

Phase- and Frequency-Domain Analysis of the Intracardiac Signals of Persistent Atrial Fibrillation in Humans

Thesis submitted for the degree of

Doctor of Philosophy

at the University of Leicester

by

Nawshin Dastagir Sakwan

Department of Cardiovascular Science

University of Leicester

2017

Phase- and Frequency- Domain Analysis of the Intracardiac Signals of Persistent Atrial Fibrillation in Humans

Nawshin Dastagir Sakwan

Abstract

Identification of critical areas for successful ablation in persistent atrial fibrillation (persAF) patients remains a challenge. Atrial electrograms (AEGs) with high dominant frequency (HDF) are believed to represent atrial substrates with periodic activation responsible for maintaining persAF. Phase is a descriptor that tracks the progression of the action potential through atria and has been demonstrated to be effective in analysing spatiotemporal changes during persAF. DF has been used as a way to express local atrial activation rate of the AEGs during AF. HDF sites were analysed consecutively to produce HDF density maps and its spatiotemporal behaviour during persAF was investigated. An algorithm based on topological charge index was also implemented to obtain phase singularity points (PSs). This algorithm's performance was compared with two other PS detection techniques for detecting PSs and has been demonstrated to have more accurate results with reduced processing time (near-real time) to calculate targets. Additionally, the effect of varying filter type and settings on the detection of PSs was also studied, From this it is understood that filter settings could affect PS detections, which result in misleading identification of the atrial substrate and hence ablation targets. Furthermore, the spatiotemporal dynamics of the PSs was also investigated by tracking them in space and time to identify 'rotors'. Rotors were not seen very often and were associated with higher atrial rate as well as disorganised AEGs. Finally, the combination of frequency and phase analysis was studied to elucidate the mechanism of wave propagation and to identify potential drivers perpetuating persAF. There is some evidence of a

cause-effect relationship between the HDF and PS density maps which leads to the spatiotemporal organization in the activation patterns during sustained A. Consequently, analysing the behaviour of the two parameters can help clinicians to develop strategies for ablation.

Acknowledgments

In the name of Allah, the Most Gracious and the Most Merciful Alhamdulillah, all praises to Allah for the strengths and His blessing in completing this thesis.

Undertaking this PhD has been a truly life-changing experience for me and it would not have been possible to do without the support and guidance that I received from many people. Hence, I would like to take this opportunity to show my gratitude to those who have assisted me in a myriad of ways.

I would first like to express my special appreciation and sincerest thanks to my supervisors, Dr. Fernando S Schlindwein and Professor G André Ng, you have been tremendous mentors for me. I would like to thank you for encouraging my research and for allowing me to grow as a research scientist. Your advice on both research as well as on my career have been priceless. I gratefully acknowledge the funding received towards my PhD from the Leicester Biomedical Research Unit (NHS) and EPSRC. I would also like to thank my internal panel members, Dr Frank Proudlock and Dr Emma Chung for serving as my committee members. Also, I believe that I am tremendously fortunate to have worked with outstanding individuals (Dr João L Salinet, Dr Frederique Vanheusden, Dr Tiago P Almeida, Dr Xin Li and Dr Gavin S Chu) and am deeply appreciative to each of them for their important contributions.

My time at Leicester was made enjoyable in large part due to the many friends and groups that became a part of my life. To my friends (Dhuha, Amnani, Moomi, Easter, Baber, Saman, Irum, Nk, Anas, Ali, Reza, Mazin, Chris, Ahmed, Sadi and Nayeem) thank you for listening, offering me advice, and supporting me through this entire process. Razia and Ramy, thank you for all the laughter and friendship. The best outcome from these past three and half years is finding my best friends (Galib Talukder, Sadaf Afreen and Kevser Sevim) who spent sleepless nights with and were always my support in the moments when there was no one to answer my queries both in work and personal life. I love you. Special thanks to Patan, without whose never-failing sympathy and encouragement this thesis would have been finished in half the time. To my friends and family scattered around the world, thank you for your thoughts, well-wishes/prayers, phone calls, e-mails, texts, snaps, visits, and being there whenever I needed a friend. I would also like to say a heartfelt thank you to my uncles and aunt (Judge Quamrul Siddique, Mr Newton Sarwar, Mrs Kanij Fatema, Dr Emran Khan and Major Mojaffar Ahmed) for always believing in me and encouraging me.

Very special thanks to my family. Words cannot express how grateful I am to my mother (Dr Kamrun Nahar Dastagir), brother (Barrister Faisal Dastagir), sister-in-law (Tamanna Dastagir), my sister (Dr Salma Dastagir) and brother-in-law (Dr Farhan Mehedi) for all of the sacrifices that you've made on my behalf. I have been extremely fortunate in my life to have such family who have shown me

unconditional love and support. I knew I always have my family to count on when times are rough. Also, I am beyond grateful for this new addition to my family, Filzaah, my niece. The first time I laid eyes on her, my heart melted and I knew she's going to be one of the best things that ever happened to me, phuppi loves you more than anything.

I would also like to express my sincere gratitude to my husband, Sakwan, who has been a constant source of support and encouragement during the last challenges of my Ph.D. journey and for offering your editing expertise throughout this process. I am truly thankful for having you in my life. Thank you very much for your love, care and support as well as for demonstrating rare and amazing patience whenever I panicked. Your kindness means a lot to me. I love you a lot.

A special note of gratitude for you, Ammu. There are no words to convey how thankful I am to you. The relationship and bond that I have with you hold an enormous amount of meaning to me. I admire you for all of your accomplishments in life, for your independence, for your hierarchical role in our family, and for all of the knowledge and wisdom that you have passed on to me over the years. Ammu, your prayers for me was what sustained me thus far. I am forever grateful to you.

Lastly and foremost, everything is incomplete if I didn't mention the most important person of my life, my Abbu (Late Alhaj Dastagir Chowdhury).

Abbu, I was very young when you left me and I never got the opportunity to tell you how much I love and respect you. Although you are not with us, your belief in me has made this success possible. It hurts a lot to think that you are not here anymore. Although I can't help but smile with tears in my eyes to think of how we cherished each and every moment of our lives together when you were alive. I miss you Baba. Your life has ended, but your legacy of wisdom, integrity and courage will go on forever. You are a great man, you are my inspiration. I know you'd be proud of the career I built so far and the young woman I've become. You are gone, but you left fingerprints of grace on my life. That's the funny thing about death: just how alive it really is. I miss you.

আল্লাহ আপনাকে জান্নাতুল ফেরদৌস দান করুন.. আমিন।

Again, I would like to thank everyone (even if I did not mention the name) who have one way or another helped me in making this study a success.

*This thesis is dedicated to the memory of my beloved father,
Late Alhaj Dastagir Chowdhury.
It is your shining example that I try to emulate in all that I do.*

I love you.

Contents

Abstract	i
Acknowledgments	iii
List of Figures	xi
List of Tables	xviii
List of Abbreviations	xix
Introduction	1
1.1 Why is atrial fibrillation important?	1
1.2 Research objectives	2
1.2.1 Main development of the thesis	3
1.2.2 Study design	4
1.2.3 Patient recruitment and ethical approval	4
1.2.4 Electrophysiological set-up	4
1.3 Outline of the thesis	6
Introduction to cardiovascular system and atrial fibrillation	8
2.1 The need for a circulatory system	8
2.2 The structure of human heart and the arrangement of the cardiovascular system	9
2.2.1 Anatomy of the heart	9
2.2.2 Blood supply to the heart	10
2.2.3 Junctional tissues of the heart	12
2.3 Electrical conduction system of the heart	13
2.4 Cardiac cycle	15
2.5 The electrical activity of the heart	18
2.5.1 Cell membrane potential	18
2.5.2 Maintenance of ionic gradient	20
2.5.3 Action potential of a cardiac cell	21
2.5.4 Measuring the cardiac electric activity	22
2.6 Arrhythmias caused by abnormal action potential generation	23

2.7	Atrial fibrillation	24
2.7.1	What is atrial fibrillation?	24
2.7.2	Epidemiology of AF in UK	25
2.7.3	Risk factors for AF	26
2.7.4	Related arrhythmias	26
2.7.5	Classification of AF	27
2.7.6	Signs and symptoms of AF	27
2.7.7	Consequences of AF	27
2.7.8	AF management and treatment	28
2.7.9	Mechanisms of AF	29
	Mapping and signal processing tools to analyse cardiac signals	33
3.1	Mapping systems	33
3.1.1	Contact mapping system	35
3.1.2	Non-contact mapping system	35
3.2	Spectral analysis	37
3.2.1	Spectral analysis and arrhythmia	37
3.3	Signal processing	38
3.3.1	Digital filters	38
3.3.2	Removal of ventricular influence	39
3.3.3	Frequency domain analysis	40
3.3.4	Dominant frequency and organisation index	42
3.4	Phase analysis	43
3.4.1	Extraction of phase data	44
3.4.2	Phase analysis and arrhythmia	46
	Using High Dominant Frequency Density Maps to Understand Spatiotemporal Behaviour of Atrial Electrograms in Persistent Atrial Fibrillation	49
4.1	Introduction	49
4.2	Materials and methods	50
4.2.1	Patients	50
4.2.2	Electrophysiological set-up	50
4.2.3	Signal analysis	51

4.2.4	Frequency domain analysis	51
4.2.5	HDF density maps	52
4.2.6	HDF temporal behaviour	54
4.2.7	Radiofrequency ablation	55
4.2.8	Statistical analysis	55
4.3	Results	55
4.3.1	Temporal stability of HDF regions	55
4.3.2	Spatial distribution of HDF regions	59
4.4	Discussion	60
4.4.1	Characterisation of high-density HDF sites	62
4.4.2	Effect of LA ablation on the HDF density maps	62
4.5	Conclusion	63
Phase analysis and Phase Singularity detection		65
5.1	Introduction	65
5.2	Methods	67
5.2.1	Study population	68
5.2.2	Electrophysiological set-up	69
5.2.3	Pre-processing techniques of VEGMs	69
5.2.4	Digital filters	69
5.2.5	Phase analysis	72
5.2.6	PSs detection technique implemented in the database	72
5.3	Results	78
5.3.1	Comparison of the three PS detection techniques	78
5.3.2	Distinguishing between different filter types	82
5.3.3	Distinguishing between different filter settings	86
5.4	Discussion	88
5.4.1	Comparing PSs identification using three different techniques	89
5.4.2	Effect of pre-processing on PS detection	90
5.4.3	Clinical significance	95
5.5	Conclusion	96

Spatiotemporal Complexity of Phase Singularities as observable in the Atrial Electrograms in Human Persistent Atrial Fibrillation	97
6.1 Introduction	97
6.2 Methods	98
6.2.1. Patient characteristics	98
6.2.2. Electrophysiological set-up and electro-anatomical mapping	98
6.2.3 Data acquisition and signal processing	99
6.2.4 Phase, phase singularities and rotor tracking	99
6.2.5 Rotors and DF	101
6.2.6 Radiofrequency ablation	102
6.2.7 Statistical analysis	102
6.3 Results	103
6.3.1 Spatial distribution of PSs during AF	103
6.3.2 Analysis of rotor lifespan during persAF	104
6.3.3 PersAF dynamics and organization	104
6.3.4 Effect of DF guided ablation on the longstanding rotors	106
6.4 Discussion	108
6.4.1 Characterizing long-lived PSs	109
6.4.2 Long lived PSs and their organisation	110
6.5 Conclusions	111
Combination of Frequency and Phase to Characterise the Spatiotemporal Behaviour of Cardiac Waves during Persistent Atrial Fibrillation in Humans	112
7.1 Introduction	112
7.2 Methods	113
7.2.1 Patient characteristics	113
7.2.2 Electrophysiological set-up and electro-anatomical mapping	113
7.2.3 Data acquisition and signal processing	113
7.2.4 Highest dominant frequency (HDF)	114
7.2.5 Phase and phase singularity points	114
7.2.6 Combining highest DF, phase maps and PS points	115
7.3 Results	120

7.3.1	Observing behaviour of HDF and PSs spatiotemporally	120
7.3.2	Correlation between HDF sites and PSs	124
7.3.3	Comparing OI values of the PSs and HDF density maps	129
7.4	Discussion	129
7.4.1	Dynamic behaviour of PSs in the LA regions	130
7.4.2	Correlation between HDF vs. PSs density maps	131
7.4.3	OI for the localisation of AF sources	132
7.4.4	Ablation strategy suggestions based on HDF and PSs density maps	133
7.5	Conclusion	133
	Main findings and future investigations	135
8.1	Main findings	135
8.2	Future investigations	138
8.2.1	Propagation of HDF region	138
8.2.2	Phase vector plots	140
8.2.3	DF guided persAF ablation	142
8.2.4	Implementing ablation strategy	143
8.3	Publications, conferences and supervisions	144
8.3.1	Journal publications	144
8.3.2	Journal publications in preparation	144
8.3.5	Conferences	145
8.3.6	Papers presented at scientific meetings	146
8.3.7	Supervisions and co-supervisions	149
8.3.7.3	Achievements and research prizes	150
	References	151

List of Figures

Figure 1: Intra-procedural fluoroscopy showing the presence of LA and RA non-contact arrays (white asterisks), electrodes (white arrow heads) and ablation catheter.	5
Figure 2: Anatomy of the human heart and the pathway of blood flow through the heart.	12
Figure 3: Flowchart showing the mechanical events in a cardiac cycle.	18
Figure 4: Action potential of the cardiac (ventricular) muscle cells.	22
Figure 5: A depiction of an action potential of the cardiac (ventricular) muscle cells illustrating the atrial and ventricular depolarisations (P and QRS interval), followed by the ventricular repolarization (T wave) as well as highlighting the region through which the impulse is travelling. (SN: sinus node, AV: atrioventricular, BB: Bachman's bundle, PF: Purkinjie Fibre).	23
Figure 6: Mechanisms underlying atrial fibrillation. Electrical impulses that propagate throughout the cardiac tissue in a disordered way can be maintained through a variety of mechanisms. (a) A rapidly discharging ectopic focus. (b) Single re-entry circuit. (c) Multiple functional re-entry circuits. (LUPV, left upper pulmonary vein; LLPV, left lower pulmonary vein; RUPV, right upper pulmonary vein; RLPV, Right lower pulmonary vein).	29
Figure 7: Illustrates the schematic diagram of excitation of cells during (a) normal rhythm and (b) arrhythmia. In (a), the recirculation cannot take place because when the stimulation completes a cycle (excitation in red), the cells at that point are still in the refractory period (dotted region) and hence can't re-trigger. Whereas during arrhythmia (b), the cells might re-trigger with shorter refractory period. Modified from (Mines, 1913).	31
Figure 8: General block diagram illustrating QRS-T subtraction.	40
Figure 9: Phasor Diagram of a Sinusoidal Waveform (blue) and a delayed version of that waveform (red).	44

Figure 10: Illustration of extraction of phase data from unipolar virtual electrograms (VEGMs). (a) Shows a VEGM segment from a persistent AF patient. (b) Illustrates the phase computation using phase-space plots of the VEGM. (c) Hilbert transformation has been used to generate an analytic signal (phase-shifted signal by 90°) of the VEGM. (d) The instantaneous phase is extracted using the inverse tangent calculation of analytic signal. (e) A 2D phase frame (and its respective 3D plot of the LA) with a color-coded activation episode is highlighted for visualisation. 46

Figure 11: (a) Illustration of accumulation of HDF clouds in order to produce a density map. The region HDF visited more or less often is indicated by the colour bar. (b) HDF density maps of one patient. Each map reflects the HDF dense regions when using different lengths of VEGM recordings. 53

Figure 12: (a) Temporal behaviour of the HDFs of one persistent AF patient. For this case, the exponential fit has a time constant of 9.81 s. Results measure the stability of the behaviour of the HDF clouds. (b) Summary of indices for all patients comparing the HDF density map produced using a particular time segment with the ultimate HDF density map produced using 300 seconds. (c) SD plots of the indexes comparing the HDF density maps. 56

Figure 13: (a) (i) Scatter graphs (for one patient) showing different directions and strengths of correlation of HDF density maps (produced using several segments of VEGM recording) when compared to the HDF density map created using 300 seconds of VEGM recording. (ii) The histogram and distribution of the similarity indices (for one patient) comparing the similarity of every HDF density map (produced using 75 seconds) with each other. The histogram at this site exhibited high kurtosis with a sharp peaked distribution and negative skewness. This site exhibited a high similarity index with a mean of 0.71. (b) Incidence of HDF dense regions – before ablation – in the different LA regions, namely: MV, PVs, roof, posterior wall, anterior wall, LAA, MVI, septum and floor. (c) The mean and SD of the HDF of MVR (occurrences of the HDFs > 80%) and LVR (occurrences of the HDFs ≤ 80%). The mean ± SD of frequency in MVR nodes is 6.32 ± 0.49 Hz, significantly different from 5.87 ± 0.95 Hz of LVR ($p < 0.001$). (d) The frequency organization of the electrograms of HDF regions as measured with OI and RI in the nodes of MVR is significantly lower (0.36 ± 0.13 vs 0.39 ± 0.14 , 0.432 ± 0.13 vs 0.437 ± 0.14 , $p < 0.0001$) than that of LVR. 58

Figure 14: (a) Location of CoGs (pink dots) in LA of two persistent AF patients obtained for a specific time window. In this case the CoGs are located outside the HDF cloud's (red region) boundaries. The position of the CoGs is not a true representative of the HDF 'cloud'. (b) Comparison of HDF density maps with CoG distribution in order to compare the spatiotemporal distribution of the two techniques.	61
Figure 15: The mean and SD of the global HDF and spatiotemporal coverage area of the VEGMs for both pre- and post-ablation.	63
Figure 16: Flowchart guides through steps of extracting phase and identifying PSs as well as highlighting the parameters that could eventually affect the overall detection.	68
Figure 17: An overview of PS illustration in 2D LA and how it is detected using the topological charge technique. (a) Phase map at an instance of time of a persAF patient. b) A map displaying arrows representing the phase vector (size indicating the magnitude and orienting representing the direction of activation. (c) & (d) A plot of the topological charge in 3D and 2D to identify the location of the PS, where the topological charge equals +1 or -1.	74
Figure 18: Schematic representation of two different methods (triangulation mesh technique and image processing technique) of PS detection and steps.	76
Figure 19: Schematic representation of tracking PSs. Each PS is considered as the same PS if it is between the maximum spatial ($\Delta d_{max} \leq 3$ nodes) and temporal separation ($\Delta t_{max} \leq 10$ ms) between the detected PS. If conditions are met, the tracking continues, else it stops tracking and reports the lifespans of the PS.	77
Figure 20: (a) An example of the PS detection using 3 methods with a series of phase gradient thresholds. (b) PS histograms of 8 s VEGM using 3 methods with different phase gradient thresholds. (c) the effect of changing the phase gradient thresholds on the number of PSs for each patient.	79

Figure 21: (a) Box plots illustrating the effect of adjusting the phase threshold on the number of PSs per frame for the TCT. (b) The processing time of TCT, TMT and IPT using default thresholds (mean \pm SD: 0.9 ± 0.2 s vs. 335.4 ± 14.4 s vs. 596.6 ± 144.0 s ($P < 0.0001$), respectively). (c) i) A frame of the phase clip and the region selected as the 'gold standard'; ii) The PS histogram generated with the manual annotation (red rectangular region); iii) The shorted path/distances on the surface of 3D atrial mesh between PSs using manual annotation and the PSs using each method with revised thresholds; iv) The PS histogram generated using each method. 81

Figure 22: Box plots showing number of PSs identified for all patients using the raw signal and the three filters. Mean highest number of PS were found within the raw signal (97784 ± 12768) followed by the EF signals (30580 ± 12835), BF (26985 ± 13691) and finally the ICF (17476 ± 8904). 83

Figure 23: Comparison of 3D scatter plots of all PSs found in BWF patient data (left) and only rotors (right). The reduction of total number of points makes comparison of relevant PS locations which is of more interest. 84

Figure 24: 3D scatter plots of centre points for all consistent rotors found using each filter and the raw signal. X and Y are the spatial directions and the Z-axis shows the time interval at which the PS cluster was found. From visual inspection, the clusters identified from the raw signal were seen to be more dispersed than those found from the filtered signals. Despite having the fewest number of rotors, the rotors identified using the ICF showed significant overlap with the rotors found using the other two filters. 84

Figure 25: Scatterplots of rotors identified from one patient without any filtration (left) and with BF filter applied (right) showing on the XY plane. Unfiltered scatter plot shows a greater area of the atrium covered compared to the BWF scatterplot. 91

Figure 26: Scatter plot of all rotors identified from one patient signals using each of the three filters separated by colour, BF clusters in red, ICF clusters in magenta and EF clusters in green, showing variations in x-axis and time. Although rotors mostly appear in the same regions as those from other filtered signals there is little overlap at the same time window as shown by the gaps in the z-axis (time) between groups of rotors. 92

Figure 27: The location of the PSs were identified in 3D and 2D and tracked spatiotemporally to detect rotors. Its X, Y coordinates were also recorded and each LA was reshaped into 2D block for observing its behaviour. The chirality of each PS was also recorded. 101

Figure 28: Shows the VEGM of a persAF patient, its frequency spectrum and the phase data extracted from it. The spectra and the phase are further analysed to study the atrial activity and dynamics of the rotor behaviour in the LA. 102

Figure 29: (a) Shows a representative example of one such plot where the cumulative distribution of PSs is shown. (b) Evolution of PSs (and their chirality) over time. In both (a) and (b) complex clusterings of PSs were seen in some instances when several PSs were detected close to each other (highlighted in red). 103

Figure 30: Shows the VEGM and the corresponding HDF value in presence of rotor(s). For the mother rotor fibrillation, the mean HDF is 8.24 ± 0.33 Hz significantly different from short lived PSs window 7.95 ± 0.42 Hz ($p < 0.0001$) (see figure 33 (a)). The complexity of the FFT spectra as represented by the OI for mother rotor and short lived PSs window were significantly different as well (OI: 0.732 ± 0.05 vs 0.76 ± 0.05 , $p < 0.0001$) (see figure 33 (b)). 104

Figure 31: (a) Density maps of short lived PSs vs. rotor. For short lived PSs, a broad distribution of PSs can be seen. (b & c) Locations of rotors in the anatomical regions of the LA for both (b) pre vs. (c) post ablation data. From our results, prior to ablation, rotors were observed in several regions, with the septum having the highest incidence. (LUPV: Left upper pulmonary vein; LLPV: Left lower pulmonary vein; RUPV: right upper pulmonary vein; RLPV: right lower pulmonary vein; POS: posterior wall; ANT; anterior wall; LAA: left atrial appendage; Sept: Septum). 105

Figure 32: (a) The number of PSs observed (Pre vs Post) at any instant for all 10 persAF patients' cases. (b) The lifespan of tracked PSs (Pre vs. Post) in milliseconds. 107

Figure 33: The mean and SD of the (a) HDF and (b) OI of rotor vs short lived PSs (for both pre vs. post ablation data). 108

Figure 34: The figure shows the relative importance of factors that maintain the paroxysmal, persistent and permanent AF (pAF, persAF and permanent AF respectively). For pAF, it is the triggers; for persAF, it is combination of both triggers and substrate modification; for permanent AF, it is only the substrate modification which is sustaining AF. 113

Figure 35: Illustration of the parameters characterising the atrial substrate. For one patient corresponding (a) phase, (b) PSs, (c) HDF and all the parameters combined for three different instances are shown in order to study the spatiotemporal relationship between among them. 116

Figure 36: Illustration of corresponding 3D and 2D HDF maps for one patient for several windows. It can be seen that the HDF regions are not consistent in every window and that sometimes they reoccur in the same region after a certain while. 117

Figure 37: Illustration of how K-Means clustering algorithm. The algorithm depends on the assignment of information to a given set of partitions also known as cluster centres or the K centroids. In this study, it was defined as 2 (clockwise and anticlockwise centroids). At every step of the algorithm, each data value is assigned to the nearest centroid based on some similarity parameter that is calculated using Euclidean distance measurement. Then, the centroids are recalculated based on these hard assignments. With each successive pass, a value can change the centroid it belongs to, thus altering the values of the centroid at every pass. 119

Figure 38: The illustration shows the colour bar of the density map with threshold set at 100 %, 75 %, 50 % and 25 % (from left to right). The cumulative history colour bar is the same except the bottom colour will be the trace background colour. 120

Figure 39: (a) shows box plot of the cumulative number of PSs (for all 10 patients) appearing over time in the septum of the LA. (b) Summary showing the mean and SD of the number of PSs appearing at each region every two seconds. (c) Shows the best fit line for all the regions and the corresponding slope (m) value of the best fit. 123

Figure 40: Comparison of the density maps of HDF and PSs to understand the overall summary of the spatiotemporal behaviour for three different patients, a, b and c. 124

Figure 41: Shows HDF and PS detection in several regions of LA in corresponding frames. 126

Figure 42: (a) shows an example of the PSs clustering appearing around a HDF cloud in a consecutive interval of time. The arrows indicate the propagating waves travelling across the atria giving rise to fibrillatory conduction and (b) they seem to be related to the drift direction of the HDF 'clouds' (see chapter 8). 128

Figure 43: The mean and SD of the OI value for HDF and PS density map with change in density threshold set at 100 % (T_{100}), 75 % (T_{75}), 50 % (T_{50}) and 25 % (T_{25}). 129

Figure 44: (a) 3D map of the left atrium showing the centre of a high DF area in black. The circles with the corresponding sign indicate clockwise and counter-clockwise PSs respectively. (b) Schematic diagram defining the direction of PSs with opposite chirality. We examine the situations when HDF channels through these PSs (arrows in the middle). 139

Figure 45: Representation of phase vector plots with the phase value in the background in 2D and 3D human LA. The color represents a phase in the excitation recovery cycle and the arrows representing the corresponding magnitude and direction the phase. 141

Figure 46: Representation of the cumulative HDF clouds stacked on the 3D LA (left-hand side) of 2 human persAF patients. 143

List of Tables

Table 1: Overview of the patients' database.	4
Table 2: Rate of generation of impulses of various tissues of the heart (Modified from <i>Sherwood 2011</i>).	13
Table 3: Summary of mean values with SD of SSIM and CORR indices obtained comparing all filter types and RAW signal for all the patients. Overall highest value of SSIM (0.69 ± 0.06) and CORR (0.64 ± 0.12) indices found between the BWF and EF.	86
Table 4: Total number of PSs and rotors identified using different filter settings. Highest mean number of PSs found using the low pass filter (70630 ± 7832) followed by 4 to 12 Hz (64482.7 ± 107994), 4 to 10 Hz (48488 ± 87425) and finally the 1 Hz bandpass filter (8844 ± 2023). Also shows the total number of rotors found followed which also followed the same trend as the number of PSs identified. Highest mean number of rotors found using the low pass (42.3 ± 17) followed by 4 to 12 Hz (19.4 ± 8.7), 4 to 10 Hz (8.0 ± 6.0) and finally 1 Hz bandpass (1.4 ± 2.0).	87
Table 5: Summary of mean values with SD of SSIM and CORR indices obtained comparing all filter settings for all the patients. Overall highest value of SSIM (0.66 ± 0.10) and CORR (0.62 ± 0.082) indices found between the settings 1 Hz BPF at HDF and 4 to 12 Hz BPF.	88
Table 6: Summarises the spatial shifts of all the PSs from the HDF region in all corresponding frames for all the 10 patients.	126

List of Abbreviations

3D	Three dimensional
ADP	Adenosine diphosphate
AEG	Atrial electrograms
AF	Atrial fibrillation
AFL	Atrial flutter
ATP	Adenosine triphosphate
AV	Atrioventricular (node)
BPF	Band-pass filtering
BWF	Butterworth
CM	Contact mapping
CoG	Centre of gravity
CONFIRM	Conventional ablation with or without focal impulse and rotor modulation
CORR	Pearson's correlation
CS	Coronary sinus
CV	Conduction velocity
DF	Dominant Frequency
DFT	Discrete Fourier Transform
EAM	Electro-anatomical mapping (system)
ECG	Electrocardiogram
EF	Elliptical
EP	Electrophysiology procedure
FFT	Fast Fourier Transform
FIRM	Focal impulse and Rotor Modulation
HDF	Highest DF

HT	Hilbert Transform
ICF	Inverse Chebyshev
IPT	Image processing based technique
LA	Left atrium
LAA	Left atrial appendage
LLPV	Left lower pulmonary vein
LUPV	Left upper pulmonary vein
LV	Left ventricle
LVR	Least visited regions
MEA	Multi-electrode array
MV	Mitral valve
MVR	Most visited regions
NCM	Non-contact mapping
OI	Organization index
PA	Pulmonary artery
pAF	Paroxysmal AF
PersAF	Persistent AF
PS	Phase Singularity point
PV	Pulmonary Veins
PVI	Pulmonary Veins isolation
r^2	Linear regression coefficient
RA	Right atrium
RFA	Radiofrequency ablation
RI	Regularity index
RLPV	Right lower pulmonary vein
RP	Refractory period

RUPV	Right upper pulmonary vein
RV	Right ventricle
SA node	Sino-Atrial (node)
SD	Standard deviation
SSIM	Structural similarity index
SVC	Superior vena cava
TCT	Topologic charge technique
TMT	3D triangulation mesh technique
VEGM	Virtual unipolar electrogram
τ	Time constant

Chapter 1

Introduction

1.1 Why is atrial fibrillation important?

Atrial fibrillation (AF) is the most common type of cardiac arrhythmia (abnormal heart rate and/or rhythm). AF produces a rapid and irregular heartbeat, during which the atria quiver (or fibrillate) instead of beating normally. Coronary or rheumatic heart disease, hypertension, obesity and diabetes have all been identified as major risk factors of AF (Abed *et al.* 2013). It affects approximately 33.5 million individuals around the world as per 2010 (Chugh *et al.* 2014). More than 0.5 million of people in the UK had AF in 1995 (Stewart *et al.* 2004) and 2 million people in the United States (Fuster *et al.* 2006) are affected by it. It is estimated to affect 15 million individuals by 2050 in US (Natale and Jalife 2008). Moreover, evidence is emerging that not only is AF associated with increased mortality and morbidity, but also it can be considered an independent risk factor as well. In some specific individuals, the triggers initiate AF, and in other individuals it does not induce, regardless of having the similar signs and symptoms. Therefore, despite the intensive knowledge we have today regarding AF, the research to find ultimate treatment is ongoing. The main underlying reasons causing AF are still being researched. AF also accounts for approximately one-third of hospitalizations for cardiac rhythm disturbances. The cost of clinical care of AF includes hospital costs, medication, follow-up, disability and emergency measures, adding up to 1% of the National Health Service budget in the United Kingdom and around US\$ 20 billion of annual expenses in the United States of America (Chugh *et al.*, 2014). The pursuit of efficient and successful treatment for AF is, therefore, important.

1.2 Research objectives

AF is a serious problem as it can lead to stroke and heart failure, with increased mortality. To further complicate the problem, the precise electrical mechanisms underlying AF are still, despite intensive research, not well understood. The number of individuals affected with AF is increasing rapidly, and there is considerable debate regarding which treatment strategy is best for patients with AF. Pharmacological therapy is typically preferred as the first line of treatment for ventricular rate control and to avoid clot formation in most patients with AF, but it is usually followed by strong side effects, such as increasing the probability of heart failure, bradycardia or heart block (Calkins *et al.* 2012).

One effective, as well as most accepted interventional procedure treatment for AF, is radiofrequency catheter ablation (RFA), whereby areas in the atria and/or nearby locations are targeted and ablated (or 'burned'). Triggers in the pulmonary veins (PVs) have been shown to be important in the initiation and perpetuation of the arrhythmia in early stages (Haïssaguerre *et al.* 1998). Consequently, PV isolation (PVI) performed by RF ablation became the standard treatment for paroxysmal AF (pAF), with success rates as high as 80% (Oral *et al.* 2002). PVI is, however, less effective in patients with persistent AF (persAF), with success rates varying from 20% to 90% of the cases using different ablation strategies (Lim *et al.* 2015). This inconsistency in persAF ablation outcomes is possibly due to extensive atrial substrate remodelling induced by long-term AF and little knowledge of the mechanisms involved in the perpetuation of AF (Oral *et al.* 2002). Hence, short term results are variable, with a significant number of patients requiring repeated procedures if AF recurs. Long term results are even less encouraging. One of the main issues with ablation is the decision on where to ablate for maximum efficacy and safety. Improving understanding of the precise electrical mechanisms underlying AF is crucial to minimising the amount of ablation and maximizing the results. There are several parameters that help to identify the abnormal atrial substrates and that can guide clinicians to perform the ablation procedure. Different parameters target different atrial regions. Therefore the work done in this study mainly

focussed on studying two different parameters, the Dominant Frequency (DF) and Phase, in order to characterise the changes of the electrical signals during AF and tracking the activation patterns.

1.2.1 Main development of the thesis

It is important that clinicians thoroughly understand the indications for treatment, the latest technologies, the fundamental physiological principles, the epidemiology, and the pathogenesis of AF so that patients can be optimally managed and so that more approach can be made toward preventing and eradicating AF. Improving our knowledge of the underlying AF conduction is an important contribution towards enhancing patient results for AF.

DF mapping has been used to identify the excitation frequency distribution and phase mapping has been used to represent the electrical activation-recovery cycle of cardiac tissue and for the identification of re-entry during AF. For DF analysis, this work focussed on demonstrating a comprehensive understanding of the spatial and temporal behaviour of the DF of the cardiac waves and for phase analysis, phase maps were computed as well as points with ambiguous activation known as Phase Singularity points (PSs) are also located. The behaviour of DF regions along with PS points was also analysed by combining DF, phase and PS maps. The work tracked persistent PS points, also known 'rotors', in order to locate the tip of functional re-entry activity during AF. Overall the work in this report is a contribution to the identification of abnormal atrial substrate during AF, as well as to providing information that can be used to aid ablation strategy either before or during the ablation procedure.

1.2.2 Study design

The section discusses patients' recruitment and electrophysiology procedure (EP) system used to treat persAF patients during catheter ablation procedure.

1.2.3 Patient recruitment and ethical approval

A cohort of 10 volunteers with symptomatic persAF were recruited at Glenfield General Hospital, Leicester, UK. They were undergoing first time ablation for drug-refractory persAF and, prior to study, were asked for permission for using their data which includes blood sampling and electrical recordings of the atria during the RF ablation for research. The study was approved by the local ethics committee and all procedures were carried out after informed consent. Clinically relevant information of the cohort is given in Table 1-1.

Table 1: Overview of the patient's database.

Number of Patients	10 (10)
Age (mean \pm SD) (years)	58 \pm 13
Male/Female	10/0
Height in cm (mean \pm SD)	178.07 \pm 5.57
Weight in kg (mean \pm SD)	99.83 \pm 20.12
Smokers	
Current (%)	2 (20%)
Never (%)	2 (20%)
Ex (%)	6 (60%)
Ablation Procedure:	
Radiation Time in min (mean \pm SD)	77.72 \pm 22.01
Radiation Dose in μ Gy (mean \pm SD)	7451.7 \pm 3484.4

1.2.4 Electrophysiological set-up

All antiarrhythmic drugs, apart from amiodarone, were stopped for at least five half-lives before the procedure. Subjects were under general anesthesia during the entire procedure and were anticoagulated with heparin to maintain an activated clotting time above 300 seconds. For all patients, bi-atrial three dimensional (3D) electro-anatomical mapping (EAM) was performed. First, a noncontact multi-electrode array (MEA) (EnSite Velocity, St. Jude Medical, USA) and a conventional deflectable ablation catheter were deployed into the right

atrium (RA) with an anchoring point in the superior vena cava (SVC). Similarly, an EnSite array was positioned transeptally into the left atrium (LA) with an anchoring point at the left upper pulmonary vein (LUPV). Further to this, a 7F coronary sinus (CS) catheter (Inquiry, St Jude Medical) was deployed from the left femoral vein to support pacing protocols. A fluoroscopic image of the setup with both balloons in place is shown in Figure 1.

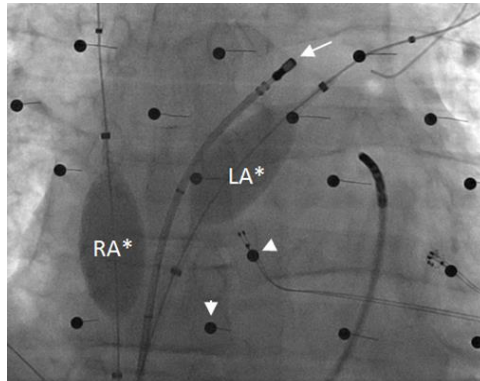


Figure 1: Intra-procedural fluoroscopy image showing the presence of LA and RA non-contact arrays (white asterisks), electrodes (white arrow heads) and ablation catheter (white arrow). Picture taken at Glenfield General Hospital before a catheter ablation procedure.

For the cohort, detailed atrial geometries were reconstructed with EAM software (EnSite, St Jude Medical) using the ablation catheter and anatomical landmarks including PV ostia, left atrial appendage (LAA), roof, septum, anterior, PVs and mitral valve (MV) annulus were annotated. After mapping, both arrays were kept in position to avoid distortion of the reconstructed isopotential maps (Chinitz and Sethi 2006). Electrocardiogram (ECG) leads were positioned on the extremities to allow for QRST segmentation and cancellation.

Following this, AF ablation proceeded as per standard practice. The primary highest DF (HDF) site was identified, its centre of gravity (CoG) (Salinet *et al.* 2013c) was determined and ablation started by targeting the CoGs and their trajectory. A post procedure recording was collected for up to 5 minutes. The MEA was removed and that was followed by standard PVI by targeting the PVs ostia, aimed at the electrical isolation between the potential firing triggers localized in the PVs (Jais *et al.* 1997) and the LA.

1.3 Outline of the thesis

AF is a complex disorder. To understand AF and to decide the best ablative therapy for each patient, it is necessary to understand the nature of AF from as many angles as possible. This work provides a multi perspective look at the disease using different characterising tools. Each chapter of this thesis deals with a different analysing tool of AF which is widely being used/recognized by experts in the evolving field of cardiac electrophysiology.

The next chapter (chapter 2) focusses on the clinical perspective of the human cardiology, describing the physiology and electrophysiology of a normal heart and how it differs during AF. It also consists of detail information on the anatomy of the atrium, physiology of the atrium, characteristics of the cell membrane and channels, factors affecting the cell membrane, action potential and atrium electrical propagation, epidemiology of AF, highlights the economic aspects, classification, mechanisms of AF, signs and symptoms, underlying risk factors and finally the current clinical treatments.

Chapter 3 discusses the mapping and engineering/mathematical techniques that are currently used for this study. It provides information regarding the type of software used for this study, electro anatomical mapping systems, spectral analysis of the signals, filter settings, AEGs, and the methodology for removal of ventricular influence.

Chapter 4 assesses the stability of DF during persAF as well as mainly focusses on the development of density maps to analyse the spatiotemporal behaviour of the HDF in the LA of patients with persAF while using non-contact mapping (NCM). This chapter also investigates the post ablation effect on the virtual unipolar electrograms (VEGMs) using the HDF density maps.

Chapter 5 describes phase analysis of the cardiac waves. In this chapter the study of how different types of filtering techniques on the intracardiac signals affect the phase data is also reported. Furthermore, the chapter compares and discusses three different methods for identifying PSs as well as the technique for tracking PSs with time.

Chapter 6 analyses the behaviour of long-standing PSs utilizing a novel non-contact methodology and compares this to real time DF analysis. In this chapter, the complexity of the atrial activity dynamics as observable using NCM in persAF patients is investigated and the dynamics of the long-standing PSs after DF guided ablation is studied.

Chapter 7 investigates the relationship between PSs and HDF density maps and a thorough analysis and careful interpretation of atrial dynamics is incorporated.

And finally, Chapter 8 summarizes the main findings from this thesis and highlights potential future investigations.

Chapter 2

Introduction to cardiovascular system and atrial fibrillation

2.1 The need for a circulatory system

All known living organisms are made of up of cells. All cells require metabolic substrates (e.g. oxygen) and a mechanism by which they can remove waste (e.g. carbon dioxide). Single cell organisms, such as amoeba, allow oxygen into them and carbon dioxide out by diffusion with the environment. However, multicellular organisms require a larger surface area for the exchange of gases and nutrients to occur and hence they have a circulatory system. The circulatory system carries nutrients, dissolved gases and hormones to body cells as well as waste products away from the body cells (Klabunde 2011). Most multicellular animals such as mammals have a heart which pumps fluids around the body. The basic components of a circulatory system are,

- Fluid: such as blood, to carry materials around the body
- Blood vessels: spaces for fluids to move
- Heart: the pump that pushes fluids through the body.

This is known as the cardiovascular system. This system ensures the adequate blood flow is delivered to the organs in order for the exchange to take place (Klabunde 2011).

2.2 The structure of human heart and the arrangement of the cardiovascular system

2.2.1 Anatomy of the heart

The heart is located in the middle of the chest (Schneek 1999). It is medial to both lungs and rests on the superior surface of the diaphragm. The heart is enclosed within a fibrous and serous membrane known as the pericardium. The fibrous pericardium firmly clamps the heart in position as well as restricts its excessive movement. The serous membrane is a slippery layer that reduces the friction and lubricates the region facilitating the beating of the heart. The heart is cone shaped with a broad base at the top and a narrow apex at the bottom.

The heart wall is made up of layers. Each layer has a different function that primarily aids its pumping action, allowing blood to flow around the body (Schneek 1999). There are three layers which are known as,

- Epicardium- A thin membrane that outlines the heart. It is a visceral layer of the serous pericardium. It consists of fatty tissues known as adipose tissues, connective tissues (such as collagen, elastics tissue and fibres) and mesothelium tissues (Van Wynsberghe *et al.* 1995, Tortora and Derrickson 2011).
- Myocardium- This layer is the middle muscular layer of the heart walls. It forms the thickest layer of the heart wall and is full of cardiac muscles that enable cardiac conduction. It also consists of blood vessels. The myocardium has three functions: providing a scaffolding for the heart chambers, assisting in contraction and relaxation of the cardiac walls so that blood can pass between the chambers and conducting electrostimulation through its tissues into the epicardium (Van Wynsberghe *et al.* 1995, Tortora and Derrickson 2011).

- Endocardium- This layer lines the entire inner surface of the heart. It consists of endothelium, subendothelial connective tissues and subendocardial layer (Van Wynsberghe *et al.* 1995, Tortora and Derrickson 2011).

The heart consists of 4 chambers that are connected by heart valves (Schneek 1999) (Figure 1). The upper two chambers are called atria. The atria are separated by a septum into the LA and the RA. The lower two chambers of the heart are called ventricles. They are separated by a septum into the left ventricle (LV) and right ventricle (RV) (Schneek 1999). The atria receive blood returning from the body and the lungs whereas the ventricles pump blood from the heart to the body and lungs. Due to their function, the atria and ventricles have their specific criteria of the heart walls. The LA and RA have thinner walls as they receive the blood compared to the LV and RV who have thicker walls as they have to pump blood to a further distance (Klabunde 2011). The right side of the heart receives deoxygenated blood whereas the left side of the heart receives oxygenated blood. The blood flows in one direction (atria to ventricles) in the heart. In order to prevent back flow of the blood, valves are present between the upper and lower chambers known as atrioventricular (AV) valves. The AV valve between the RA and RV is known as tricuspid valve (as it has three cusps/flaps) and the AV valve between LA and LV is known as bicuspid/mitral valve (Sherwood 2011). The two main blood vessel emerging from the RV and LV are pulmonary artery (PA) and aorta they also have valves known as pulmonary and aortic semilunar valves, which also prevent backflow of blood (Klabunde 2011).

2.2.2 Blood supply to the heart

The heart pumps almost 5.7 litres of blood per minute and beats more than 100,000 times a day (Winner 2007). The heart itself requires blood supply to get nutrients to pump blood efficiently. Two branches exit from the base of the aorta known as the left and right coronary arteries and supply oxygenated blood to the left and right side of the heart respectively

(Klabunde 2011). The deoxygenated blood is removed by the coronary veins. The coronary veins are made up of two subgroups, the greater and smaller cardiac venous system. All the veins collect together and form a large blood vessel known as coronary sinus. The coronary sinus drains the deoxygenated blood to the RA. This circulation of supplying oxygen and removing carbon dioxide from the myocardium cells is known coronary circulation (Klabunde 2011).

The cardiovascular system is comprised of two types of circulation: systemic circulation and pulmonary circulation (Klabunde 2011). The systemic circulation is between the heart and the whole body. It carries blood from the heart to rest of the tissues of the body and then returns it to the heart (Sherwood 2011). Oxygen rich blood is pumped from the left ventricle into the aorta. The aorta then makes an inverted U-turn to form the aortic arch, which gives rise to branches that supply the head, neck and upper limbs. The aorta continues posterior to the heart travelling through the thoracic and abdominopelvic cavities. It supplies the organs of these cavities and lower limbs. In the systemic capillaries, oxygen is exchanged for carbon dioxide, resulting in deoxygenated blood (Klabunde 2011, Sherwood 2011). The deoxygenated blood enters the RA via the superior and inferior *vene cavae*. The pulmonary circulation carries blood from the heart to the lungs for gas exchange and then returns it to the heart. Deoxygenated blood is pumped from the RV into the pulmonary trunk. The large pulmonary trunk divides into right and left PA. These arteries transport blood to the right and left lungs. In pulmonary capillaries, carbon dioxide is exchanged for oxygen. This result in oxygen-rich blood that then flows through the PV and enters the LA (Klabunde 2011). Pulmonary circulation is the circulation between the lungs and the heart.

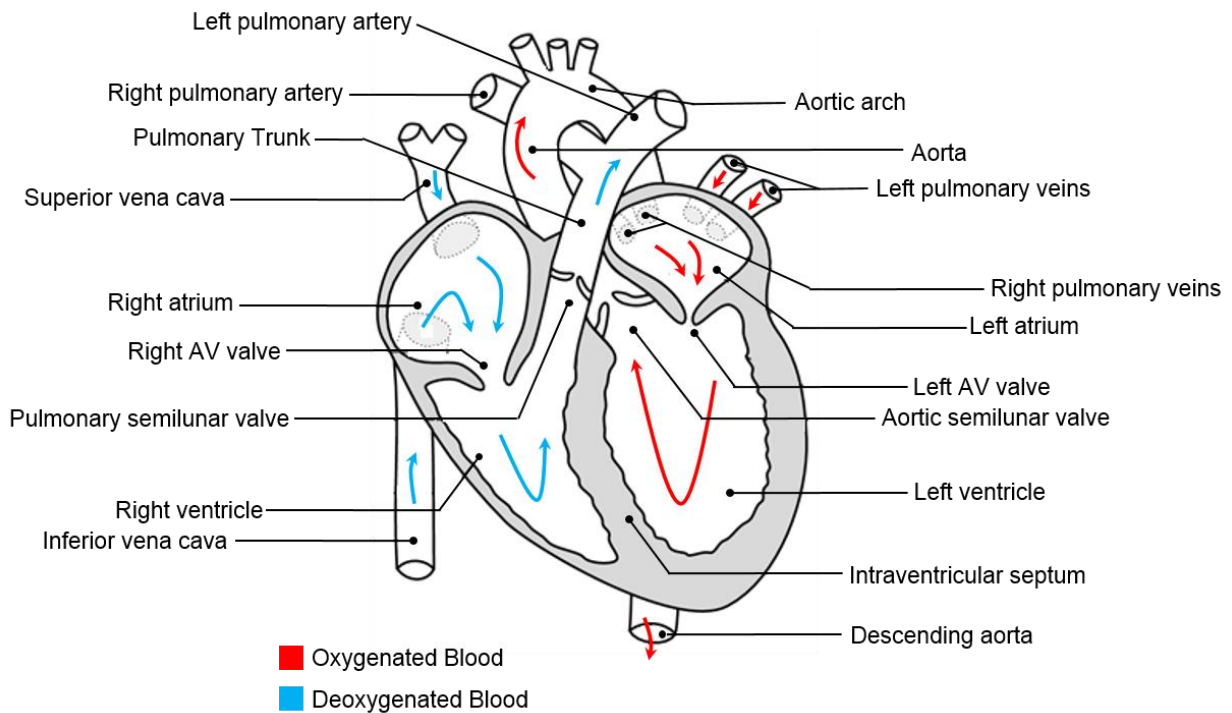


Figure 2: Anatomy of the human heart and the pathway of blood flow through the heart.

2.2.3 Junctional tissues of the heart

There are some specialized fibres in the cardiac muscles which can generate cardiac impulses and transmit them to all parts of the myocardium. They are called junctional tissues or conduction system of the heart. The junctional tissues are as follows (Sherwood 2011):

- SA node (Sino-Atrial node)
- The inter-nodal pathways:
 - o Anterior
 - o Middle
 - o Posterior
- AV node
- AV Bundle or the Bundle of His and its right and left branches
- Purkinje fibres

Rate of generation of their impulses are shown in the table below:

Table 2: Rate of generation of impulses of various tissues of the heart (Modified from Sherwood 2011).

Junctional Tissues	Impulse/minute	Conduction Speed (m/s)	Functions
SA node	70 – 80	0.05	Generates the normal cardiac impulse
AV node	40 – 60	0.05	Delays the passing of the impulse from the atria to the ventricles
AV bundle	30 – 36	1	Transmit impulse from atria to ventricles
Purkinje fibres	15 – 40	4	Transmit the impulse to all parts of the ventricles

2.3 Electrical conduction system of the heart

Various parts of the conduction system and the myocardium are capable of spontaneous discharge. The SA node discharges most rapidly and the impulses generated from it are transmitted to the AV node and other parts of the conductive system (Van Wynsberghe *et al.* 1995). As a result these parts are triggered by the SA node and discharge at the rate commanded by the SA node. The impulse is transmitted to the myocardium, which also discharges at the rate of SA nodal discharge. Thus, normally the rate of impulse discharges of the SA node determines the rate at which the heart beats (Sosnowski *et al.* 2011).

The depolarization/cardiac impulses from the SA node spread radially through the entire atrial muscle. The impulses then reach the AV node through the cholinergic pathways and then the AV bundle and its branches. The AV node is normally the only conducting pathway between the atria and the ventricles. There is a delay in transmission of the cardiac impulse from the atria to the ventricles, caused by the AV nodes, due to the inter-nodal delay, which

is about 0.09 seconds. The causes of AV node delay is due to (Van Wynsberghe *et al.* 1995, Sherwood 2011, Sosnowski *et al.* 2011):

- the very small size of the junctional fibres of the AV nodes
- very few gap junctions between the successive muscle cells of the AV node which is a great resistance to conduction of excitatory ions from one cell to the next
- prolonged refractory period of the AV nodal fibres.

The advantages of such delay are that it allows time for the atria to empty their blood into the ventricles before the ventricular contractions begin.

A special characteristic of the AV bundle is the inability, except in abnormal states, of action potential to travel back from the ventricles to atria (Sherwood 2011). This prevents re-entry of cardiac impulses and allows only forward conduction from atria to the ventricles. Furthermore, the atrial muscle is separated from the ventricular muscle by a continuous fibrous barrier (Van Wynsberghe *et al.* 1995, Sherwood 2011, Sosnowski *et al.* 2011). This barrier normally acts as an insulation that prevents passage of cardiac impulses between atrial and ventricular muscle through any other route.

After crossing the AV bundles and its branches, the cardiac impulse reaches the Purkinje fibres. The Purkinje fibres arise from the branches of the Bundle of His, spread from the interventricular septum directly into the papillary muscles and directly into the lateral walls of the ventricle, ending ultimately with the sub-endocardial network (Sherwood 2011). Its fibres spread to all parts of the ventricular myocardium. The functions of the Purkinje fibres are to initiate impulse and conduct the impulses quickly to every part of ventricular muscle at a rate of 15-40 impulse/minute (Sherwood 2011).

Finally, the cardiac impulse reaches all the ventricular muscles. Depolarization of ventricular muscle therefore starts at the side of the interventricular septum and the septal activates from left to right (Sherwood 2011). This is then followed by the activation of anteroseptal region of the ventricular myocardium and major portion of ventricular myocardium from

endocardial surface. Finally, the last stage of the electrical conduction of the heart is the late activation of the posterobasal portion of the left ventricle, the pulmonary conus and the upper portion of the septum (Sherwood 2011).

2.4 Cardiac cycle

The cardiac events that occur from the beginning of one beat to the beginning of the next are called the cardiac cycle. A cardiac cycle usually takes 0.7-0.8 seconds. The events of cardiac cycles are (Sherwood 2011),

- Mechanical events;
- Pressure changes in ventricles, atria, aorta, pulmonary artery and jugular veins;
- Changes in volume of ventricle and atria;
- Production of heart sound and apex beat;
- Production of pulse and appearance of pulse wave;
- Electrical changes in the heart;
- Systematic, coronary and pulmonary circulation.

The mechanical events comprise of the 2 phases of a cardiac cycle: Systole and Diastole (Sherwood 2011). The phases occur in both the atria and ventricles known as atrial systole, atrial diastole, ventricular systole and ventricular diastole.

Atrial systole lasts for only 0.1 second. It initiates the cardiac cycle as the pacemaker is in the RA. About 30% of ventricular filling occurs actively during atrial systole. It has two phases,

- Dynamic phase (0.05 second): During the first half of the atrial systole, there is maximum contraction of the atrial muscles and inter-atrial pressure rises. This part is known as dynamic phase (Sherwood 2011).

- Adynamic phase (0.05 second): The second half of the atrial systole is known as the adynamic phase because during this period force of contraction of atrial muscles decrease and the inter-atrial pressure decreases (Sherwood 2011).

Atrial diastole begins after atrial systole and lasts for 0.7 seconds. During the first half of the atrial diastole, the atria collect blood from vene cavae and pulmonary veins and the AV valves remain closed. During the second half, the AV valves open and blood passes from the atria to the ventricles. About 70-80% of the ventricular filling occurs passively in diastole (Sherwood 2011).

Ventricular systole begins after atrial systole and this phase lasts for 0.3 seconds. It has three phases:

- Isometric contraction phase: It is the interval between the closure of the AV valves and opening of the semilunar valves. At the onset of ventricular systole, the AV valves close and produce the first heart sound (Sherwood 2011). The ventricular muscles contract but muscle length does not shorten which is called isometric contraction. The ventricles contract as a closed cavity and no blood gets out. The intraventricular pressure rises sharply as the myocardium presses on the blood in the ventricle. When intraventricular pressure exceeds the pressure in the aorta and the pulmonary trunk, the semilunar valves open and this phase ends. The importance of this phase is that in this period there is a sharp rise of intraventricular pressure, which helps large amounts of blood to be pumped out of the ventricles in the next phase;
- Maximum ejection phase: In this phase, ventricles pump about 80% of the blood (Sherwood 2011);
- Slow ejection phase: In this phase, ventricles pump about the remaining 20% of the blood (Sherwood 2011).

Ventricular diastole starts at the end of ventricular systole and lasts for 0.5 seconds. It has 5 phases,

- Protodiastolic phase: It is the interval between the onset of diastole and the closure of the semilunar valves. In this phase, ventricles relax, however some blood still gets out of the ventricle due to the momentum of the blood. So the intraventricular pressure falls. When intraventricular pressure falls below the pressure in the aorta and the pulmonary trunk, the semilunar valves close producing the second heart sound and thereby ending this phase (Sherwood 2011);
- Isometric relaxation phase: It is the interval between the closure of the semilunar valves and the opening of the AV valves. In this phase, the ventricles relax as a closed cavity and no blood enters the ventricles. So the intraventricular pressure falls sharply. When the intraventricular pressure falls below the atrial pressure, the AV valves open and this phase ends (Sherwood 2011);
- First rapid filling phase: It begins with the opening of the AV valves. Blood rushes rapidly from the atria into the ventricles and produces the third heart sound (Sherwood 2011);
- Diastasis or slow filling phase: The amount of filling in this phase is minimum. The filling is slow as (Sherwood 2011)
 - Ventricles are already filled unto a large extent;
 - Atrial pressure falls and ventricular pressure slowly rises;
 - The AV valves remain in a fluttering condition.
- Last rapid filling phase: It coincides with the atrial systole. Due to atrial contraction, blood rushes into the ventricles in this phase and produces the fourth heart sound (Sherwood 2011).

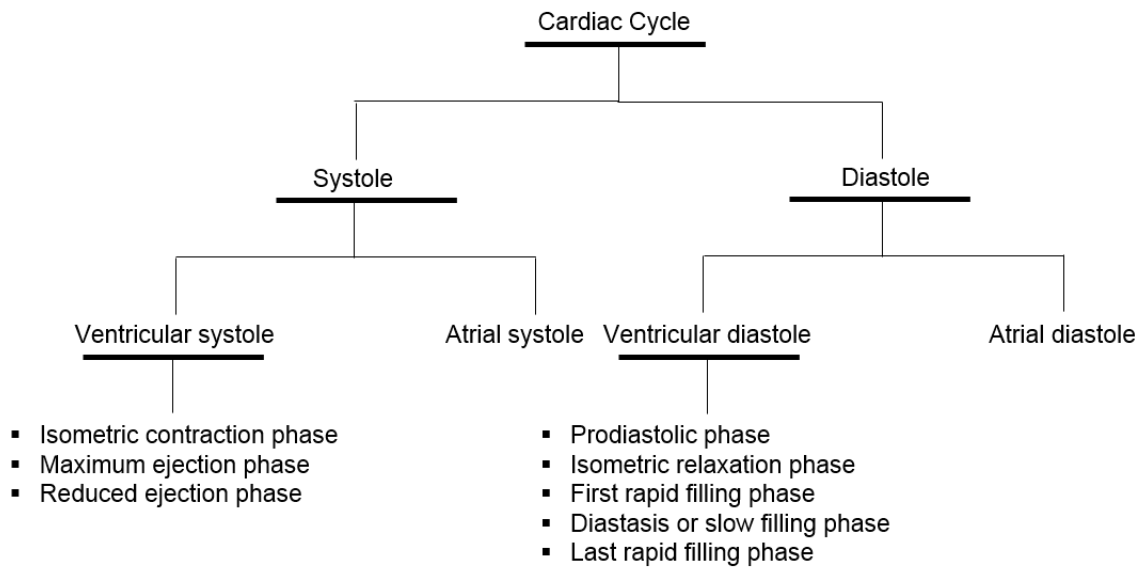


Figure 3: Flowchart showing the mechanical events in a cardiac cycle.

2.5 The electrical activity of the heart

The main function of the myocardial cells is to contract. The heart has four key properties that allow it to conduct and generate electricity (Sherwood 2011):

- Automaticity- the ability of the myocardial cells to spontaneously generate an electrical impulse without being stimulated by other sources;
- Excitability- the ability of the myocardial cells to respond to this impulse;
- Conductivity- the ability of the cells to propagate the stimuli to the next cell and so on;
- Contractility- the cells' ability to contract when triggered by an impulse.

2.5.1 Cell membrane potential

The myocardial cells use electrical signals to function. Therefore they have an electrical potential across the cell membrane. Specialised protein channels are present in the cell membrane that allows the ions to flow between the external environment and inside of the cell. Two types of gradient, chemical and electrical, determine the direction of flow of ions. Conventionally, the external environment of the cell is considered to be at 0 mV (Hall and Guyton 2011). Therefore, comparatively, the interior of the cell is negatively charged with respect to the external environment. The difference in charge between the inside of a cell

and its environment is known as the membrane potential. The difference in inside of a cell and environment is maintained by various types of ion channels or pumps, such as the Na⁺/K⁺ that pumps three Na⁺ out of the cell and two K⁺ ions into the cell. Although all cells (such as muscle cells) have a membrane potential, neurons have the unique ability to actively change their membrane potential (Hall and Guyton 2011, Klabunde 2011). The membrane potential is established due to a difference in the concentrations of ions in the cytosol of the cell, and the external environment. K⁺ is the most concentrated inside the cell, and Na⁺ is most concentrated outside the cell (Klabunde 2011, Sherwood 2011). Cl⁻ ions are also present both in inside the cell and external environment, however the membrane potential only changes based on the change of concentration of Na⁺, K⁺ and Ca²⁺ only. This creates the chemical gradient in the cell membrane (Klabunde 2011).

When K⁺ moves out from the cell, a potential difference arises between the external and internal environment of the cell. This potential difference itself drives the K⁺ back into the cell as the concentration of positive ions is high in the external environment. An equilibrium state is then reached and the potential difference between the external and internal environment is called equilibrium potential for K⁺ (Klabunde 2011). In order to quantify the equilibrium potential, Nernst equation can be used (equation 1.1).

$$E_x = \frac{Rt}{zF} \ln \frac{[X]_1}{[X]_2} \quad (1.1)$$

Where,

R = Gas Constant (8.314 JK⁻¹ mol⁻¹)

T = Absolute Temperature (K)

Z = Charge number of the ion (+2 for Ca ions, +1 for Na ions)

F = Faraday Constant (96,500 C mol⁻¹)

[X]₁ = Concentration of ions in the external environment of the cell

[X]₂ = Concentration of ions in the internal environment of the cell

Na^+ plays an important role in changing the membrane potential of the cell. The equilibrium potential for any ion can be found using the *Nernst* equation. Therefore, at 37°C the *Nernst* potential for K^+ is -96 mV . Similarly, the *Nernst* potential for Na^+ and Ca^{2+} are $+52\text{ mV}$ and $+134\text{ mV}$ respectively. Membrane potential is very important and is the basis for action potentials (Hall and Guyton 2011, Klabunde 2011).

2.5.2 Maintenance of ionic gradient

The cell membrane is selectively permeable, that is, it allows only certain types of molecules to pass into and out of the cell. The concentrations of some ions outside the cell are different from those in the cytosol of the cell (Klabunde 2011). The resultant charge or the overall potential of a cell should be neutral. Therefore, the number of positive and negative ions should be balanced between the internal and external environment of the cell. Membrane potential is highly dependent on the ionic concentration across the membrane (Klabunde 2011).

The maintenance of ionic gradient across the membrane is an example of active transport process. This process can move the ions against the concentration gradient and requires energy expenditure in the form of the breakdown of ATP (adenosine triphosphate). The Na^+/K^+ exchange pumps moves Na^+ out of the cell and K^+ into the cell. The carrier protein for the Na^+/K^+ exchange is embedded in the cell membrane. Three Na^+ and an ATP molecule combine with the carrier protein on the inside of the cell membrane. The ATP is broken down into ADP (adenosine diphosphate) and phosphate. Simultaneously the carrier protein changes shape and Na^+ ion are transported across the membrane and released on the outside. In its new configuration, the carrier protein can now bind K^+ in the outside of the cell (Hall and Guyton 2011). Two K^+ are attached to the carrier protein and phosphate attached to the carrier protein is released. The carrier protein changes its shape again reverting into its original configuration and delivering the K^+ across the membrane to the inside of the cell (Hall and Guyton 2011, Klabunde 2011).

In the case of Ca^{2+} , its concentration is higher in the external environment than the internal environment. During action potential, there is an influx of Ca^{2+} into the cell. There is also a slight leakage of Ca^{2+} when the cell is in resting potential (Klabunde 2011). Accumulation of higher concentration of Ca^{2+} may lead to cell dysfunction. Hence, there are two methods that enable the removal of Ca^{2+} ions from inside the cell and therefore also maintain an equilibrium of the Ca^{2+} . The two methods are (Hall and Guyton 2011):

- ATP dependant Ca^{2+} pump: that uses energy to transport Ca^{2+} out of cell;
- Sodium calcium exchanger.

2.5.3 Action potential of a cardiac cell

The coordinated contractions of the heart result from electrical changes that take place in the cardiac myocytes. Cardiac myocytes can contract as a result of stimulus. This stimulus can generate from: a neuron, nearby cardiac muscle cell or due to its auto rhythmicity property. This allows the system to generate action potentials that spread throughout the heart, triggering contractions in the contractile cells. An action potential is a short lasting electrical event on the plasma membrane of the cell. An action potential can be divided in up to five different phases (Hall and Guyton 2011):

- Phase 0: Depolarisation, due to influx of Na^+ by Na^+ channels;
- Phase 1: Early repolarisation, due to closure of Na^+ channels;
- Phase 2: Plateau, due to Ca^{2+} influx through slower but prolonged of voltage-gated channels;
- Phase 3: Late rapid repolarisation, due to closure of Ca^{2+} channels and K^+ efflux through various types of K^+ channels;
- Phase 4: Resting membrane potential.

The plateau phase greatly prolongs the period of depolarization and causes the contraction of the heart muscle to last for this same relatively long period. Hence, as a

result of the prolonged period of contraction of heart muscles, heart can pump all its blood (Hall and Guyton 2011).

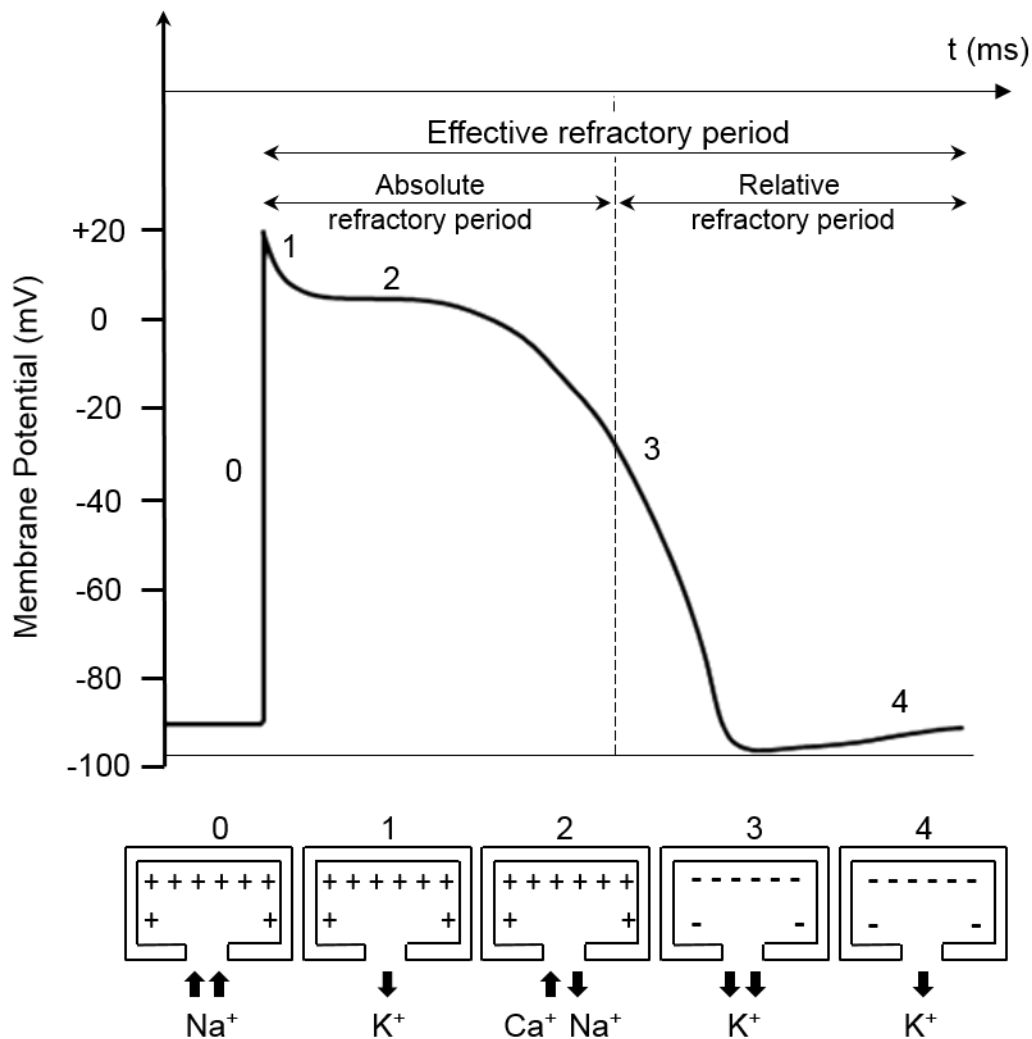


Figure 4: Action potential of the cardiac (ventricular) muscle cells.

2.5.4 Measuring the cardiac electric activity

The very first test clinicians perform on a patient is an ECG to examine the heart's electrical activity and rhythm. For an ECG small electrodes are placed in specific places on the arms, chest and legs of the patient. When the heart beats, the electrodes pick up voltage signals and the ECG is the record of these voltages. The differences in electrical activity (by looking at ECG's morphology) are clearly distinguishable in a healthy heart and in altered heart structure. The morphology of the ECG wave comprises of the P wave, QRS complex and T wave. The regions (atria, AV node, bundle of HIS, Bachman's bundle, Purkinjie fibres,

ventricles) through which the electric impulses travel at each stage of the action potential and the P-QRS-T wave of the ECG are shown in Figure 5.

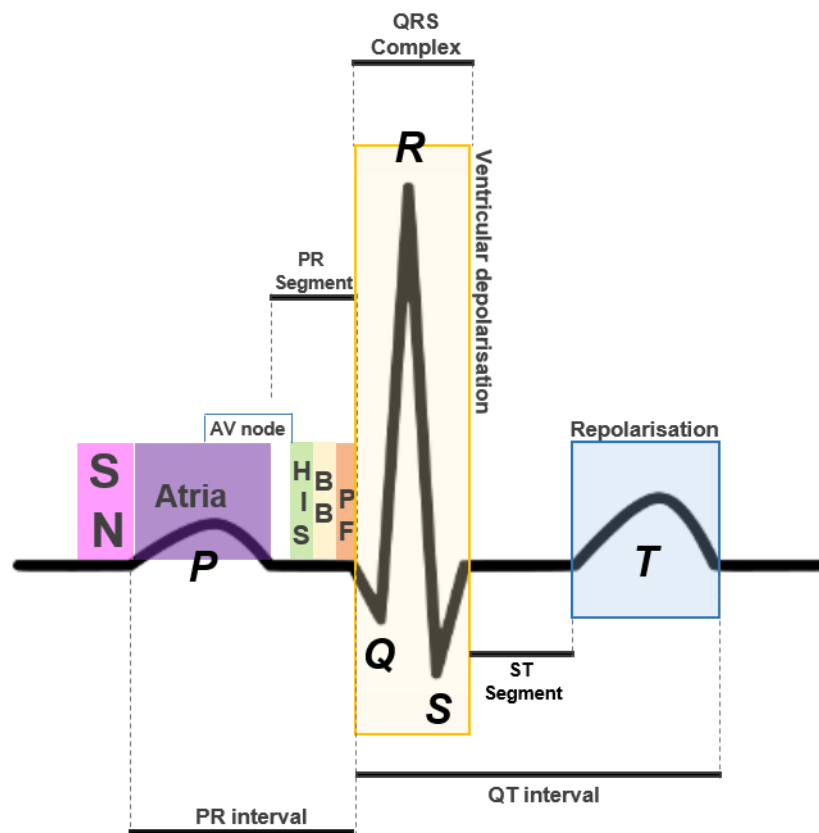


Figure 5: A depiction of an action potential of the cardiac (ventricular) muscle cells illustrating the atrial and ventricular depolarisations (P and QRS interval), followed by the ventricular repolarization (T wave) as well as highlighting the region through which the impulse is travelling. (SN: sinus node, AV: atrioventricular, BB: Bachman's bundle, PF: Purkinje Fibre).

2.6 Arrhythmias caused by abnormal action potential generation

An arrhythmia is a disturbance in the electrical activity of the heart. In some cases, the SA node could be slowed or the action potentials could be absent. Often it could be due to receiving less or more sympathetic or parasympathetic nervous system impulses as a result of which the number of action potentials generated vary accordingly and the heart gets out of rhythm. The arrhythmia can also arise due to the damage of the SA node which slows down the action potentials or even, in severe cases, stops acting as the pacemaker of the heart.

Blockage of the conduction from SA node could also lead to arrhythmia (Klabunde 2011). The most common blockage is the AV node region and this could be caused by ischemia or fibrosis from myocardial infarction, myocarditis from viral infection or other factors that damages the tissues of the AV node. The pathway of the action potentials can also be disrupted, for example due to scar tissues, as a result of which the action potentials travel around it and often creates a circuit as it travels completely in a circular manner in order to depolarize the rest of the tissues (Klabunde 2011). By the time the circuit ends, the tissues start repolarizing again and the circuit continues. People get more prone in developing arrhythmia with age as scar tissues form and damages myocardium over time. Other pathological issues such as anxiety, fever, pregnancy, anaemia, heart failure, drugs, etc. affects both the anatomy and physiology of the heart as well.

2.7 Atrial fibrillation

2.7.1 What is atrial fibrillation?

AF is a heart condition that causes the heart to race and beat in an irregular rhythm (Fuster *et al.* 2006). It is the most common type of arrhythmia (Cottrell 2012). In AF the electrical impulses do not originate in the SA node but from all over the atria. These abnormal electrical signals become rapid and disorganised radiating through the atrial walls and therefore the atria are stimulated very fast, at a rate of 300-600 beats per minute (Nattel 2002, Cottrell 2012) and quiver in an uncoordinated manner. Usually the ratio of atrial activity (P-wave) to the ventricular activity (QRS wave) of a normal heart in sinus rhythm is 1:1 whereas in AF, the ratio of P: QRS wave is irregular. Therefore, AF is characterised by disorganised atrial deflections and an irregular AV conduction sequence, resulting in a grossly irregular pattern of the QRS complex. The distances between R-waves vary beat to beat, with no discernible pattern and there is no fixed relationship between episodes of ventricular depolarisation (Camm *et al.* 2010). Furthermore, there are no identifiable P-waves (Bellet 1963).

Due to this irregular pattern, the atria do not coordinate with the ventricles and the heart gets out of rhythm. Since in AF the atria do not contract regularly, blood does not empty efficiently into the ventricles and might pool in the atria especially in the atrial appendages. This pooling of blood causes clot formation, and the dislodged clots can travel in the bloodstream eventually reaching the brain. The clot can potentially obstruct narrow blood vessels, often the middle cerebral artery, and prevent the normal flow of blood. The reduced supply of blood and oxygen to a particular part of the brain can result in tissue death leading to ischaemic stroke (Miller *et al.* 1993, Fuster *et al.* 2001, Hart and Halperin 2001, Kimura *et al.* 2005).

2.7.2 Epidemiology of AF in UK

AF is the commonest heart disease and influences around 8.8 million adults in the European Union (Krijthe *et al.* 2013) and up to 800,000 people in the UK (NHS 2013). It accounts for approximately one-third of the hospitalizations for cardiac rhythm disturbances and in UK, consuming up to 1% of the National Health Service budget in the UK (approximately 2500 per patient annually (Chugh *et al.* 2014)). For each patient the total clinical cost can be broken down into hospital expense (52%), drugs (23%), follow up and further examination (17%) and miscellaneous (8%) (Fuster *et al.* 2006).

2.7.2.1 Projected prevalence of AF through 2060

AF is a pandemic type of disease where incidents have been increasing over decades and is expected to double from 2010 to 2060 (Krijthe *et al.* 2013) in the European Union. The number of AF patients is expected to rise due to patients developing congestive heart failure, which is a risk factor for AF (Flaker *et al.* 1992) as well as due to increase in life expectancy. As the prevalence of AF increases with age, men are more prone to AF than women at any age group (Flaker *et al.* 1992). Along with AF prevalence, the proportion of strokes attributable to AF also increases (Kimura *et al.* 2005) with age by up to 5 times (Camm *et al.*

2010). From Framingham study (Wolf *et al.* 1991) it is seen that 20% of strokes are attributable to AF, so this is a major public health threat.

2.7.3 Risk factors for AF

There are many risk factors that indicate the high incidents of AF. Such possible risk factors include increasing age, family history, smoking, hypertension (high blood pressure) and obesity. Also, if the patient has other conditions such as heart failure, diabetes and coronary artery disease (atherosclerosis) then the patient has a higher risk of developing AF.

2.7.4 Related arrhythmias

AF arises secondary to many different disease states, both intrinsic and extrinsic to the heart. AF may occur alone or along with different arrhythmias including atrial flutter (AFL) and atrial tachycardia (Jais *et al.* 1997, Wyse and Gersh 2004). AFL arises by a very specific mechanism. In this arrhythmia a loop of depolarizing activity circulates constantly within the wall of the diseased RA discharging depolarizing current into the LA in a re-entrant loop which rotates discharging into the LA at approximately 300 discharges per minute. If the ventricular electrical activity for this moment from the ECG is viewed, the discharge of the depolarizing current from the re-entrant loop produces large negative deflections in the electrograms which are known as the flutter waves (f-waves) creating a 'saw-tooth'-patterned characteristic of AFL. AFL may degenerate into AF and AF may improve to AFL. Identification of elements of this underlying pattern is the key for diagnosis of this arrhythmia and distinguishing it from AF (Fuster *et al.* 2006). Whereas in case of atrial tachycardia, a condition when the atria is beating abnormally fast, a recent study by Youshida *et al.* (Yoshida *et al.* 2009) suggested that the presence of atrial tachycardia during ablation period could be the drivers of AF.

2.7.5 Classification of AF

When patients are first diagnosed, a period of AF is experienced which can be momentary or even last for days. AF gets more critical with time. It is important to detect it early because the longer the heart is out of rhythm, the harder it is to return to normal rhythm. AF can be classified in three types (Camm *et al.* 2010, Cottrell 2012):

- (1) pAF - is characterised by small episodes which last less than 7 days and that can terminate spontaneously;
- (2) persAF - is characterised by episodes that last more than 7 days. It could also last less than 7 days if pharmacologic or electric cardioversion is performed;
- (3) Permanent AF- is characterised by AF persisting for more than a year. In this case the heart may not restore its normal rhythm at all.

AF occurring in the absence of structural heart disease is called lone AF. Therefore AF can be classified by its clinical relevance and temporal patterns.

2.7.6 Signs and symptoms of AF

There are many signs and symptoms of AF. Patients usually describe uneven or racing heartbeat. Due to such irregular pulses of the heart the patients usually feel shortness of breath, light headedness, dizziness, as well as fatigue, increased sweating, chest pain and discomfort such as palpitations (Shea and Sears 2008, MacRae 2009, Cottrell 2012). In some of the cases patients usually do not realise having AF episodes. In rest, the symptoms might be mild or severe or could vary in lasting period and may even discontinue on their own (Association 1995).

2.7.7 Consequences of AF

As mentioned previously, if the patient does not have symptoms of AF, the heart could still be out of rhythm and is still at risk of other complications such as:

- Stroke risk: The clot formations in the atria could travel to the brain and cause stroke. A person in AF is 5 times more likely to have a stroke than a person who does not have AF;
- Remodelling: If AF is left untreated, it can change the size and shape of the heart by a process called remodelling. This is a permanent change in the heart that can occur in a very short time. Since in AF the heart beats more often, the cardiac tissues can be damaged. The atria increases in size and its wall thickens. (Kabra and Jagmeet, 2010);
- Others: AF patients may feel weak and exhausted as the heart is not pumping properly. In some cases the condition can keep the person from enjoying exercise and everyday activities (Shea and Sears, 2008).

2.7.8 AF management and treatment

There is a comprehensive approach in treating the risks of AF. AF management prioritises three treatment goals: rate control, stroke prevention and maintenance of the sinus rhythm.

There are several ways AF can be treated:

- For managing rate control of AF, the clinicians prescribe medications (such a beta blockers or calcium channel blockers) to slow down the rate at which the heart beats (Markides and Schilling 2003). Rate control medications reduces the heart rate and do not concentrate on the irregular rhythm or pattern of AF;
- Clinicians prescribe specific anti-arrhythmic medications targeting the rhythm of the heart in AF. Rhythm treatment regulates the heart rhythm but has very small or no effect on the rate the heart beats. Combination of rate and rhythm control medications may be recommended to slow the heart rate down and when rhythm control is added the goal is to retain heartbeat at normal rhythm. (Heist *et al.* 2011);
- If medications are not effective, the clinicians may perform 'cardioversion' in which electric current is used to restore a normal heart rhythm. (Waktare 2002);

- Radiofrequency catheter ablation is a procedure that stops the heart from generating the 'faulty' electrical signals that cause the chaotic heartbeats of AF;
- Surgical ablation is a surgical procedure to destroy the cardiac cells that causes abnormal heart rhythm. It may be used when other treatments have not worked. The surgeon treats the surface of the heart directly rather than relying on catheters and X-rays to reach the heart. Such an example is Cox-Maze procedure. (Damiano and Bailey 2007);
- For some patients atrial pacemakers may be implanted under the skin to generate electrical signals to regulate heartbeat. (Waktare 2002)

2.7.9 Mechanisms of AF

Standard therapy for AF still remains suboptimal since the precise electrical mechanisms causing AF are still not well understood (Aliot *et al.* 2008, S.M. Narayan *et al.* 2012). Recent advances from ongoing researches of human AF propose three classical mechanisms for human AF (Van Gelder and Hemels 2006) (as shown in Figure 6):

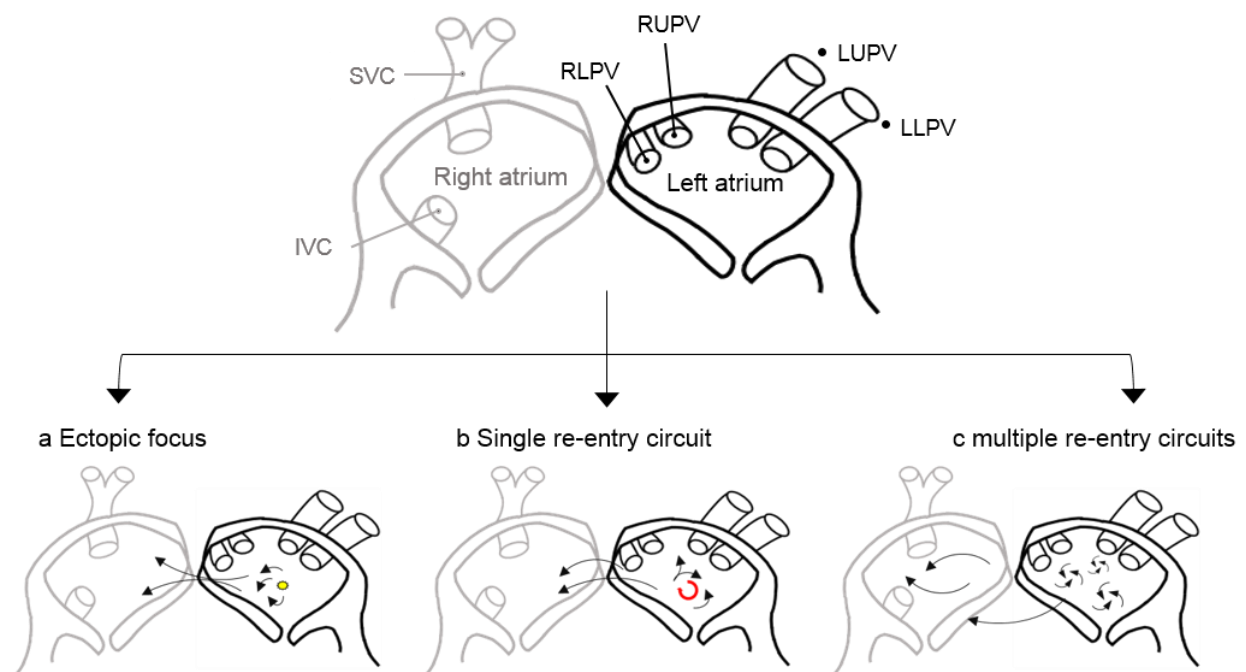


Figure 6: Mechanisms underlying atrial fibrillation. Electrical impulses that propagate throughout the cardiac tissue in a disordered way can be maintained through a variety of

mechanisms. (a) A rapidly discharging ectopic focus. (b) Single re-entry circuit. (c) Multiple functional re-entry circuits. (LUPV, left upper pulmonary vein; LLPV, left lower pulmonary vein; RUPV, right upper pulmonary vein; RLPV, Right lower pulmonary vein).

- Initiating Mechanism: It describes the source that triggers AF. Ectopic foci have been highlighted as one of the sources from which electrical signals spread as a ripple-type effect throughout the cardiac tissue which increases its automaticity along with the independent activity of the SA node (Winter and Crijns 2000). Forty years later, it has also been proven by AF modelling by Scherf and his group in 1947 (Scherf 1947). Usually, ectopic foci alone leads to tachyarrhythmia (Pak *et al.* 2006). Haïssaguerre *et al.* (1998) (Haïssaguerre *et al.* 1998) studied patients in whom they found 94% of the ectopic foci located at the PVs. Since then other researchers also shown that focal sources have been indicated to be common in the PVs that are initiating pAF (Haïssaguerre *et al.* 1998) as well in the other areas of the atria as AF develops. Mines (Mines 1913) introduced the concept of single re-entry circuits and concluded that the cardiac cells that have been depolarised earlier are reactivated due to the revisit of the wave fronts.

This thereby creates a circuit where wave fronts re-enters and thus maintains a self-sustaining AF (Allessie *et al.* 1973, Mandapati *et al.* 2000). This phenomenon of circus movement of re-entry circuits is illustrated in the schematically in Figure 7b. Mines (Mines, 1913) also stated that the product of the refractory period (RP) and conduction velocity (CV) gives the wavelength of the propagating wavelets. This explains that the shorter the RP and CV are, the shorter would be the wavelength of the wavelets. As a result this would lead to the formation of re-entry circuits and AF by reducing the size of the minimum circuit (Uetake *et al.* 2013). Since RP duration limits the frequency of action potentials, based on this theorem, many medicines

have been developed for suppressing the arrhythmia by increasing the RP of the cardiac cells.

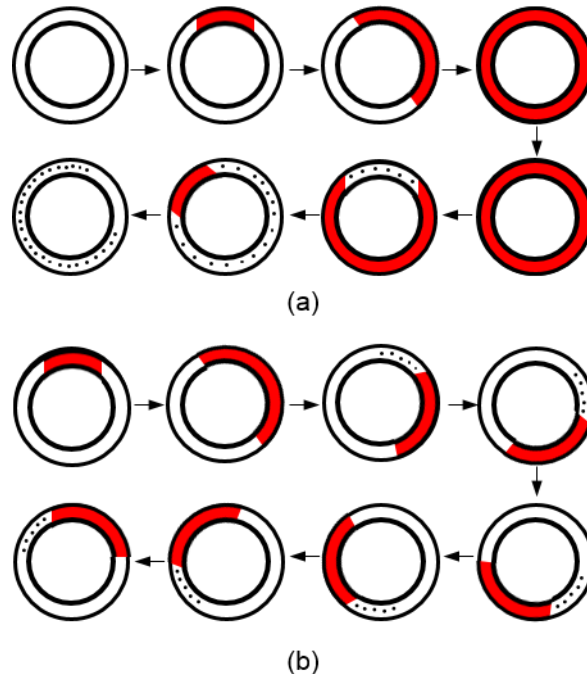


Figure 7: Illustrates the schematic diagram of excitation of cells during (a) normal rhythm and (b) arrhythmia. In (a), the recirculation cannot take place because when the stimulation completes a cycle (excitation in red), the cells at that point are still in the refractory period (dotted region) and hence cannot re-trigger. Whereas during arrhythmia (b), the cells might re-trigger with shorter refractory period. Modified from (Mines, 1913).

- Maintaining mechanism: In 1962, Moe *et al.* (Moe 1962) have shown, using a computer simulation, that localized re-entry circuits and focal impulse sources describe the complex AF behaviour poorly and that meandering waves exists which might be sustaining the AF. Therefore by performing experimental work on animal models, Allesie and his group (Allesie *et al.* 1985) demonstrated the presence of multiple re-entry circuits existing which causes continuous activation of the cardiac

tissues due to the random propagation of the several wavelets in the atria. Though pAF is believed to be induced by focal ectopic sources (Haïssaguerre *et al.* 1998, Aliot *et al.* 2008), the multiple re-entry circuits are believed to be responsible for persAF (Aliot *et al.* 2008).

- Other Mechanisms: Schuessler *et al.* (1992) (Schuessler *et al.* 1992), using canine RAs have shown that with increase in concentrations of acetylcholine, the behaviour described by various re-entrant circuits changed over to a particular high frequency re-entrant circuit that remained fixed in position and brought about fibrillatory conduction. Subsequent advances in the understanding of useful re-entrant rhythms have prompted the idea of "rotors", defined as excitable spiral waves propagating around an unexcited core (Jalife *et al.* 2002). Narayan and Krummen (Narayan and Krummen 2012) defined rotors as isochrones around a focal point where wavelets radiate outwards that help sustaining AF. These rotors are self-sustained, are understood to be either stationary or if not, and they may meander around preferential anatomical heterogeneities in the tissue (Jalife *et al.* 1998). Narayan and colleagues (Narayan *et al.* 2012) also recently demonstrated in a trial known as CONFIRM (Conventional ablation with or without focal impulse and rotor modulation) that AF is maintained by a small number of such stable localised rotors and the results stated that ablating such rotors will terminate AF.

Therefore, the combination of these mechanisms leads to various forms of AF and hence the complexity of finding the correct treatment for curing AF.

Chapter 3

Mapping and signal processing tools to analyse cardiac signals

Electrophysiological testing and radiofrequency ablation have evolved as curative measures for a variety of rhythm disturbances (Saxon *et al.* 1996, Earley *et al.* 2006). For the prevention of AF, an effective drug treatment is yet not available. Catheter ablation has been widely accepted as a strategy to treat AF (Kirchhof and Eckardt 2010). In addition, recent studies showed that the use of catheter ablation to maintain the sinus rhythm was more efficient than the use of antiarrhythmic drugs (Kirchhof and Eckardt 2010, McCarthy *et al.* 2010, Calkins *et al.* 2012).

The abnormal heart rhythms during AF arise from multiple different locations. Mapping the atria allows us to find the problematic areas and analyse them. The fundamentals before intervening arrhythmia treatment require understanding the arrhythmia, targeting the atrial substrate for ablation and finally ablating those critical areas (Hing 2009). In order to achieve that, the main steps include a) achieving an accurate atrial map and b) characterising the abnormal tissues. In this chapter the electro anatomical mapping system, as well as the signal processing and analytical tools used to extract features of the atrial EGMs to characterise the behaviour of the cardiac waves of AF patients are discussed.

3.1 Mapping systems

Electro anatomical mapping systems allow the acquisition of a high resolution 3D map of the chambers of the heart. The 3D maps of the heart are created when the physician carefully guides a catheter through the blood vessels until it is inside the heart's cavity. It uses non-fluoroscopic methods for endocardial mapping to generate a 3D anatomical map of the heart's chambers (Rolf *et al.* 2014a, Rolf *et al.* 2014b). The image is colour coded to show different regions of the heart and other electrical activity (Sra and Akhtar 2007, Hing 2009,

LaPage and Saul 2011, Tsuchiya 2012). The advantage of using such a system is that it allows rapid acquisition of the maps, automatic and continuous annotation of the mapped regions and most importantly, it allows simultaneous collection of electrical and anatomic data from many data points. The maps generated have a high definition and enhance the arrhythmia visibility. The mapping systems employ an optimal blend of magnetic and impedance location technologies to generate validation map such as activation or voltage maps that help to plan the ablation for successful termination of the disease. In addition to the electro anatomical mapping system, cardiac anatomy maps can also acquire either using computed tomography or magnetic resonance image. With recent advancement in technologies, such images can also be achieved real time, simultaneously with electro anatomical mapping systems (Ahmed and Reddy 2009). The advantages of using conventional mapping technique are that more comprehensive anatomy of the cavity can be achieved and also that it is more likely to accrue with accurate view of the heart's cavity as it is not dependant on the catheter or the operator (Burkhardt and Natale 2009). Using such images simultaneously along with the electro anatomic maps allows more accuracy due to the exact identification of the anatomical positions (Ahmed and Reddy 2009, Piorkowski and Hindricks 2009, Sy *et al.* 2012, Tsuchiya 2012). The advantages of using electro anatomical mapping are that it leads to reduced fluoroscopy time, radiation dose, procedure time and reduced expenses (Macle *et al.* 2003, Estner *et al.* 2006).

The technology of electro anatomic mapping can be of two types a) contact mapping (CM) and b) non-contact mapping (NCM) system. As the NCM system is the used mapping system used in this study, it will be the focus of the following discussion.

Contact mapping system

The two most common types of CM technique are point-by-point mapping and using a contact basket catheter in order to record the endocardial electrical activity during the arrhythmia. In point-by-point mapping systems, voltage maps are achieved by collecting sequential data over many cardiac cycles by the catheters that are in contact with the intracardiac chamber as well as the endocardial surface. In the latter technique, the catheter is also in contact with the endocardial surface which allows collection of up to 32 simultaneous atrial electrograms.

The two most common CM systems used for electrophysiological study are the Ensite NavX® system (St Jude Medical, St. Paul, MN, USA) and the CARTO® system (Biosense Webster, Baldwin Park, CA, USA) (Scherr *et al.* 2007, Aizer *et al.* 2008).

3.1.1 Non-contact mapping system

The noncontact mapping system used in this thesis utilizes a MEA catheter (Ensite, Endocardial Solutions Inc., St. Paul, MN, USA) to simultaneously record multiple areas of cardiac chambers. The MEA is a high resolution mapping catheter that has a balloon with 8 splines with a 64 electrodes design that facilitates rapid collection of intracardiac signals (Bhakta and Miller 2008). The basket design and bidirectional steer ability allows manoeuvrability throughout the heart chambers. It is a 7.5 mL cylindrical balloon type array in which the 64 electrodes are located at equidistant from each other. It has the ability to collect electrical activity of the cardiac surface simultaneously as well as to interpolate the electrical activity of neighbouring cardiac cells (Gojraty *et al.* 2009). For this study, up to 2048 points (a matrix of 32 × 64 spatial points) along the geometric coordinates (x, y, z) of the inner wall of the atrium have been exported (Friedman 2002). This is of a great advantage since electrical potentials of the cardiac surface can be collected without the presence of the physical contact of the electrodes (Friedman 2002) unlike CM. Such recordings are also known as VEGM. Therefore NCM allows continuous monitoring of all the electrograms from the endocardial surface of the atrium simultaneously and thereby helps

the clinicians to develop an efficient strategy before RF ablation is performed. Advantages of using the MEA catheter over CM are that: a) it does not require remapping of the atrium after ablation (Andrikopoulos *et al.* 2009), b) the whole intracardiac chamber can be mapped, unlike CM where only the region of interest could be mapped, c) it is suitable for non-sustained, polymorphic or hemodynamically unstable arrhythmias (Tsuchiya 2012), d) it is faster compared to using single catheter, e) it is not dependant on the contact or pressure of the catheter (Sy *et al.*, 2012) and hence ability to collect accurate signals and f) does not require a positional reference catheter in order to align the geometry map of the chambers. Some limitations of the MEA are that it is expensive, that it occupies a good amount of space in the cardiac chamber due to its size (18mm x 40mm) and is restricted to only movement in two axes. In 1998-9 the validation of NCM was carried out by Schilling *et al.* (Schilling *et al.* 1999) and Kadish *et al.* (Kadish *et al.* 1999) who concluded that the accuracy of VEGMs is high and that it produces high-resolution potential maps for regions within 40mm from centre of the balloon array.

3.1.1.1 Virtual unipolar electrograms

A unipolar catheter records the electrical activity of the cardiac cells surrounding the electrode and unipolar electrograms are obtained by the potential difference between this single electrode and the reference electrode which is at a distant position (intravascular but outside the heart). It contains both local and remote information and provides information about the directionality of the wave fronts (R wave- coming towards the electrode; QS- emanating away from electrode). Hence, it can be understood that it contains the information of the ventricular influence as represented by the QRS complex in the electrograms. Therefore, unipolar signals provide localization of abnormal sites for ablation and a characteristic morphology at specific regions inside the heart. However, low-amplitude local signals might get concealed (Eckardt and Breithardt 2009) as a result of which it is not so helpful in cases where low signal amplitude is necessary, for example, scar-based arrhythmias.

3.2 Spectral analysis

Determining the frequency content of a waveform is termed spectral analysis, in which a waveform is decomposed into its frequency components (Semmlow 2004). Spectral analysis has been widely used to study the physiological cardiovascular system behaviour in both normal and arrhythmic intracardiac signals. This analysis is advantageous as it is able to detect the periodicities in the data.

3.2.1 Spectral analysis and arrhythmia

Studies have shown that the time duration of the wave front during fibrillation correlated with the DF of the intracardiac electrograms (Skanes *et al.* 1998). DF mapping was used to identify the excitation frequency distribution during AF (Berenfeld *et al.* 2000). This study concluded that this technique provides accurate sites of the activity, gives stable demonstration for AF maintenance and that different parts of the atria have different frequency characteristics when studied in an isolated sheep heart. In a study by Jalife *et al.* (Jalife *et al.* 2002) they concluded that atrial regions harbouring high DF may represent sites with fast periodic activation, driven by either ectopic activity or re-entry circuits. Husser *et al.* (Husser *et al.* 2004) reviewed a study about the usefulness of spectral analysis in AF and confirmed that it is helpful for guiding AF therapy. Therefore, frequency domain representation of a waveform has been extensively studied on model as well as real human and animal data to provide more useful information.

Many researches in AF employing DF study concluded that AF has significant periodic elements with different degrees of regularity and that certain areas may show higher activation frequencies. This might indicate the drivers of AF and could be the potential targets during ablation (Skanes *et al.* 1998, Mansour *et al.* 2001, Lazar *et al.* 2004, Pachon *et al.* 2004, Sahadevan *et al.* 2004, Sanders *et al.* 2005, Huang *et al.* 2006). Ablation strategies based on targeting DF of the intracardiac signals resulted in successful termination of AF (Sanders *et al.* 2005). Other studies also suggested DF analysis to estimate the atrial activation rates (Ng and Goldberger 2007). It is also experimentally

observed by Matsou and his colleagues (Matsuo *et al.* 2012) that ablating the PVs with high DF lead to termination of pAF. Recently, Uetake (Uetake *et al.* 2013) analysed the frequency characteristics in persAF patients and examined the correlation of the DF between the intracardiac signals and surface ECGs. The study concluded that DFs from the intracardiac signals of whole LA showed good correlation with the ECGs and also that it is an important indicator of AF termination. Though it may show strong correlation between the intracardiac signals and surface ECGs, Jarman *et al.* (Jarman *et al.* 2012) stated that the DF generated in the left atrium is not spatiotemporally stable when analysed using NCM. The ability of DF analysis to show the true atrial rate is highly dependent on how the intracardiac signals are processed. In spectral analysis the frequency of the VEGMs are approximated by sinusoidal function with a frequency equal to the activation rate. The VEGMs may be incorporated with undesired frequencies. These electrograms need to be filtered in order to remove the noise and improve the signal to noise ratio. The following section discusses about the signal processing techniques and the technique for estimation of the DF of the VEGMs.

3.3 Signal processing

3.3.1 Digital filters

The VEGMs exported from the intracardiac chamber of the persAF patients might be contaminated by the interference, noise, or other signals, including voltages associated to ventricular activation. Digital filtering can be used in order to eliminate or reduce some of these artefacts. Mathematical software, such as MATLAB® (The Mathworks Inc., MA, USA, version 2015a) has been used for the whole processing of getting rid of the unwanted signals. There are many filter configurations and designs that also affect the way the signal is filtered (more discussed on chapter 5). For this study, 2048 VEGMs and surface ECG were collected with a sampling frequency of 2034.5 Hz. The signals were band-pass filtered (1-150 Hz), exported and analysed further. For each patient, 8 s of VEGMs were resampled to 512 Hz using a cubic spline interpolation method to reduce processing time. Ventricular

far-field activity was removed from the recorded VEGMs using a QRST subtraction technique described in the following section.

3.3.2 Removal of ventricular influence

The unipolar VEGMs are significantly influenced by the far-field ventricular activity as a result of which the power spectrum produced after spectral analysis will not reflect only the atrial activity of the heart (Traykov *et al.* 2012). Therefore, the 'far-field' ventricular influence needs to be removed before the unipolar VEGMs are processed further. Husser *et al.* (Husser *et al.* 2004) concluded that subtraction of the QRST complexes from an intracardiac signal allows the power spectral analysis to show larger inter-individual variability and also that this measurement correlates well with intra-atrial cycle length.

There are several techniques developed to perform the ventricular template subtraction including blind source separation methods (Rieta *et al.* 2000), principal component analysis (Langley *et al.* 2000) and spatiotemporal 'QRST cancellation' methods (Stridh and Sornmo 2001). These methods have some limitations that do not preserve the true atrial activity corresponding to the QRS-T interval (Salinet *et al.* 2013a).

In our research group, Salinet *et al.* (2013) (Salinet *et al.* 2013a) have implemented an effective method to allow subtraction of ventricular far-field influences from unipolar electrograms to allow realistic DF mapping analysis in patients with persAF. The technique, prior to the subtraction, performs the segmentation of the QRS-complex and detection of T-wave in the ECG by using Madeiro *et al.* (Madeiro *et al.* 2012) and Qinghua *et al.* (Qinghua *et al.* 2006)(Qinghua *et al.*, 2006) techniques respectively. Then the corresponding time of the QRST-complex were marked accordingly in the VEGMs. A QRST-pattern with highest cross-correlation was located from the VEGMs and is used as a template to subtract from the intracardiac signals (Salinet Jr *et al.*, 2013). This method allows to investigate atrial EGMs with reduced presence of ventricular activity and consequently

performing it prevents the signals hampering the analysis and possibly distorting results (Gojraty *et al.* 2009, Ahmad *et al.* 2011, Salinet *et al.* 2013a).

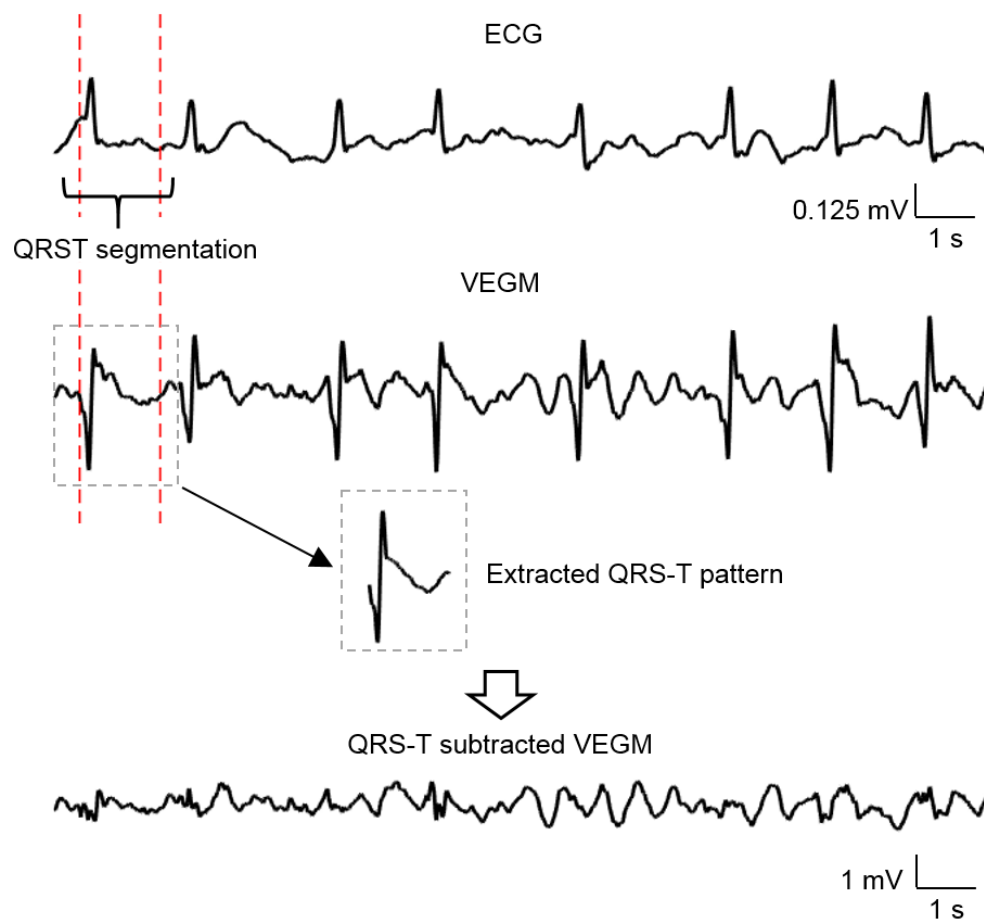


Figure 8: General block diagram illustrating QRS-T subtraction

3.3.3 Frequency domain analysis

To analyse signals in the frequency domain, a mathematical transformation called Fourier transform (FT) is applied to transform signals between time domain and frequency domain due to continuous signals can be represented as a sum of weighted sinusoid functions.

3.3.3.1 Continuous Fourier transform

FT is applied which transforms signal between time domain and frequency domain, and determines the complex sinusoids of that signal (Smith 1997). The continuous notation for

the FT considers infinite cycle duration. The continuous Fourier transform of a continuous signal, $f(t)$, can be expressed as

$$F(j\omega) = \int_{-\infty}^{\infty} f(t)e^{-j\omega t} dt \quad (3.1)$$

The absolute value of the FT of above equation is denoted as the frequency spectrum of $f(t)$. The spectrum components correspond to the energy of the particular frequency component in the signal.

3.3.3.2 Discrete Fourier transform and fast Fourier transform

The Discrete Fourier Transform (DFT) is the equivalent of the continuous Fourier transform for signals known only at N instants separated by sample times T (i.e. a finite sequence of data). Each sample can be regarded as $f[k]$ and the DFT of the signal, $f(t)$ mentioned above, can be expressed as

$$F[n] = \sum_{k=0}^{N-1} f[k] e^{-j\frac{2\pi nk}{N}} \quad (3.2)$$

$(n = 0 : N - 1)$

For this study, to analyse signals in the frequency domain another mathematical transformation called Fast Fourier Transform (FFT) is used. The DFT is a slower algorithm approach for spectral estimation as it depends principally on the number of multiplications involved, since these are the slowest operations. The FFT it is a more efficient method to obtain the DFT. For the DFT of N points, the complexity is proportional to N^2 , while for the FFT the complexity is proportional to $N \log_2(N)$ (Ingle and Proakis 2012).

There are also some factors that need to be considered during FFT such as:

- Total length of the time window: reflects the frequency resolution.
- Total number of samples in the time domain- determines the number of frequencies in the frequency domain.
- The Nyquist sampling theorem states that the sampling rate has to be at least larger than twice the maximum frequency component of the signal. (Smith 1997).

- Spectral “leakage”- for a waveform that is not periodic in time, the temporal effect of the sample window becomes visible in the Fourier transform by showing undesirable effects in the frequency spectrum domain due to abrupt discontinuities in the beginning or in the end of the segment (Harris 1978). “Windowing” amplitude modulates the input signal so that the spectral leakage is evened out and thereby, reduces the amplitude of the samples at the beginning and end of the window, altering leakage. Windowing is implemented by multiplying the input signal with a windowing function.
- Zero padding- refers to increasing the number of samples with zero elements to improve spectral estimation representation. It provides a smoother spectrum by interpolation without affecting spectral resolution. (Ingle and Proakis 2012, Traykov *et al.* 2012).

3.3.4 Dominant frequency and organisation index

DF is defined as the frequency of the signal at which the power spectrum has the maximum value. DF can summarise the behaviour of the arrhythmia over short time segments and provide further understanding about AF drivers. In the present work, DF was defined as the frequency with highest amplitude within the physiologically relevant range (4 to 10 Hz) (Salinet *et al.* 2013b). This range was defined as it considers the expected physiologically range of AF (240-600 beats/minute) (Nattel 2002).

Everett and collaborators introduced the study of organization index (OI) (Thomas H. Everett *et al.* 2001) and Rosenbaum and Cohen introduced regularity index (RI) (Rosenbaum and Cohen 1990) for measuring AF organization. The indices give a measure of how ‘dominant’ the DF is within the AF physiological relevant range. OI represents the ratio of the area under the DF peak and its harmonics to the area of all the frequency spectrum. Low OI represents high variability of frequency and, consequently, lower organization of the electrograms (Takahashi *et al.* 2006). Whereas RI represents the ratio of the area only under the DF peak to the areas of all the power of the frequency spectrum. High RI indicates high

influence of that particular frequency in the signal as it exhibits its dominance since no other peaks including the harmonics are ‘competing’ with it. The equation for OI and RI are as follows:

$$OI = \frac{\text{Area (DF peak + Harmonics)}}{\text{Area below the frequency spectrum}} \quad (3.3)$$

$$RI = \frac{\text{Area (DF peak)}}{\text{Area below the frequency spectrum}} \quad (3.4)$$

3.4 Phase analysis

In the late eighties, phase analysis was introduced to study cardiac fibrillation (Winfree 1997). In this work, phase analysis has been performed on the VEGMs of persAF patients. The phase data of the electrograms tells us about the activation of a particular region. Analysing phase data of the persAF signals over time can provide information about the activation patterns. The waveform of each signal during fibrillation can be considered as a series of sinusoids that are at the same frequency as, or multiples of, the waveform frequency.

Mathematically, phase can be expressed as the different stages within 1 cycle of a signal divided into 360° or 2π radians. Each signal can be represented on a complex plane at different stages around a unit circle known as phasor plots (Figure 9). The position of the vector in a phasor plot can be represented in angle “θ” in polar coordinates or “a + j b” in Cartesian coordinates, where, ‘j’ represents the imaginary part of the complex number.

Another signal at a constant phase difference or having a delay (θ) can be understood as another activation, therefore, this can be interpreted as an activation wave front that is travelling in the cardiac tissue.

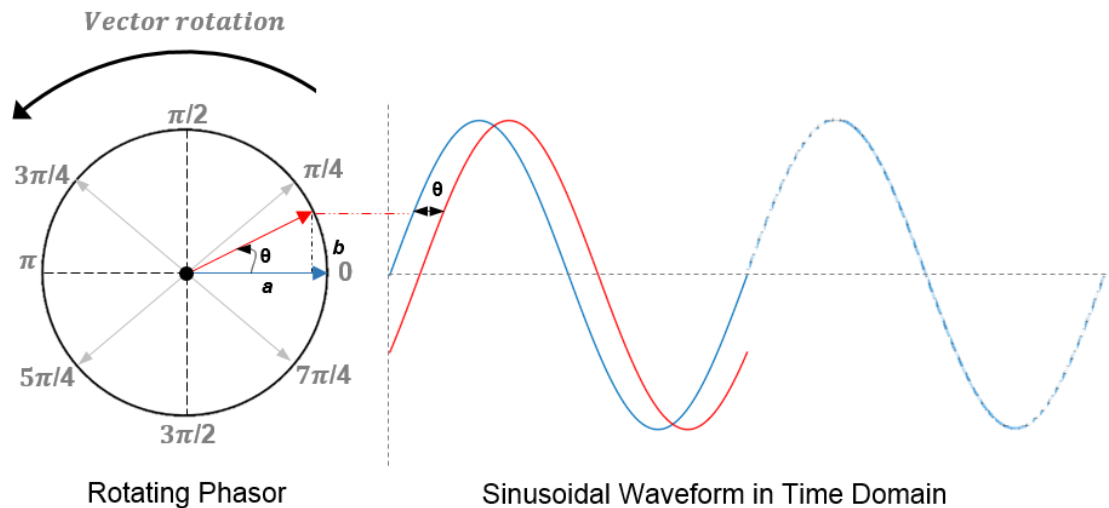


Figure 9: Phasor Diagram of a Sinusoidal Waveform (blue) and a delayed version of that waveform (red).

Therefore phase analysis allows to capture the wave dynamics which exhibits the activation-recovery cycle of the intracardiac tissues by elucidating the sequence of the activation, which is not directly available from the morphology of the signal (which is in voltage over time) (Roney *et al.* 2016).

3.4.1 Extraction of phase data

A phase space plot shows the trajectories of a dynamical system in the phase plane. The idea was developed by Ludwig Boltzmann in late 19th century. In a phase space plot, the signal is plotted against the signal with a 'θ'. Therefore the phase space plot appears as one circle-shaped trajectory with one fixed centre if the delay is constant. The instantaneous phase of each instant could be extracted by applying inverse tangent calculation of the 2 coordinates. However, if the signal is irregular and chaotic (such as AF signal), the phase plot is comprised of many circle-shaped trajectories which are dispersed yet fixed around one centre (Figure 10(b)). As a result of its complex trajectory, choosing an ideal value for 'θ' is difficult.

Another mathematical tool, the Hilbert Transform (HT) can also be used for phase analysis. It was first used in 1905 concerning analytical functions. The basic property of the HT is to

generate a phase-shifted signal by 90°. For this study, HT have been used to extract phase of the intracardiac signals of the persAF patients. It is applied to the VEGMs to produce an analytic signal in the form of (Umapathy *et al.* 2010a, Clayton and Nash 2015, Ortigosa *et al.* 2015)

$$z(t) = x(t) + jH[x(t)] \quad (3.5)$$

where H is the HT operator and is defined as,

$$H[x(t)] = \frac{1}{\pi} \int_{-\infty}^{\infty} \frac{x(\tau)}{t-\tau} d\tau \quad (3.6)$$

This complex signal enables the instantaneous phase to be extracted using the inverse tangent calculation of the imaginary and real part of the analytic signal:

$$Phase, \phi(t) = \arctan \left(\frac{Im [z(t)]}{Re [z(t)]} \right) \quad (3.7)$$

Figure 10 shows phase calculation in a single VEGM. For each sample, the calculated phase was limited between $-\pi$ and $+\pi$ and the colour scale of an activation is also illustrated. Once phase analysis was applied to all 2048 VEGMs, sequential 2D and 3D phase maps were developed.

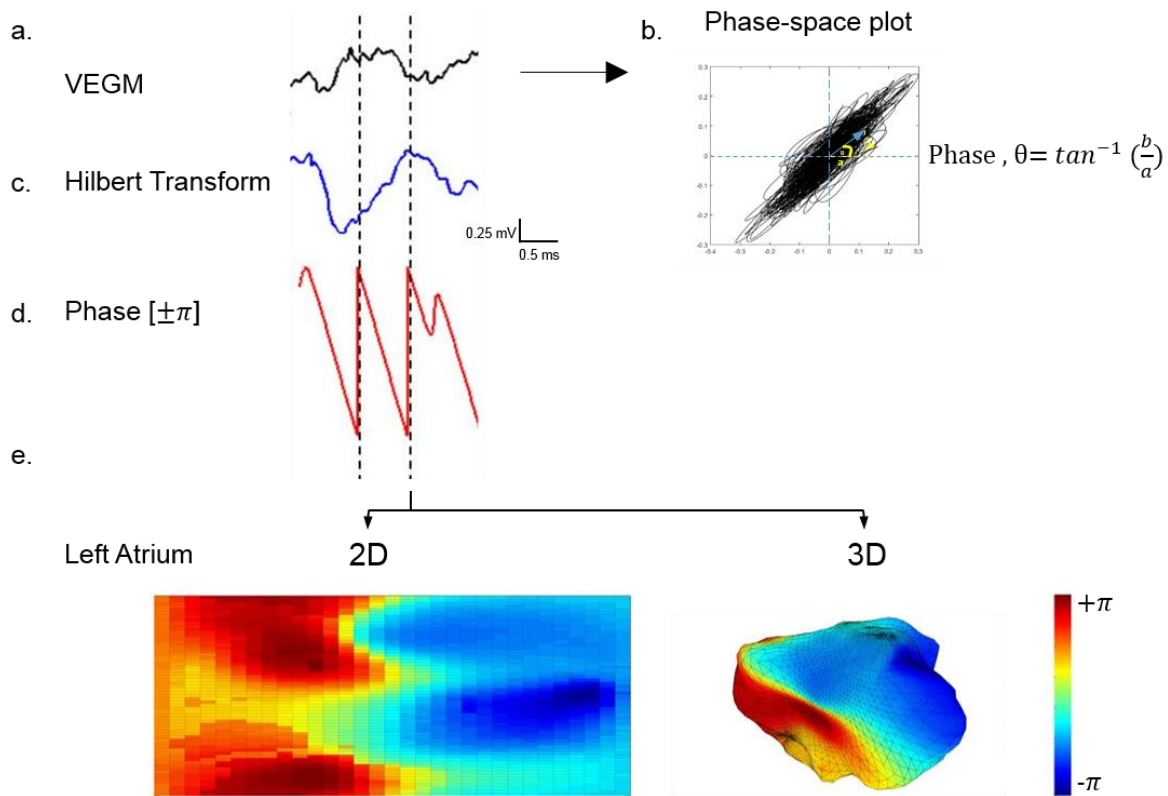


Figure 10: Illustration of extraction of phase data from unipolar virtual electrograms (VEGMs). (a) Shows a VEGM segment from a persistent AF patient. (b) Illustrates the phase computation using phase-space plots of the VEGM. (c) Hilbert transformation has been used to generate an analytic signal (phase-shifted signal by 90°) of the VEGM. (d) The instantaneous phase is extracted using the inverse tangent calculation of analytic signal. (e) A 2D phase frame (and its respective 3D plot of the LA) with a color-coded activation episode is highlighted for visualisation.

3.4.2 Phase analysis and arrhythmia

As mentioned earlier, phase analysis aids the visualisation of the progression of an action potential through a defined region of cardiac tissue. It is very useful in analysing spatiotemporal changes during AF (as the electrograms are not periodic and exhibit time-varying cycle) and allows observation of the activation patterns. Studying phase maps gives an understanding into the fibrillatory dynamics and helps clarify its mechanisms (Gray *et al.* 1998, Samie *et al.* 2001, Bray and Wikswo 2002, Umapathy *et al.* 2010b, Pandit and Jalife

2013). From phase maps, identification of the regions where the phase progresses through a complete cycle from $-\pi$ to $+\pi$ is important in fibrillation. At these points, the phase becomes indeterminate and the activation wave fronts hinge on these points and rotate around them in an organized fashion forming re-entrant circuits (Samie *et al.* 2001, Umapathy *et al.* 2010, Pandit and Jalife, 2013). These points are called phase singularity points (PSs) in the phase map. Re-entry has been understood as one of the mechanisms of AF (as discussed in chapter 2). In early 20th century, Sir Thomas Lewis (Lewis 1909, Lewis 1921) first introduced this concept. Fifty years later the leading circle theory of re-entry was suggested by Allesie and his group (Allesie *et al.* 1973) and soon another concept of 'rotors' was proposed. In 1990, Davidenko *et al.* provided the very first evidence of rotors (Davidenko *et al.* 1990). The rotor concept widely got accepted as more evidence was gathered from experimental and modelling studies (Davidenko *et al.* 1990, Gray *et al.* 1998).

Phase mapping provides in depth understanding of re-entry in AF by the identification of PSs. PSs can be formed when a wave breaks and can form the centre of the re-entry circuits. Tracking PSs in space and time can identify rotors (Umapathy *et al.* 2010b). Pak *et al.* (Pak *et al.* 2003) reported ablation of PSs can terminate ventricular arrhythmia. Recent studies by Jalife and colleagues (Jalife *et al.* 2002, Pandit and Jalife 2013, Berenfeld and Jalife 2014) also stated that a stable rotor is known to induce fibrillatory conduction, and thereby is a key for sustaining AF. Rotors are believed to passively activate the surrounding regions thereby allowing to 'control' the tissues. As a result wave fronts collide creating fibrillatory conduction and hence contributing to the appearance of global disorganization in the cardiac chamber. Narayan *et al.* (Narayan *et al.* 2012), identified rotors using near-real-time mapping in AF patients and hypothesized that human AF may be sustained by rotors whose elimination could lead to the outcome of AF ablation (Sanjiv M. Narayan *et al.* 2012, Narayan *et al.* 2013a, Narayan *et al.* 2013b).

Therefore analysing the complex spatiotemporal patterns and identifying the sites about where all phases of the depolarization/repolarization cycle exist simultaneously can be

greatly simplified by identifying the PSs. PSs can lead to the analysis of the arrhythmia and improve understanding of its electrophysiology. In this study, further investigations of PSs (chapter 5, 6 and 7) have been performed in more detail in human persAF data in order to understand the clinically important implications and to develop effective ablative strategies.

Chapter 4

Using High Dominant Frequency Density Maps to Understand Spatiotemporal Behaviour of Atrial Electrograms in Persistent Atrial Fibrillation

4.1 Introduction

AF is the most common rhythm disorder seen in clinical practice (Calkins *et al.* 2012). Catheter ablation is a well-established therapy for AF (Dagres *et al.* 2015). PVI electrically isolates the region around PVs in wide encircling lesion and destroys the tissue and causes scar tissue to form. This scar tissue blocks the extra electrical signals from the PVs so the area can no longer generate or conduct the impulses. PVI has proven to be effective in patients with pAF (Haïssaguerre *et al.* 1998), but less so in persAF (Tan *et al.* 2009) due to electromechanical remodelling and structural changes in the atrial tissue that leads to sustained AF (Dagres *et al.* 2015). Hence, an effective ablation technique for patients with persAF is subject of intense discussion (Nademanee and Oketani 2009, Narayan *et al.* 2014, Rolf *et al.* 2014b).

DF analysis has recently gained interest as a means for studying the pathophysiology of AF (Ng *et al.* 2006). Studies suggest that AF can originate from a single source (Jalife *et al.* 2002, Jalife 2003) and that this source activates at the fastest rate. To identify the region containing this source, DF mapping has been used in animals and humans. Studies have reported that DF mapping identifies localized sites of high frequency activity (Sanders *et al.* 2005, Ng *et al.* 2006) and that it offers potential advantages for the substrates mapping of AF episodes (Goldberger 2000, Sanders *et al.* 2005). Another study (Haberl *et al.* 1988) also found frequency analysis to be more specific than time-domain analysis without loss of

sensitivity in patients with arrhythmia. Due to the chaotic nature of AF (Ng and Goldberger 2007), consistency with DF findings is necessary as its spatiotemporal organization has previously been demonstrated to be unstable (Schuessler *et al.* 2006).

Therefore, in order to assess the stability of DF during persAF, this study mainly focussed on producing density maps to analyse the spatiotemporal behaviour of the HDF in the LA of patients with persAF while using NCM and to understand the post ablation effect on the unipolar virtual electrograms VEGMs using HDF density maps.

4.2 Materials and methods

4.2.1 Patients

Ten persAF patients undergoing catheter ablation for the first time were included. All antiarrhythmic drugs were stopped at least 5 half-lives before the procedure. The study protocol was approved by the Glenfield General Hospital's Ethics Committee, and all procedures were carried out after obtaining written informed consent. The patients' characteristics are detailed in Table 1 (see chapter 1).

4.2.2 Electrophysiological set-up

Prior to the electrophysiological study, patients were given heparin to reduce the risk of blood clot formation. Under fluoroscopic guidance, a quadripolar catheter and steerable decapolar catheter were placed at His position and CS, respectively via femoral access. Following trans-septal puncture, anticoagulant drugs were given and repeated doses were administered to maintain an activated clotting time between 300 – 350 seconds. Electro-anatomical mapping was performed in all patients to achieve detailed 3D LA geometry (which includes RUPV, RLPV, LUPV, LLPV, atrial roof, LAA, septum, mitral valve isthmus (MVI), lateral, anterior, floor, posterior and CS).

4.2.3 Signal analysis

For all the patients, the non-contact MEA (Ensite Velocity, St. Jude Medical, USA) recorded 2048 points of VEGMs simultaneously from the endocardial surface of the LA during AF and up to five minutes of VEGM segments were analysed offline using MATLAB (Mathworks, USA). Data were resampled to 512 Hz to reduce computational costs, and QRST subtraction was applied to remove the ventricular influence using a previously described method (Salinet *et al.* 2013a).

4.2.4 Frequency domain analysis

The mean of all data values was subtracted before windowing in order to eliminate the strong component at the lowest frequency. A Hamming window was applied to the VEGMs to minimize spectral leakage effects. FFT was applied to every 4 seconds window with 50% overlap (in order to produce a smoother animation of the DF maps to help in tracking the movement of several frequency zones in the atrium) for all the 2048 points in the LA to derive an estimate of the power spectrum and find the DF, defined as the frequency component with highest power in the frequency range between 4 - 10 Hz (physiologically relevant to fibrillatory activity in the human atrium) (Salinet *et al.* 2013a). Fivefold zero padding was applied, resulting in a frequency step of 0.05 Hz in order to increase the density of the frequency spectrum, making it appear smoother.

The RI and OI were calculated for each VEGM. RI is defined as the area under the curve of the DF peak divided by the area under the curve of the entire power spectrum, whereas OI is calculated by identifying the area underneath the DF as well as its harmonics and then dividing by the total area within the frequency spectrum (Everett *et al.* 2002, Sanders *et al.* 2005).

4.2.5 HDF density maps

HDF regions in the 3D LA geometry for each individual window were defined as any node in the mesh where the calculated DF was within 0.25 Hz of the maximum DF for that window. A colour-scaled map of HDF distribution across the LA was constructed, with the HDF from each site displayed on the 3D LA geometry.

HDF density maps were created using the counting of the occurrences of HDF for each LA node. Accordingly, the atrial areas with HDF were delimited in each frame for all 2048 VEGMs. The number of times that the HDF clouds super-imposes each other were recorded and represented onto the 3D LA geometry. The size of the HDF-dense regions varies as the HDF maps are plotted over time. Figure 11 (a) shows a methodological illustration for producing a HDF density map. Here, red and grey areas are the sites that were visited the most and the least often by the HDF clouds, respectively. Figure 11 (b) shows HDF density maps of one patient. Each map reflects the HDF dense regions when using different lengths of VEGM recordings (in total 20 maps with incremental time duration of 15 seconds).

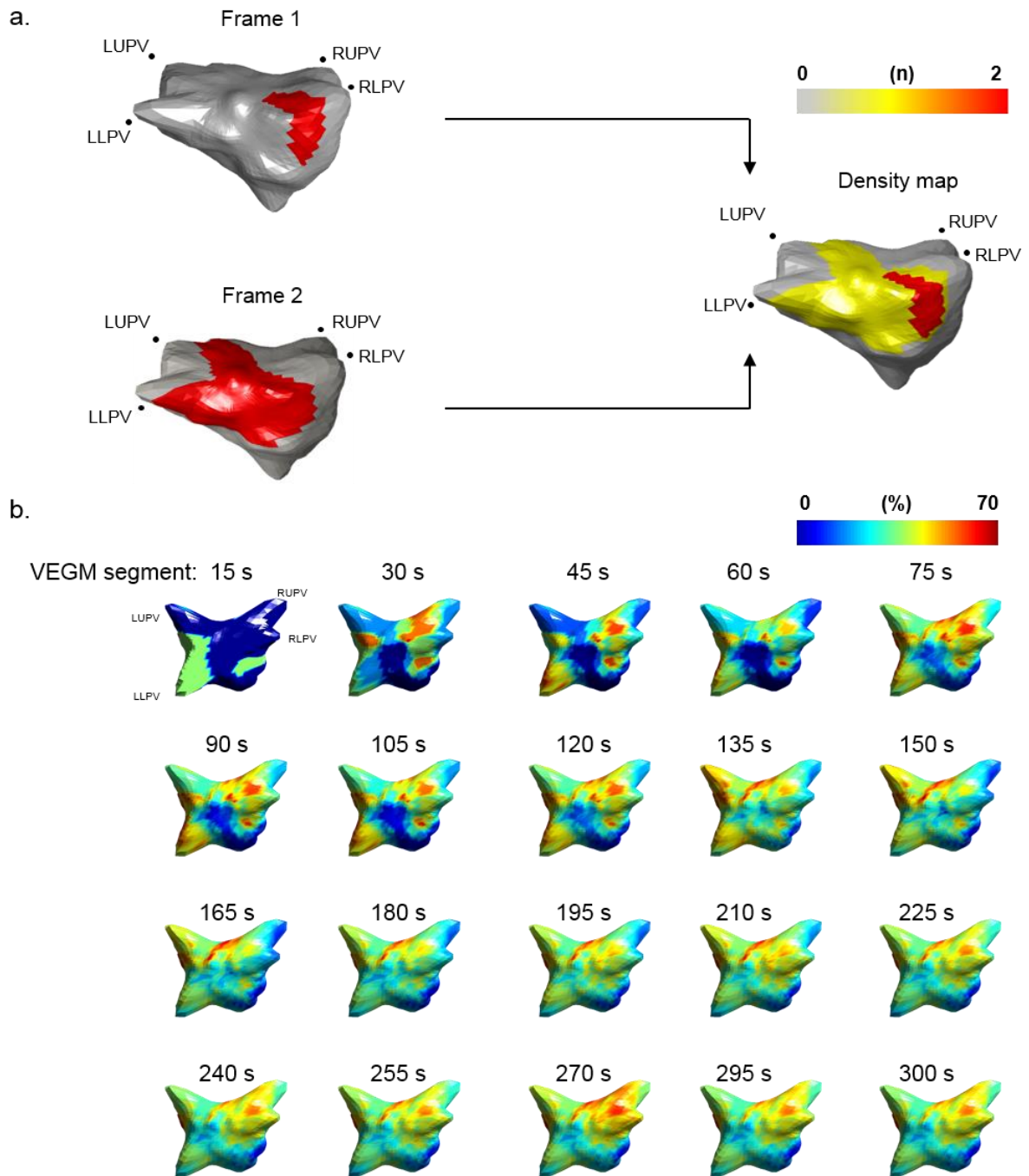


Figure 11: (a) Illustration of accumulation of HDF clouds in order to produce a density map. The region HDF visited more or less often is indicated by the colour bar. (b) HDF density maps of one patient. Each map reflects the HDF dense regions when using different lengths of VEGM recordings.

4.2.6 HDF temporal behaviour

To assess the temporal stability of the HDF clouds, the number of nodes in the LA mesh which did not host any HDF from the beginning of the mapping time was determined for every window by counting the number of nodes that did not contain HDF values in the first time window and comparing with the subsequent windows. In addition, consecutive VEGM segments were assessed to understand VEGM temporal behaviour. For each subject, VEGMs were divided into 20 segments which increased in time duration with 15 seconds to obtain segments of 15, 30, 45 s and so on, until the full duration of the segment was considered. For each segment, a HDF density map was produced, as illustrated in Figure 11 (b). A total of 200 HDF density maps of the LA were produced and every HDF density map was compared to the ultimate HDF density map (produced using the whole five minutes recording), allowing the investigation of the minimum time needed to produce a representative density map. The comparison between the HDF density maps was performed based on Pearson's correlation (CORR), structural similarity (SSIM) index (method for measuring the similarity between two images) and linear regression coefficient (r^2).

Consecutive VEGM segments of the chosen optimal time with every 50% overlap were obtained to infer about similarity of the density maps when any different EGM interval is chosen. The similarity of each map was therefore also compared to each other using all the three indices and the distribution of the similarity index was analyzed using kurtosis (shape of the distribution) and skewness (asymmetry of the distribution).

To investigate further the underlying dynamics of local atrial activation of the dense regions of the HDF, the 2048 nodes in the LA were divided into two groups according to their density, most visited regions (MVR, occurrences of the HDFs $> 80\%$) and least visited regions (LVR, occurrences of the HDFs $\leq 80\%$) and their HDF, OI and RI features were obtained.

4.2.7 Radiofrequency ablation

Radiofrequency catheter ablation guided by DF was performed on all patients. Once the primary HDF site was identified, its centre of gravity (CoG) was determined (Salinet *et al.* 2013c) and ablation started targeting the CoGs and their trajectory. A post procedure recording was collected for up to 5 minutes. The MEA was then removed and that was followed by standard PVI.

4.2.8 Statistical analysis

Nonparametric paired multiple data were analysed using the Wilcoxon matched-pairs signed rank test, while nonparametric unpaired data were analysed using the Mann–Whitney test. Linear regression and correlation coefficients were computed between different time segments of VEGMs in order to identify the minimum time segment required to reach spatiotemporal consistency of the HDF density maps. P-values less than 0.05 were considered statistically significant.

4.3 Results

4.3.1 Temporal stability of HDF regions

The number of nodes not visited by HDFs out of 2048 nodes decreased with time in an approximately exponential behaviour (Figure 12 (a)). Logarithmic curves were fitted for each patient and the average time constant (τ) of the exponential curves was (mean \pm standard deviation (SD)) 12.6 ± 8.5 seconds.

Although the gross atrial fibrillatory pattern, as represented by the HDF density maps, is reproducible with any particular time segments of VEGMs, consistency of the locations of the dense regions is important. Longer recordings can provide more accurate consistency of the density map as the activities of the drivers can be captured more with cumulative increase in the number of windows. Thus, increasingly longer recordings of VEGMs result in a convergence towards the spatially dense regions. However, for practical reasons, using

recordings that are too long is not feasible, as this leads to the patient being exposed to radiation for longer as well as resulting an increase in the risk to the patient and the cost of the procedure.

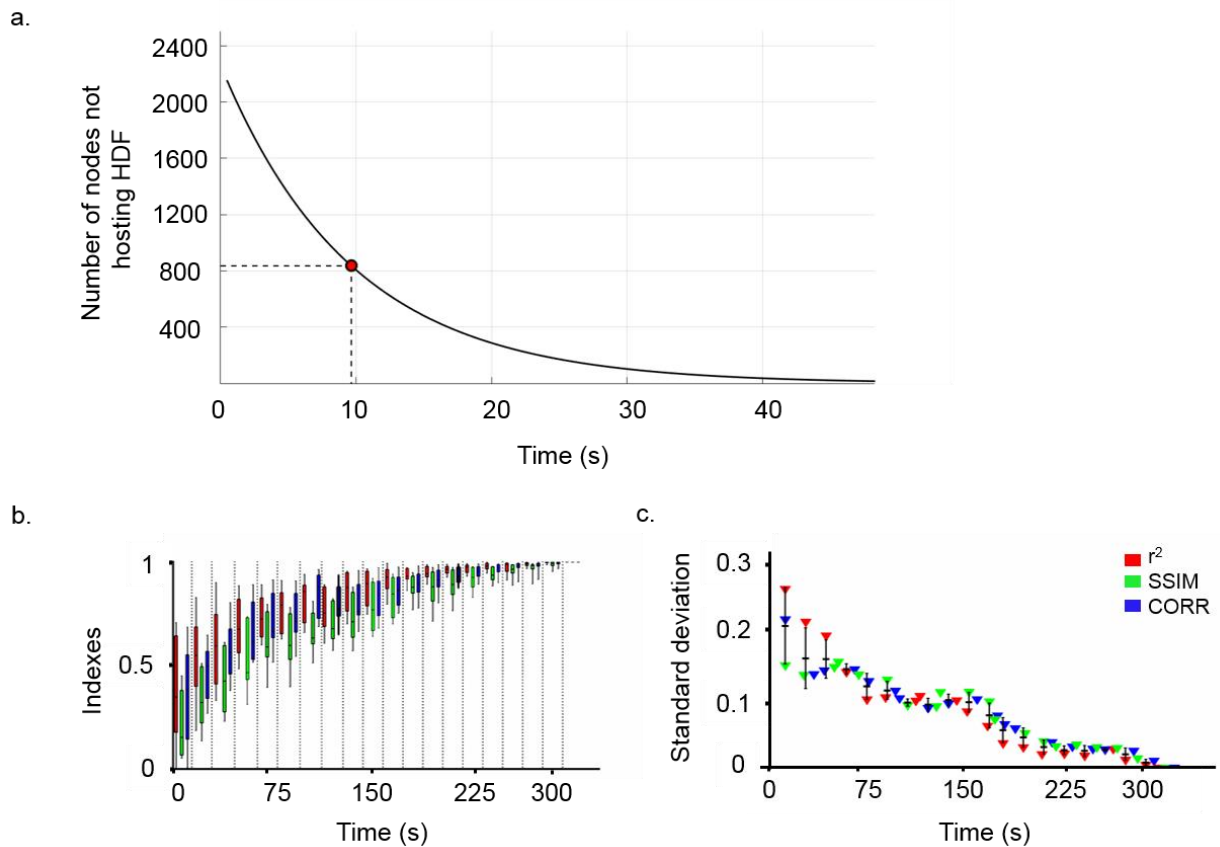
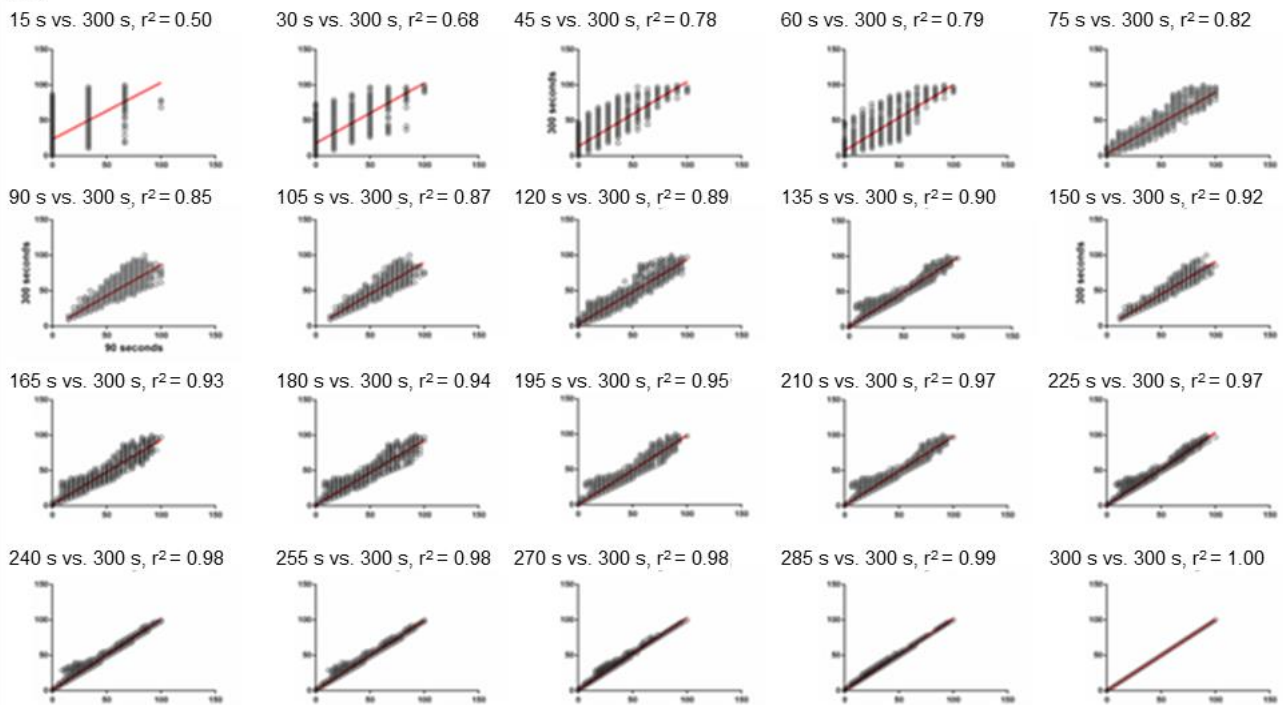


Figure 12: (a) Temporal behaviour of the HDFs of one persistent AF patient. For this case, the exponential fit has a time constant of 9.81 seconds. Results measure the stability of the behaviour of the HDF clouds. (b) Summary of indices for all patients comparing the HDF density map produced using a particular time segment with the ultimate HDF density map produced using 300 seconds. (c) SD plots of the indexes comparing the HDF density maps.

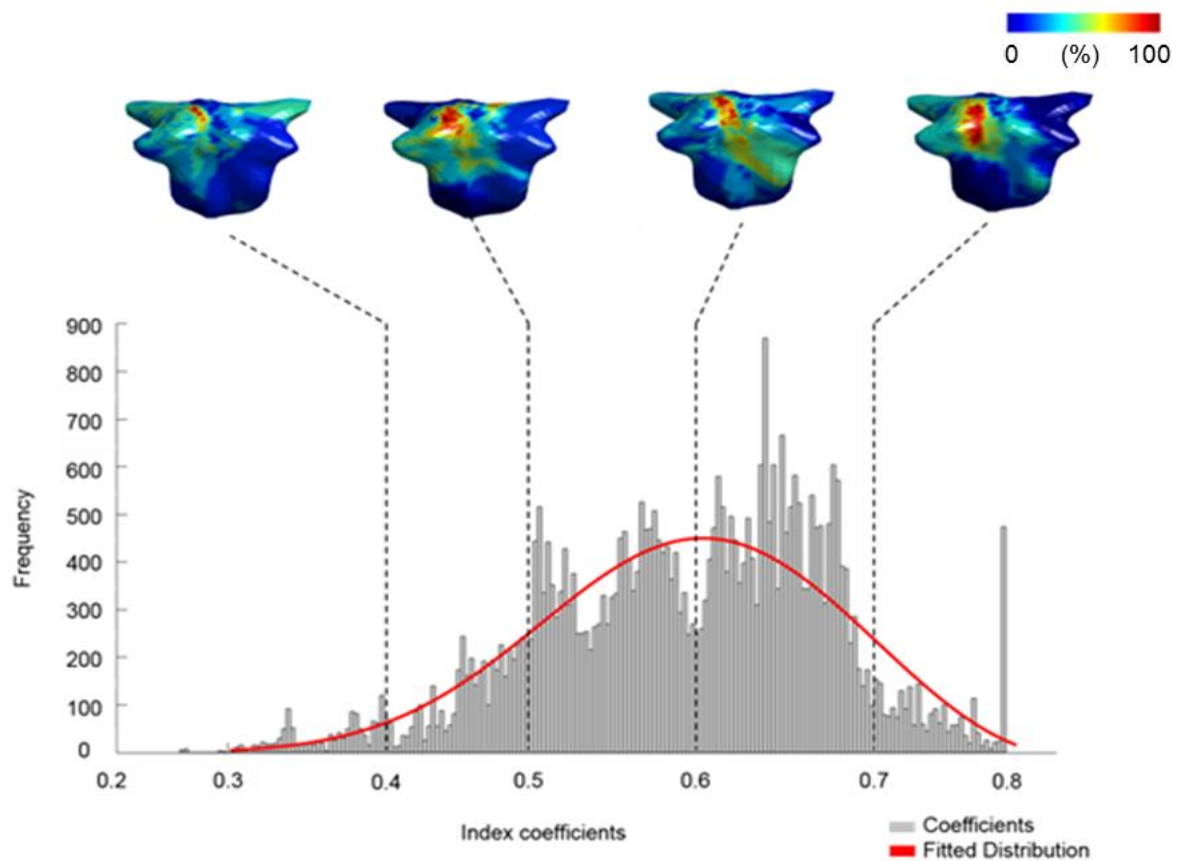
From the results, for all patients, the temporal segment of VEGMs up to 60 seconds had mean CORR, SSIM index and r^2 value less than 0.70 when compared with the 300 seconds recording. The maps obtained for 75 seconds of recording had a good mean correlation (CORR = 0.71 ± 0.12 , $r^2 = 0.73 \pm 0.09$, SSIM= 0.70 ± 0.13) (Figure 12 (b)). A trend in

decrease of the variation in data could be observed (Figure 12 (c)). Hence, from 75 seconds of VEGM recording the locations of the dense region seemed to remain consistent and therefore the density maps ought to have a predictable convergence.

a (i)



(ii)



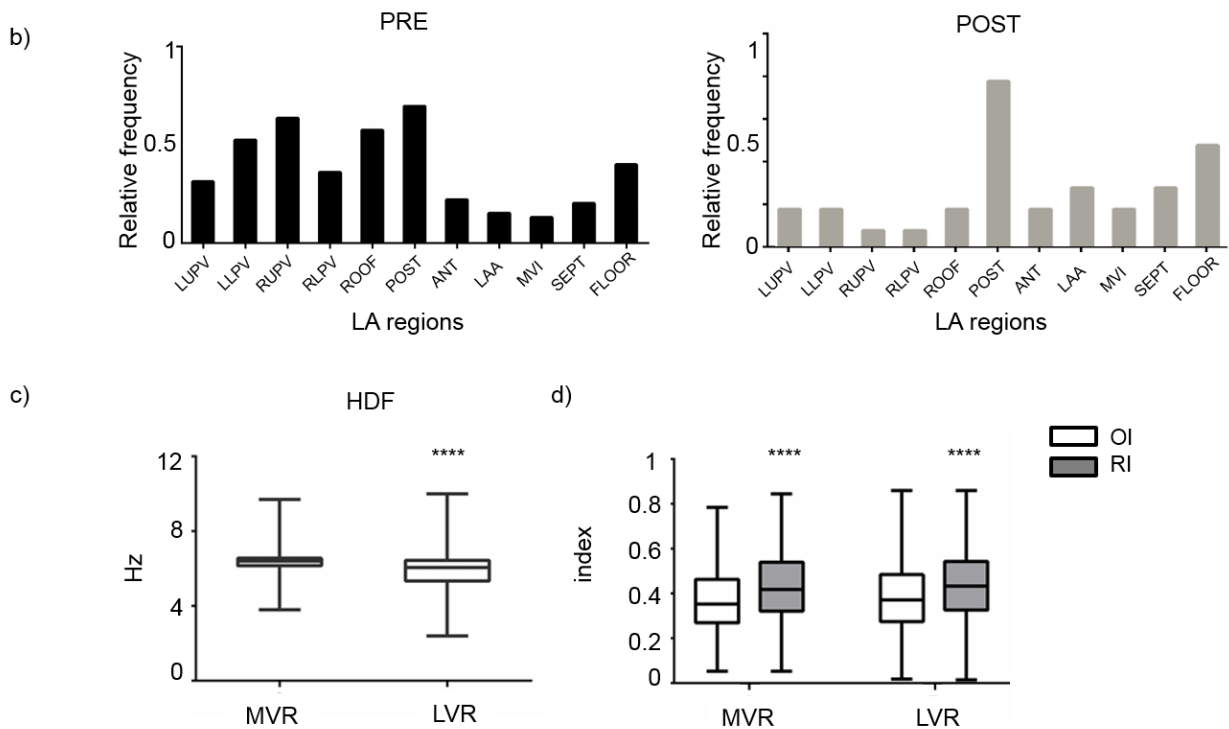


Figure 13: (a) (i) Scatter graphs (for one patient) showing different directions and strengths of correlation of HDF density maps (produced using several segments of VEGM recording) when compared to the HDF density map created using 300 seconds of VEGM recording. (ii) The histogram and distribution of the similarity indices (for one patient) comparing the similarity of every HDF density map (produced using 75 seconds) with each other. The histogram at this site exhibited high kurtosis with a sharp peaked distribution and negative skewness. This site exhibited a high similarity index with a mean of 0.71. (b) Incidence of HDF dense regions – before ablation – in the different LA regions, namely: MV, PVs, roof, posterior wall, anterior wall, LAA, MVI, septum and floor. (c) The mean and SD of the HFD of MVR (occurrences of the HDFs > 80%) and LVR (occurrences of the HDFs ≤ 80%). The mean ± SD of frequency in MVR nodes is 6.32 ± 0.49 Hz, significantly different from 5.87 ± 0.95 Hz of LVR ($P < 0.0001$). (d) The frequency organization of the electrograms of HDF regions as measured with OI and RI in the nodes of MVR is significantly lower (0.36 ± 0.13 vs 0.39 ± 0.14 , 0.432 ± 0.13 vs 0.437 ± 0.14 , $P < 0.0001$) than that of LVR.

An example of the convergence between several lengths of recordings compared to the 300 seconds recording for one patient is shown in Figure 13 (a(i)). The density maps using 75 seconds were similar to the HDF density map produced using 300 seconds. Figure 13 (a(ii)), shows the histogram and distribution of the all three index coefficients (for one patient) comparing the similarity of every HDF density map (produced using 75 seconds) with each other. From the histogram, the skewness value resulted in -0.36 (negative skewed value indicating the "tail" of the distribution points to the left) and kurtosis value resulted in 2.93 (positive kurtosis value indicating that the distribution has heavier tails and a sharper peak than the normal distribution). The combined distribution of all three indexes results in -0.49 and 2.31 for the values of skewness and kurtosis respectively. Therefore, any random segment of VEGM recording of 75 seconds exhibited higher index with a mean of 0.69 (median= 0.71 and mode= 1). Hence, it could potentially suggest consistent locations of the dense regions which could be an indicative of fixed drivers of persAF.

4.3.2 Spatial distribution of HDF regions

For all the patients, the HDF dense regions were observed to be spatially unstable. The HDF dense regions seemed to have the highest incidence at the posterior wall of the LA, followed by the RUPV, roof, other PVs, floor, anterior wall, septum, LAA and the MVI. For all the patients, it was observed that only 5.30 ± 4.06 % of the area of the HDF dense regions were the MVRs and the mean frequency in these area was 6.32 ± 0.49 Hz, significantly different from 5.87 ± 0.95 Hz of LVR ($P < 0.0001$, Figure 13 (c)). For every density map of each patient, the SD of HDF regions of the MVR was observed to be lower when compared with that of LVR (0.41 ± 0.32 Hz vs 0.55 ± 0.39 Hz). In addition, the frequency organization of the electrograms of HDF regions as measured with OI and RI in the nodes of MVR is also

significantly lower (0.36 ± 0.13 vs 0.39 ± 0.14 , 0.432 ± 0.13 vs 0.437 ± 0.14 , $P < 0.0001$) when compared with the frequency organization of LVR (Figure 13 (d)).

4.4 Discussion

FFT analysis has been shown to be a powerful analytic method for signal processing in the frequency domain (Cain *et al.* 1984, Haberl *et al.* 1988, Cain *et al.* 1991). DF analysis of atrial electrograms has been used to characterise AF, more specifically as an estimation of local atrial activation rates in AF (Ng *et al.* 2007). The HDF sites could be understood as the sites representing the main activation wave front of the VEGM that might also represent the atrial regions hosting ectopic activities or re-entry circuits driving the arrhythmia.

Ablation strategies based on targeting DF of the intracardiac signals resulted in successful termination of AF (Sanders *et al.* 2005, Atenza *et al.* 2009, Uetake *et al.* 2013). It was observed experimentally by Matsou *et al.* (Matsuo *et al.* 2012) that ablating the PVs with high DF led to termination of pAF. Sanders *et al.* (Sanders *et al.* 2005) demonstrated that ablation at a high DF site was more likely to prolong the AF cycle length. Recently, Uetake *et al.* (Uetake *et al.* 2013) analysed the frequency characteristics in patients with persAF undergoing radio frequency catheter ablation and examined the correlation of the DF between the intracardiac signals and surface ECGs. They concluded that DFs from the intracardiac signals of the whole LA showed good correlation with the ECGs and also that a significant decrease of its value when the patient is in sinus rhythm (compared to when in AF) is an important indicator of AF termination. Though there might be strong correlation between the intracardiac signals and surface ECGs, both Jarman *et al.* (Jarman *et al.* 2012) and Salinet *et al.* (Salinet *et al.* 2013c) concluded that the DF generated in the LA is not spatiotemporally stable when analysed using NCM data. It has been reported that the DF is temporally variable and that HDF regions can be transient in clinical experimentation (Habel *et al.* 2010, Kogawa *et al.* 2015). In a study based on personalized AF simulation modelling, it was also shown that the spatiotemporal behaviour of the DF was highly unstable and that this may preclude the development of effective ablation strategies (Li *et al.* 2016). Therefore,

targeting sites of HDF from a single time frame is unlikely to be a reliable ablation strategy (Salinet *et al.* 2013c). Hence, analysis of the temporal variability from the decay curves proves to be a useful tool to describe the stability of persAF content.

A previous study suggested the use of CoG of the DF clouds and their trajectory (by tracking the CoGs from several frames) to assess the spatiotemporal behaviour of the atrial substrate (Salinet *et al.* 2013c). In order to create the HDF area trajectory map, Salinet *et al.* (Salinet *et al.* 2013c) determined the CoG for the DF cloud by averaging the coordinates of each point in the cloud weighted by their particular DF values (Salinet *et al.* 2013c). This approach led to CoGs being occasionally outside the HDF cloud as in case of convex (e.g. horseshoe) shaped clouds or clouds with non-uniform spread of DF value (e.g. Figure 14 (a)).

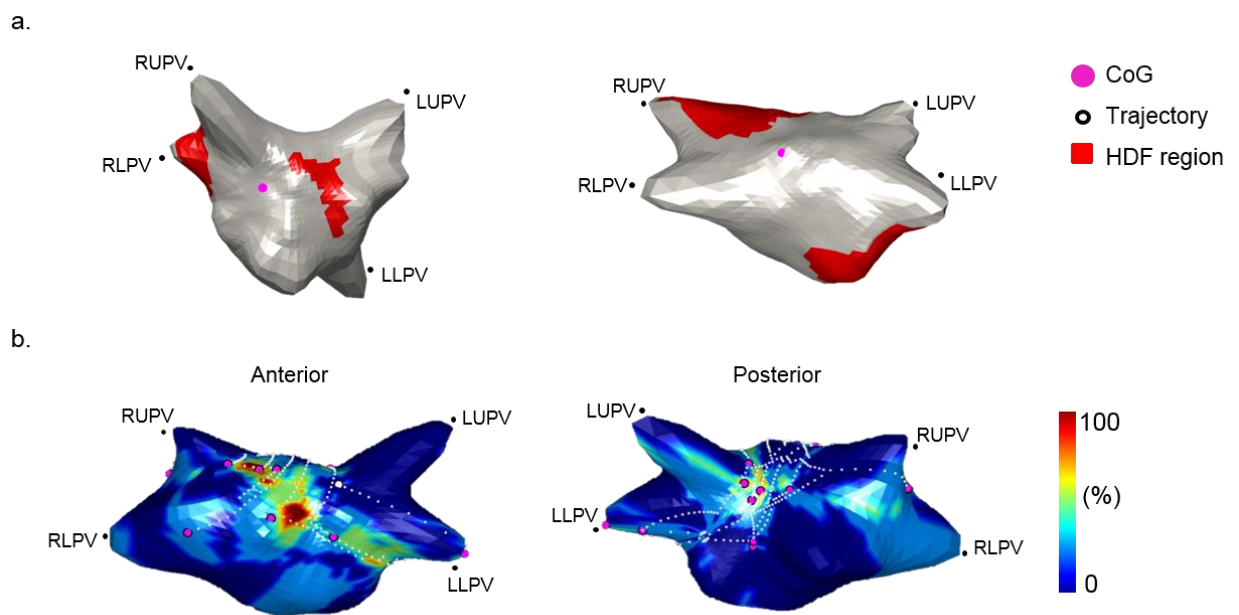


Figure 104: (a) Location of CoGs (pink dots) in LA of two persistent AF patients obtained for a specific time window. In this case the CoGs are located outside the HDF cloud's (red region) boundaries. The position of the CoGs is not a true representative of the HDF 'cloud'. (b) Comparison of HDF density maps with CoG distribution in order to compare the spatiotemporal distribution of the two techniques.

Therefore, HDF density maps (based on a histogram of occurrences) were constructed in this study in order to understand a wider perspective about the movement of the HDF clouds as these identify the regions that are being revisited most often despite the unstable dynamic behaviour. Density maps also summarise the spatiotemporal distribution of DF better than the CoGs (Figure 14 (a) and 14 (b)).

4.4.1 Characterisation of high-density HDF sites

Despite the unstable temporal nature of HDFs, the reappearance of HDFs in certain regions of the LA has provided evidence that persAF might be spatially organized. From our results, the areas of MVR have been observed to be small when compared to the total area of the HDF dense regions. Other studies have also demonstrated that despite sources being spatially and temporally stable, they exist in small regions (Davidenko *et al.* 1992, Zlochiver *et al.* 2008). Furthermore, the VEGMs from MVR of the HDF density maps are characterized by significantly higher values of HDF and lower OI and RI. This can be understood as MVR regions having higher atrial rate and showing a lower degree of organisation, thereby indicating non-dominant or multiple peaks at the VEGM's spectra which could be due to collision of uncoordinated fibrillatory waves. Previous studies reported that certain areas of the atria can have higher activation rates which could suggest the sources of the drivers maintaining AF and hence the potential targets of ablation (Skanes *et al.* 1998, Mansour *et al.* 2001, Berenfeld *et al.* 2002, Lazar *et al.* 2004, Sahadevan *et al.* 2004, Sanders *et al.* 2005).

4.4.2 Effect of LA ablation on the HDF density maps

The study also analysed the HDF density maps of the VEGMs for both pre- and post-ablation in order to assess the effect of catheter ablation on their spatial and temporal variability. From the results, DF guided ablation (prior to PVI) significantly affected the global HDF value of the LA (6.421 ± 0.67 Hz before ablation to 7.38 ± 0.67 Hz after, $p < 0.05$) (Figure 15 (a)). That could be understood as a post-ablation beneficial outcome (despite the

patients still being in AF) considering the spatiotemporal coverage of the HDF dense regions decreased from 80.8 ± 22.2 % to 65.83 ± 25.7 % of the LA thereby highlighting the more ‘dominant’ regions of the LA that could be the sources sustaining the AF (Figure 15 (b)).

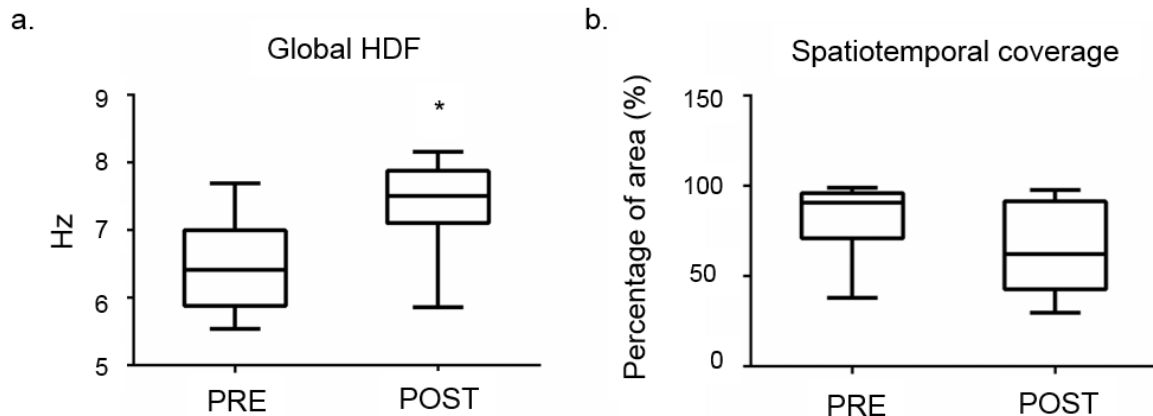


Figure 15: The mean and SD of the global HDF and spatiotemporal coverage area of the VEGMs for both pre- and post-ablation.

Patients 4, 5 and 10 converted to AFL immediately after DF-guided ablation. Interestingly, analysing their post-HDF density maps, the spatiotemporal coverage of the LA of these patients decreased significantly from 89.0 ± 7.8 % to 45.7 ± 9.7 % ($p < 0.05$). In AFL, unlike AF, electrical activity in the atria is coordinated (Winter and Crijns 2000). The post HDF density maps of the AFL patients identified localized regions of high-frequency activity. These confined sites could indicate the presence of the self-perpetuating macro re-entrant circuits causing the propagation of electrical impulses maintaining AFL (Waldo 2002). This result also supports the idea that HDF density maps could also be used as an important tool that can be used to analyse the effect of ablation.

4.5 Conclusion

HDF sites have been reported to be related to the centre of a focal-firing rotor or local re-entry circuit, based mainly on both animal studies and human studies. They have been shown to be effective targets for AF termination, thus suggesting their importance in the maintenance of AF. However, these sites change over time as a result of which

characterization of HDF spatiotemporal distribution and stability are critical to their relevance as targets for catheter ablation. HDF density map is an interesting method to investigate the spatiotemporal behaviour of HDF and to identify the occurrences of recurrent activities in patients with persAF. Spatial distribution of HDF density suggests potential sources that may reflect mechanisms driving and maintaining the fibrillatory process of AF. We suggest that HDF density maps should be considered for HDF targeted ablation rather than the centre of gravity of the HDF 'clouds'.

Chapter 5

Phase analysis and Phase Singularity detection

5.1 Introduction

Analysis of the atrial electrical activity plays an important role to reveal the underlying electrophysiological mechanisms responsible for AF's initiation, maintenance and perpetuation. In early 19th century, experiments showed that the chambers of the heart could support a circulating excitation (Mines 1913, Garrey 1914), and later studies in intact hearts found activation sequences were consistent with this re-entrant mechanism (Lewis 1920, Wiggers 1940). During re-entry, electrical activity propagates repeatedly along a closed path, forming a spiral wave of activation in 2D. With time, many experimental studies on animals and humans and computational simulation studies illustrated that this arrhythmia is sustained by re-entrant activity, and that each re-entrant wave rotates around a PS as discussed in chapter 3. Therefore, PSs could lead to characterizing arrhythmias and might provide mechanistic strategies in modulating cardiac fibrillation. The behaviour of the action potential of the cells (where its phase progresses through the activation-recovery cycle) can be visualized by transforming activation into phase maps as previously discussed in chapter 3.

Models offer replicated fibrillation data sets as they allow choosing the best set of parameters to achieve the signals and hence can simulate the principal features of critical patterns sustaining AF. They offer to investigate conditions which are difficult to deal with experimentally and that they can be controlled by parameters (Sörnmo and Laguna 2006). However, whether the signal produced is highly realistic are often associated with high complexity and therefore highly dependent on parameter estimation (Sörnmo and Laguna 2006). On the other hand, analysing fibrillation signals collected from animals and human

can provide with more 'truth' as it is real. Therefore, data collected in vivo requires pre-signal processing before phase analysis is performed. In cardiac research, filtering of the signals in time domain is becoming an increasingly important research tool. In our study, the signals undergo time domain filtering in order to enhance certain frequencies (corresponding to atrial activity) and to attenuate other frequencies that may be present (for example noise) (the term 'noise' is here used in a wide sense which includes physiological activities other than the one under study which may interfere with the desired signal). It is, therefore, important to understand how the signal is processed and also how different filtering affects the signals accordingly as this will also affect the detection of PSs.

In this chapter, we performed a comparative examination of several pre-processing techniques for persAF signals and illustrated how it affects the PSs quantification. Also, different investigators have used different approaches to identify the location of PSs, and little is known about the differences between these methods (Fenton and Karma 1998, Bray *et al.* 2001, Iyer and Gray 2001, Bray and Wikswo 2002). Three methods for detecting PSs have been discussed, among which one of them is the technique that was proposed by Bray *et al.* (Bray *et al.* 2001) based on topological charge index and which is the main basis of the algorithm that has been used to identify PSs in this study. This algorithm has been applied on fibrillation data collected from optical signals of animal's heart (Gutbrod *et al.* 2015), simulation studies of acute AF and persAF (Bray and Wikswo 2002, Bayer *et al.* 2016, Hornung *et al.* 2017), simulated bipolar AF electrogram (Roney *et al.* 2014), VF model (Bray and Wikswo 2002), contact mapping of persAF ('The Boston AF Symposium 2016 Abstracts' 2016), etc. Therefore, this technique is routinely applied to simulated fibrillation electrograms as well as unipolar/bipolar electrogram data from animals and human data, to the author's knowledge, not particularly to non-contact VEGMs collected from human persAF database. The algorithm was implemented and parameters were adjusted accordingly to track PSs. Additionally, in this chapter we also compare the implemented topological charge technique with two other PS detection techniques and performs a comparative study.

5.2 Methods

Phase analysis of atrial electrograms has become an important method in characterizing AF. Phase maps of the cardiac signals may show different patterns according to the way they are processed (Guimarães and Santos 1998). PS detection methods have been proposed and studied both in vivo and in vitro, and have been broadly used in EP studies (Bray et al. 2001, Rantner et al. 2007, Tomii et al. 2015, Unger Laura et al. 2015). It has been observed that phase analysis and number of PSs detection depends on choosing appropriate parameters for each algorithm and that if an appropriate choice is made there could be consistency in PS detection. The following flowchart guides through steps of extracting phase and identifying PSs as well as highlights the parameters that could eventually affect the overall detection.

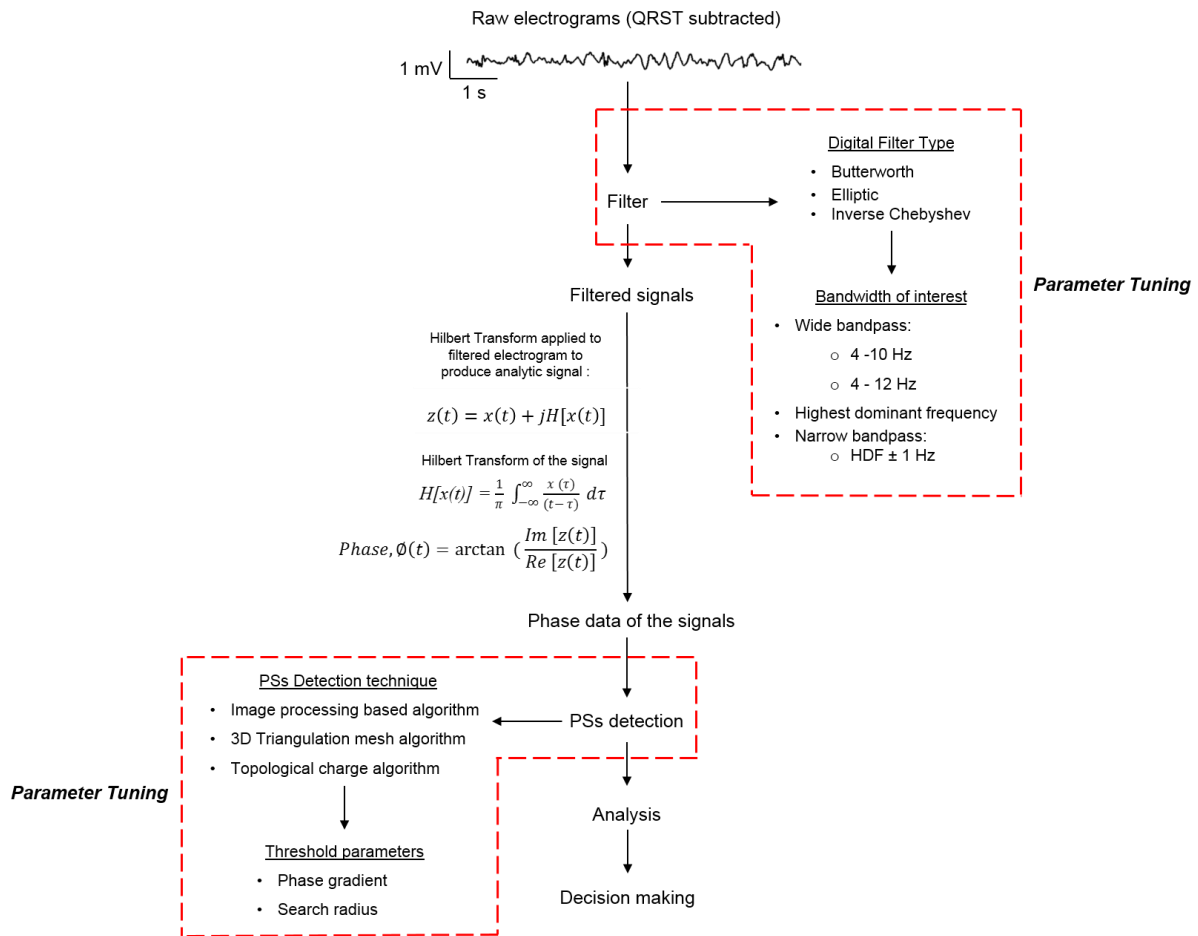


Figure 16: Flowchart guides through steps of extracting phase and identifying PSs as well as highlighting the parameters that could eventually affect the overall detection.

5.2.1 Study population

The study population consisted of 10 persAF patients (10 male; mean age 58 ± 13 years) referred to our institution for first time catheter ablation. Details of the clinical characteristics of the study subjects have been provided in chapter 1. Study approval was obtained from the local ethics committee and all procedures were performed with full informed consent. Table 1 in chapter 1 summarizes the clinical characteristics of the study subjects. All patients were treated in the Leicester Cardiovascular Biomedical Research Unit at Glenfield Hospital.

5.2.2 Electrophysiological set-up

Details of the electrophysiological study, mapping procedure, and the clinical characteristics of the study subjects have been introduced previously in chapter 1. Study approval was obtained from the local ethics committee and all procedures were performed with full informed consent.

Three dimensional LA geometry was created and VEGMs were collected by deploying a noncontact MEA catheter (EnSite Velocity, St. Jude Medical, USA) and a conventional deflectable mapping catheter. The patients underwent DF-guided ablation and a post procedure recording was collected for up to 5 min. The MEA was removed followed by standard PVI. In case this was insufficient to restore sinus rhythm, cardioversion was achieved by flecainide or internal defibrillation.

5.2.3 Pre-processing techniques of VEGMs

One of the most crucial pre-processing steps used is the filtration of signals. Filtration is necessary for noise removal but by its nature also has the potential to remove crucial components of signals. Some research has been done into the effect of filtration on phase analysis, mainly focusing on the effect BPF has on the length and position of PS (Attin and Clusin 2009, Narayan *et al.* 2012, Walters *et al.* 2015), but little research has been done into the effect of varying filter size and type. Studies investigating atrial fibrillation use a range of filters during this stage and without fully understanding the consequences of using different filters there is a potential to draw false conclusions. By investigating the similarities and differences in PS location and stability identified when using different filtering techniques, this study aims to highlight the effects of filter design in atrial substrate characterisation.

5.2.4 Digital filters

A digital filter is a mathematical transform that reduces noise and interference by a process of attenuating certain frequency components, such as baseline drift and high frequency noise (Alcaraz and Rieta 2013) from a digital signal that may arise during signal

measurement that obscures or modifies the signal in some way. Filters are usually represented visually by their frequency response to a constant magnitude sinusoidal signal. All filters have three main components (Samie *et al.* 2001),

- Passband: region of frequencies for which there is no attenuation, or attenuation is less than a specified threshold;
- Stopband: region of frequencies for which attenuation above a certain threshold takes place;
- Transition band: region of frequencies between the pass and stop bands, attenuation is neither large nor small.

The point at which the filter transitions between the pass and stop bands into the transition band is called the cut off frequency (Samie *et al.* 2001). In an ideal filter there is no transition band, the transition from pass to stop band is immediate. The frequency response of an ideal filter is also completely flat to give a consistent level of attenuation across the pass and stop bands (Samie *et al.* 2001). Filters are usually classified according to their frequency-domain characteristics as lowpass, highpass, bandpass and bandstop filters.

5.2.4.1 Filter designed for the study

The term pre-processing is employed in the current study to designate the digital filters that have been applied to highlight the frequency of interest of the signals. Pre-processing may be needed for a more precise DF result and phase mapping. Mathematical software, such as MATLAB® (The Mathworks Inc., MA, USA, version 2015a) has been used for the whole processing of the signals and three types of digital filters will be considered; Butterworth (BWF), Inverse Chebyshev (ICF) (also known as Chebyshev type 2) and Elliptical (EF). Each of these filters has specific ripples, oscillation of the frequency response, and the sharpness of the transition band. BWF has flat pass and stop bands but has a wider transition between the two compared to the other filters. ICF has some ripple in the stopband

but a steeper transition band compared to BWF. EF has a steeper transition band compared to both BWF and ICF but has ripples in both the pass and stop bands (Samie *et al.* 2001).

Applications of frequency setting of the filters are:

- (a) Band-pass filtering (BPF) at 4–10 Hz and 4–12 Hz: In the present work, DF was defined as the frequency with highest amplitude within the physiologically relevant range (4 to 10 Hz) (Salinet *et al.* 2013c). In other study, it was evaluated by analysing spectra of AF waves from a patient with AF that the major atrial frequencies correspond from 4 to 12 Hz (Xie *et al.* 1998). Therefore, these two range was defined as it corresponds to the expected physiologically range of AF (240-600 beats/minute) (Nattel 2002).
- (b) Low pass with HDF value as cut off frequency: The effect of low pass filtering with HDF value (which represents the highest atrial rate of the LA) as cut off frequency is just filtering out the signals above that particular frequency.
- (c) BPF around the HDF: Applying BPF around the HDF allows signals between two specific frequencies to pass and discriminates against signals at other frequencies. The threshold of ± 1 Hz around the HDF is applied and a very narrow BPF is created. The cut off frequency of the low pass filters and the centre of the ± 1 Hz BPF was selected by analysing the FFT of each set of each patient's intracardiac signals and identifying the HDF across all 10 patients. This value was chosen to test how the extent to which the DF can be used to decide which frequencies should be filtered.

The order of each filter was kept constant as the order of the filter also dictates how steep the transition band is. Increasing the order reduces the size of the transition band. An ideal filter would have an instantaneous transition between pass and stop bands but this would only be possible with a theoretical ∞^{th} order filter (Samie *et al.* 2001). 10^{th} order was chosen as it was in line with similar studies (Mainardi *et al.* 2008, Narayan *et al.* 2012) and by using

a relatively high order filter the frequency response is closer to having an ideal transition and stopping all frequencies outside of the pass band.

5.2.5 Phase analysis

With the first geometry surface of the LA created, the NCM system identifies 64 evenly distributed locations on the 3D geometry. Then, the software uses the boundary element method (Schawrtz and Ben-Haim 2009) to measure VEGMs from the 64 electrodes of the MEA and then performs the inverse solution for Laplace's equation at each position of the endocardial surface. Up to 2048 isopotential points across the cavity of the LA is created and thousands of reconstructed signals generated by the system are then colour-coded accordingly onto the LA's surface to project the phase data (see chapter 3 equations 1.5, 1.6 and 1.7 for extraction of phase data). The phase data was also projected on a 2D sheet of LA (using cylindrical coordinates and forcing symmetry about the z-axis).

5.2.6 PSs detection technique implemented in the database

The concept of topologic charge technique (TCT) allows the identification of PSs easily in tissues that are undergoing re-entrant excitation, thereby, revealing the dynamic behaviour of the tissues. This technique is implemented in our work to determine the PSs in the VEGMs of persAF.

A PS is detected by estimating the 'topologic charge', n_t (equation 5.1)

$$n_t \equiv \frac{1}{2\pi} \oint_c \nabla \Phi \cdot d\vec{l} \quad \text{equation 5.1}$$

Where, $\Phi(\vec{r})$ = localised phase and

\vec{l} is a line integral on a closed route c surrounding the point of interest.

PSs were identified as locations where the phase was undefined, and, upon winding around the point, the phase changes by 2π , meaning it is a site of non-zero topological

charge (Bray and Wikswo 2002). It has been shown that the phase gradient used to determine PS presence can have an effect on the number of PS located. Reducing this phase threshold would ease the required phase difference for a PS to be identified; a wave would have to rotate around a smaller proportion of a full cycle to be considered a PS 'candidate'. This could lead to the inclusion of more valid PS that would have been missed by not showing a full 2π phase shift, but could equally lead to over-detection caused by the inclusion of pseudo-PS. A complete 2π phase gradient is usually not always observed around the point, hence, a threshold gradient needs to be applied. This could be due to the 2048 isopotential points across the cavity of the LA not being spaced equally and also could be due to not having monotonic increase in the phase between the points. Therefore, a PS is identified when the topologic charge exceeds the threshold defined in the algorithm. The sign of the integral corresponds to the chirality of the PS. This is the direction in which the associated wave front circulates about the PS (clockwise or counter-clockwise). Its X, Y coordinates were also recorded and each LA was reshaped into 2D to study the number of PSs per surface unit along with time. An overview of PS illustration in 2D LA and how its detected using TCT is shown in Figure 17.

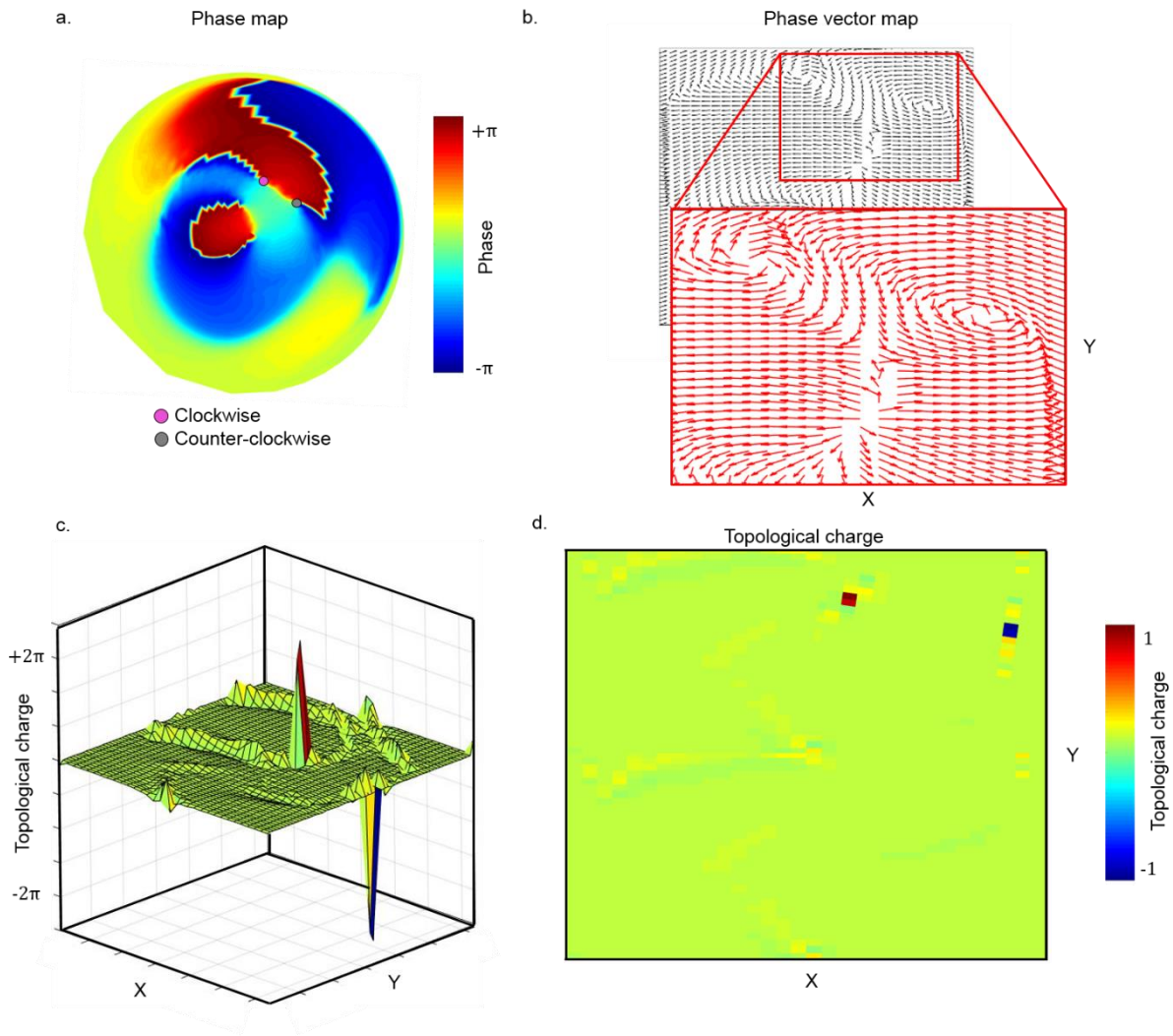


Figure 17: An overview of PS illustration in 2D LA and how it is detected using the topological charge technique. (a) Phase map at an instance of time of a persAF patient. (b) A map displaying arrows representing the phase vector (size indicating the magnitude and orienting representing the direction of activation). (c) & (d) A plot of the topological charge in 3D and 2D to identify the location of the PS, where the topological charge equals $+1$ or -1 .

5.2.6.1 Other PSs detection techniques

Two other algorithms were compared with the TC to detect PSs are 3D triangulation mesh technique (TMT) and the image processing based technique (IPT).

The first technique was developed in our research group, and is based on analysing the phase gradient around the interested point. The increment or decrease in phase is checked in a clockwise manner in the nodes around the point of interest. The point is identified as a PS if there is an overall increase in the phase and if the phase gradient is above the threshold defined in the algorithm. Though the detection was performed in 3D, the results could be illustrated to the 2D mesh as a cylindrical projection mentioned earlier.

The other method is more of an image processing technique for finding the boundaries of phase gradient within images. The canny edge detector (Canny 1986) was used for this purpose. After detection of the edges, sites at the end of the edges were marked and checked for a monotonic increase/decrease in phase value in a clockwise fashion. The phase gradient was also checked around it and if it satisfied all the parameter conditions, it was identified as a PS. Clusters of PS detection are represented using the centre of gravity of the cluster and in the 3D triangulation mesh algorithm, clusters of PSs are replaced by the point with greatest phase gradient. The default threshold chosen for both methods is 1.5π .

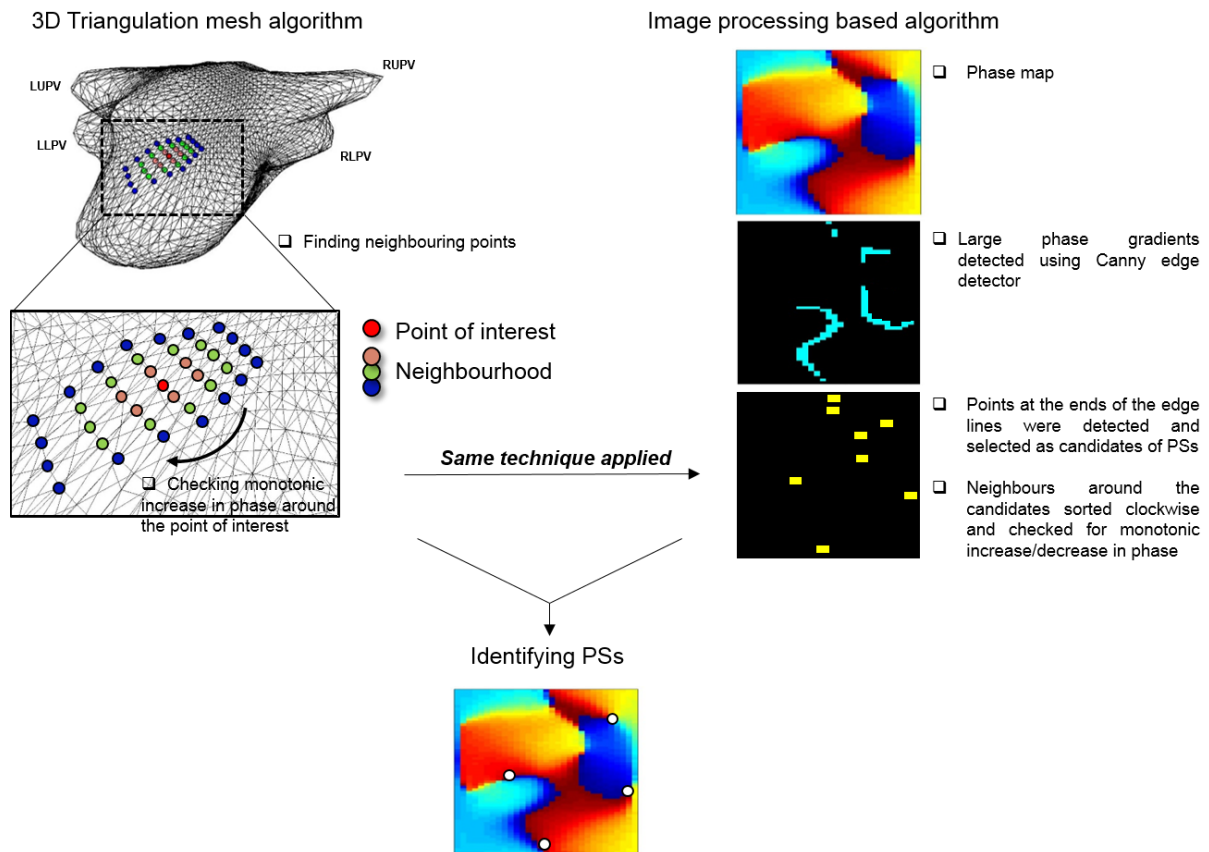


Figure 18: Schematic representation of two different methods (triangulation mesh technique and image processing technique) of PS detection and steps.

5.2.6.2 Parameter affecting PS detection techniques

Additionally, for the two PS detection techniques discussed above, the size of the ‘neighbourhood’ of the point of interest requires adjusting before the detection is performed. Therefore, the search radius is another important parameter that requires tuning, apart from the phase gradient threshold. PS detections for different combinations of the phase gradient threshold (from 0.1π to 2π) and the search radius (from 2 to 8 nodes) were performed for the three techniques. The PS histogram maps created from the PSs found using different settings were compared with the PS histogram map created from the PSs from the manual annotation (performed by an expert and is therefore referred as the ‘gold standard’). Optimised thresholds were found to improve detection accuracy and PS histograms were compared using the SSIM index and CORR. Multi-objective optimization function values

(Nocedal and Wright 2006) were calculated in order to gain the best trade-off between the two similarity indexes and the processing time as well as surface distance between PSs and the annually annotated PSs.

5.2.6.4 Tracking PS spatially and temporally

We used spatiotemporal ‘thresholds’ to track PSs in order to detect rotors. A maximum spatial ($\Delta d_{max} \leq 3$ nodes) and temporal separation ($\Delta t_{max} \leq 10$ ms) between detected PS was set. As a result of the tracking algorithm implementation, analysis of PS was more accurate and robust against losses of detection in short periods of time, for tracking long standing rotors. The overall overview of the methods is shown in Figure 19. PS lifespan was obtained as the temporal difference between two PSs and for those PS lasting ≥ 100 ms were considered as rotors.

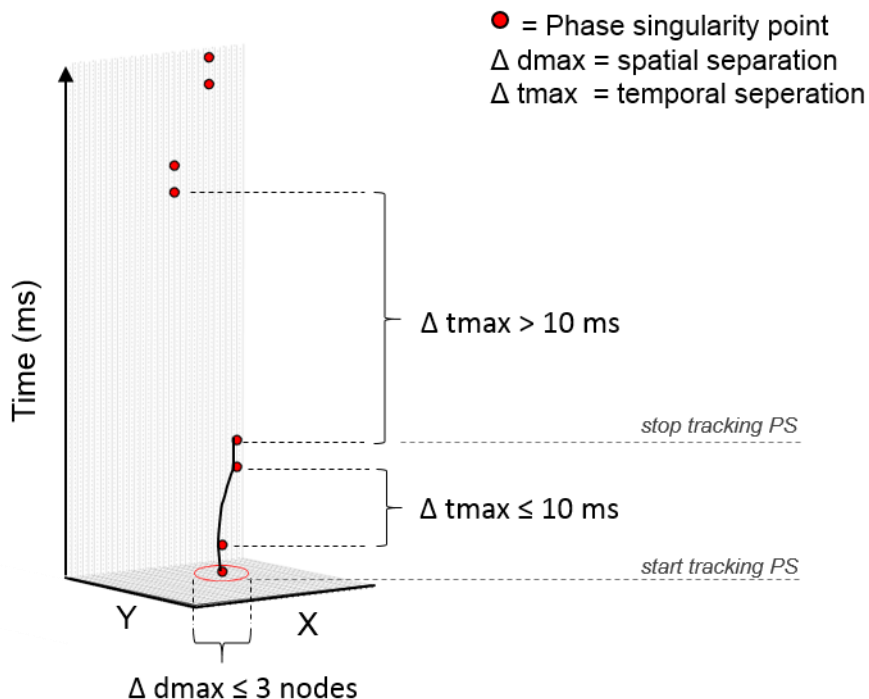


Figure 19: Schematic representation of tracking PSs. Each PS is considered as the same PS if it is between the maximum spatial ($\Delta d_{max} \leq 3$ nodes) and temporal separation (Δt_{max}

≤ 10 ms) between the detected PS. If conditions are met, the tracking continues, else it stops tracking and reports the lifespans of the PS.

5.3 Results

5.3.1 Comparison of the three PS detection techniques

The performances of the three techniques for detecting PSs were compared using PS density maps. The maps were created for 10 seconds using their default thresholds for the parameter (TCT: 1.9π ; TMT and IPT: 1.5π and nodes ≤ 3). Overall, the similarity of the density maps did not show a good agreement (SSIM and CORR: IMT vs TMT- 0.64 ± 0.08 and 0.32 ± 0.11 ; TMT vs TCT- 0.55 ± 0.15 and 0.21 ± 0.10 ; IMT vs TCT- 0.57 ± 0.17 and 0.35 ± 0.11 respectively). On average, the SSIM and CORR for all the three techniques poorly correlated 0.59 ± 0.14 and 0.30 ± 0.12 ($P < 0.001$ using Mann Whitney test) respectively.

With the search radius fixed ($n= 3$) for the TMT and IPT, the PS density maps for all the three techniques showed that different thresholds induce differences in PS occurrence concentration, annotating distinct LA regions as potential targets for ablation (Figure 20).

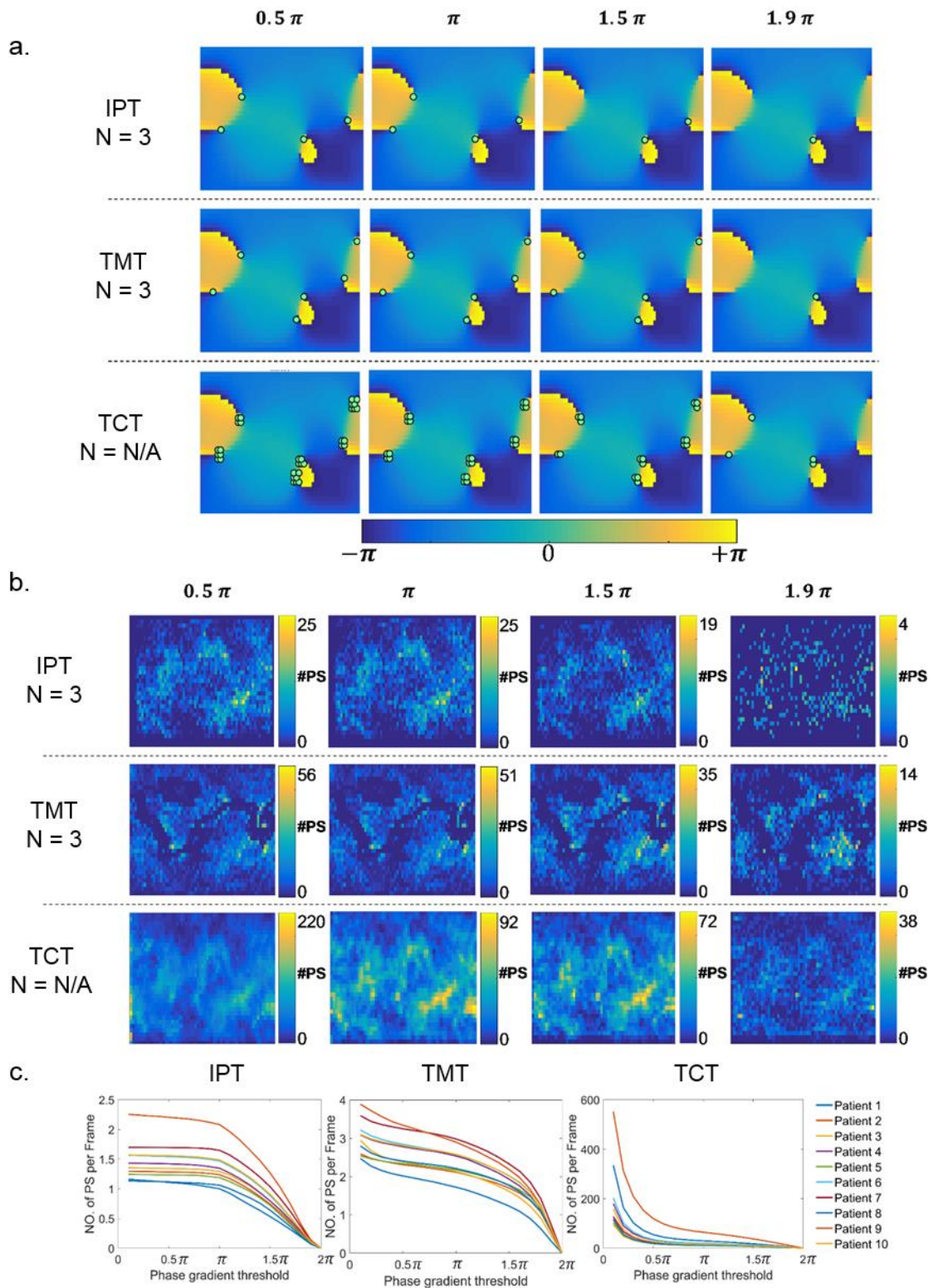


Figure 20: (a) An example of the PS detection using 3 methods with a series of phase gradient thresholds. The colorbar shows the phase value in rad. (b) PS histograms of 8 s VEGM using 3 methods with different phase gradient thresholds. (c) the effect of changing the phase gradient thresholds on the number of PSs for each patient.

Figure 21 (a) illustrates the effect of adjusting the phase threshold on the number of PSs per frame for the TCT. With increase of the phase gradient threshold of acceptance of PS points, the number of PSs significantly increased overall ($P < 0.05$ using Mann Whitney test) except between the threshold 2π and 1.75π which did not show any significant differences (threshold: mean \pm SD, $2\pi = 6047 \pm 3531$, $1.75\pi = 7034 \pm 3769$, $1.5\pi = 11948 \pm 7351$, $1.25\pi = 16815 \pm 10898$, $\pi = 18023 \pm 11216$, $0.75\pi = 21584 \pm 12197$, $0.5\pi = 20971520 \pm 0$). The TCT was independent of the search radius on the number of PSs per frame unlike TMT and IPT. In a study conducted in our research group, dramatic changes were observed when analysing more than 2 circles of neighbours. As a result, the processing time was comparatively very high for TMT and IPT. The processing time of TCT, TMT and IPT using default thresholds were 0.9 ± 0.2 s vs. 335.4 ± 14.4 s vs. 596.6 ± 144.0 s ($P < 0.0001$), respectively (Figure 21).

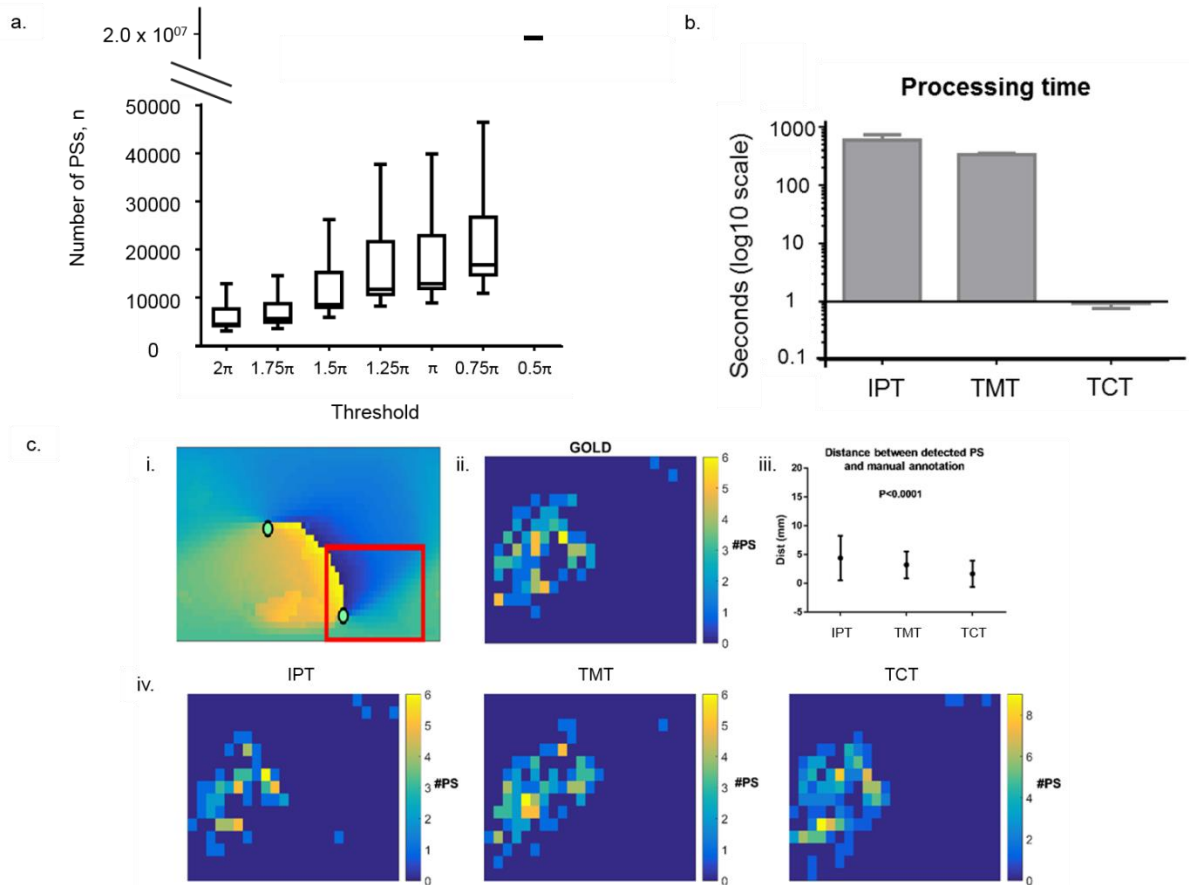


Figure 21: (a) Box plots illustrating the effect of adjusting the phase threshold on the number of PSs per frame for the TCT. (b) The processing time of TCT, TMT and IPT using default thresholds (mean \pm SD: 0.9 ± 0.2 s vs. 335.4 ± 14.4 s vs. 596.6 ± 144.0 s ($P < 0.0001$), respectively). (c) i) A frame of the phase clip and the region selected as the 'gold standard'; ii) The PS histogram generated with the manual annotation (red rectangular region); iii) The shortest path/distances on the surface of 3D atrial mesh between PSs using manual annotation and the PSs using each method with revised thresholds; iv) The PS histogram generated using each method.

PS density maps of the current setting were compared to the maps manually annotated by the expert. Multi objective optimization function values were calculated for each setting and the minimum value within each method was considered the optimal point. According the multi-objective optimization, the optimal setting for IPT resulted in 1.4π , with 2 circles of neighbours, while 0.6π , with 3 circles of neighbours for TMT, and it is 1.8π for TCT. With the

application of the revised settings, the PS density histograms were generated and compared with the 'gold standard' as discussed earlier. The surface distances between the automatically detected PSs and the PSs from manual annotations for each method are 4.38 ± 3.88 mm for the IPT, 3.19 ± 2.32 mm for TMT and 1.63 ± 2.30 mm ($P < 0.0001$) for the implemented TCT.

5.3.2 Distinguishing between different filter types

Instead of individual point by point comparison of PS locations, rotors have been tracked for each patient in order to compare the differences in the number of PSs in each filter settings in detail by filtering out very short-lived PSs and keeping only the more significant PSs for comparison. For all the 10 patients, each filter significantly detected different number of PSs ($P < 0.0001$ using Mann Whitney test) when compared with the number of PSs using raw signal (mean \pm SD: Raw = 97784 ± 12768 ; BWF = 26985 ± 13691 ; ICF = 17476 ± 8904 ; EF = 30580 ± 12835) over a 20 seconds interval. When the number of PSs was compared for each filter they also differed significantly from each other except between BWF and EF (Figure 22).

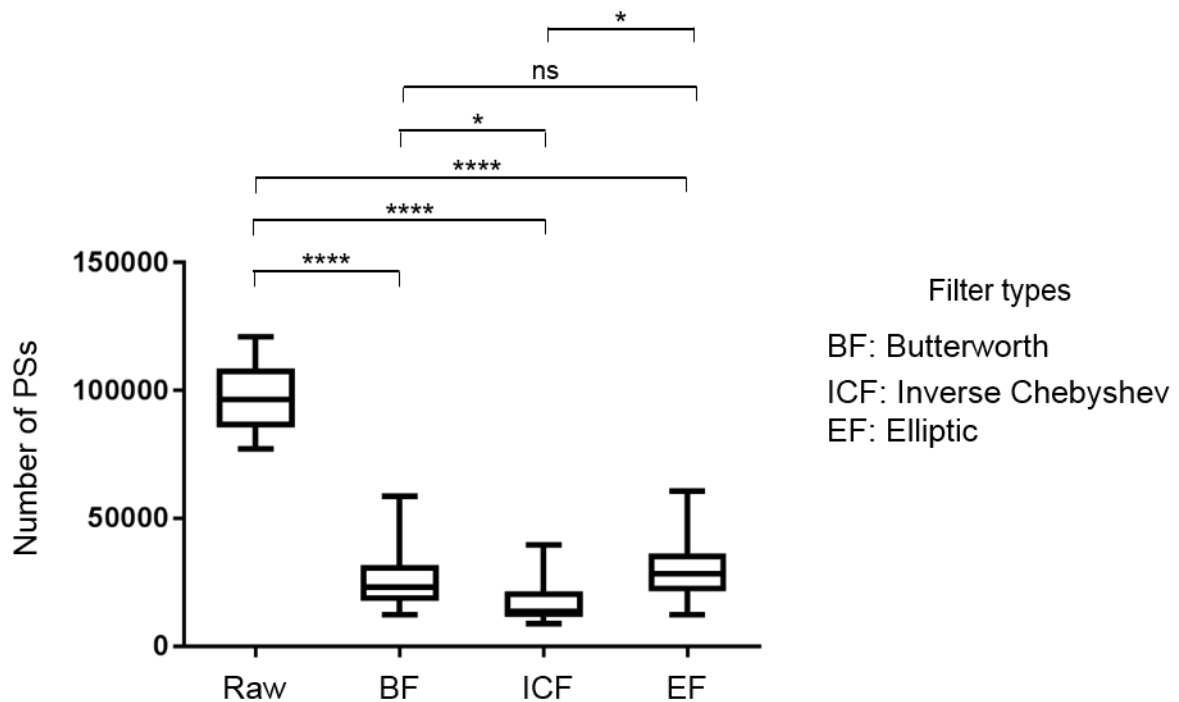


Figure 11: Box plots showing number of PSs identified for all patients using the raw signal and the three filters. Mean highest number of PS were found within the raw signal (97784 ± 12768) followed by the EF signals (30580 ± 12835), BF (26985 ± 13691) and finally the ICF (17476 ± 8904).

Grouping multiple points into a single cluster allows us to visualise the overall trend in the motion of the points. Only rotors (which lasted ≥ 100 ms) were analysed and by evaluating the locations of these rotors the differences in identification of PSs between filters are observed. This also has the added effect of filtering out some of the PSs to make comparison more significant by leaving only the more important PSs for comparison, i.e., comparing the PSs that could be considered potential targets for ablation (Krummen *et al.* 2015, McDowell *et al.* 2015, Hwang *et al.* 2016). This is demonstrated in Figure 23, which shows two scatterplots; one plotted with all PS included (left) and one including only the “consistent” rotors plotted (right).

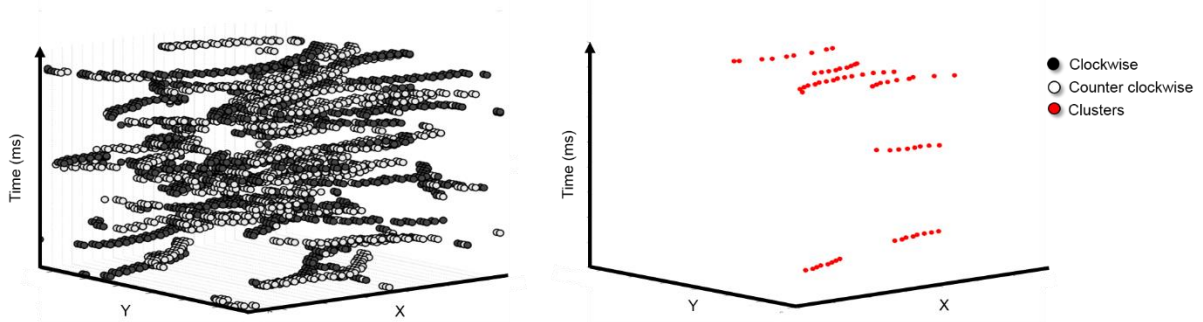


Figure 23: Comparison of 3D scatter plots of all PSs found in BWF patient data (left) and only rotors (right). The reduction of total number of points makes comparison of relevant PS locations which is of more interest.

For all the 10 patients, each filter also significantly detected different number of rotors ($P < 0.0001$ using Mann Whitney test) when compared with the number of rotors using raw signal (mean \pm SD: Raw = 107.9 ± 24.1 ; BWF = 21 ± 8.9 ; ICF = 8 ± 6.0 ; EF = 17.1 ± 9.0). When the number of rotors were compared for each filter they also differed significantly from each other except between BF and EF (BW vs. ICF: $P < 0.05$, BW vs. EF: $P = 0.362$, ICF vs. EF: $P < 0.05$).

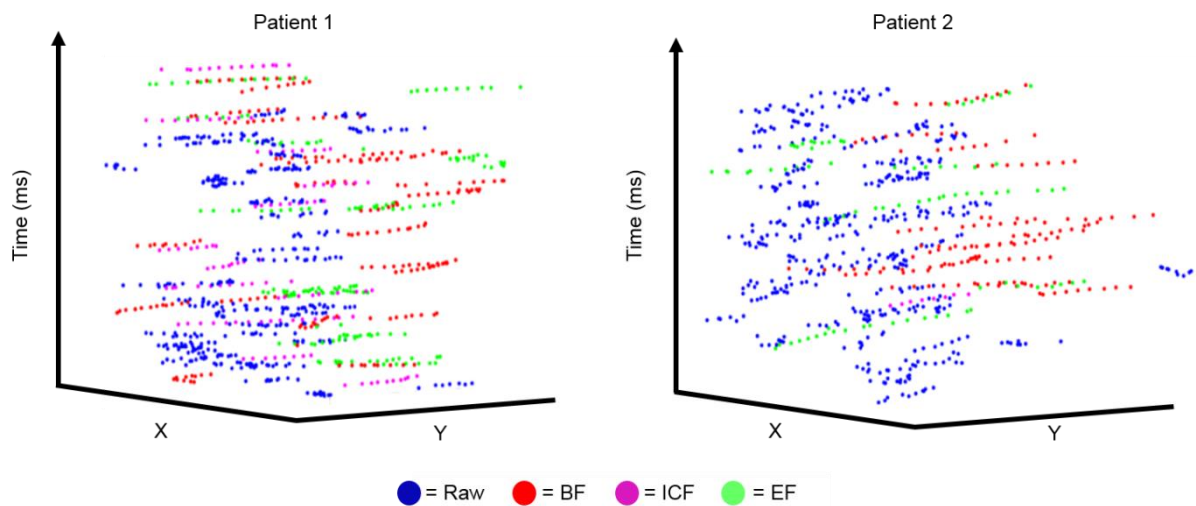


Figure 24: 3D scatter plots of centre points for all consistent rotors found using each filter and the raw signal. X and Y are the spatial directions and the Z-axis shows the time interval at which the PS cluster was found. From visual inspection, the clusters identified from the

raw signal were seen to be more dispersed than those found from the filtered signals.

Despite having the fewest number of rotors, the rotors identified using the ICF showed significant overlap with the rotors found using the other two filters.

PSs density maps are a useful tool for identifying sites where PS consistently return as they identify sites with highest PSs occurrences which could indicate areas that have a higher chance of presence of rotors (Bayer *et al.* 2016). In order to check the location of the rotors and to get a broader view of the differences of each filter type, the PS density maps have been compared for all combinations of filters for all patients. The comparison between the HDF density maps produced using each filter type was reported based on SSIM index and CORR. The table shows the comparison values of mean and SD of SSIM and CORR between all the three filters and raw data.

Highest value of SSIM and CORR were seen between PS density maps of BWF and EF followed by BWF and ICF and ICF and EF. Very low similarity was seen between raw signal density maps and those generated from filtered signals due to greater dispersion of PS due to noise present in unfiltered signals.

Table 3: Summary of mean values with SD of SSIM and CORR indices obtained comparing all filter types and RAW signal for all the patients. Overall highest value of SSIM (0.69 ± 0.06) and CORR (0.64 ± 0.12) indices found between the BWF and EF.

		Index, mean \pm SD			
		RAW	BWF	ICF	EF
RAW	SSIM	1 ± 0	0.10 ± 0.05	0.06 ± 0.02	0.11 ± 0.06
	CORR	1 ± 0	0.39 ± 0.14	0.33 ± 0.10	0.32 ± 0.16
BWF	SSIM		1 ± 0	0.64 ± 0.06	0.69 ± 0.06
	CORR		1 ± 0	0.58 ± 0.10	0.64 ± 0.12
ICF	SSIM			1 ± 0	0.56 ± 0.09
	CORR			1 ± 0	0.49 ± 0.12
EF	SSIM				1 ± 0
	CORR				1 ± 0

5.3.3 Distinguishing between different filter settings

The variation in the number of PS and rotors was also observed when the filter settings were differed. The number of PSs and rotors found between for all the 10 patients for the all 4 different filter settings are shown in Table 4.

Table 4: Total number of PSs and rotors identified using different filter settings. Highest mean number of PSs found using the low pass filter (70630 ± 7832) followed by 4 to 12 Hz (64482.7 ± 107994), 4 to 10 Hz (48488 ± 87425) and finally the 1 Hz bandpass filter (8844 ± 2023). Also shows the total number of rotors found followed which also followed the same trend as the number of PSs identified. Highest mean number of rotors found using the low

pass (42.3 ± 17) followed by 4 to 12 Hz (19.4 ± 8.7), 4 to 10 Hz (8.0 ± 6.0) and finally 1 Hz bandpass (1.4 ± 2.0).

n, Mean \pm SD								
	4 – 10 Hz		4 – 12 Hz		1 Hz BP		Lowpass	
	PSs	Rotors	PSs	Rotors	PSs	Rotors	PSs	Rotors
1	39748	18	56388	26	6699	0	44583	42
2	309056	5	386196	8	7536	4	41139	53
3	11041	1	14112	7	8644	5	41395	52
4	15509	2	23566	18	12812	0	49266	22
5	13098	17	23677	33	11390	0	47909	39
6	17933	10	21446	14	6797	0	51092	57
7	13459	3	23744	25	8460	0	37583	57
8	13386	14	18590	20	6583	1	31084	27
9	38014	5	49114	12	8976	0	56920	10
10	13576	5	27994	31	10539	4	35367	68
Total, n	48488 \pm 87425	8.0 \pm 6.0	64482.7 \pm 107994	19.4 \pm 8.7	8844 \pm 2023	1.4 \pm 2.0	70630 \pm 7832	42.3 \pm 17.0

In order to check the effect of the differences of each filter settings, the PS density maps have also been compared based on SSIM index and CORR. Table 5 shows the comparison values of mean and SD of SSIM and CORR between every filter settings.

Table 5: Summary of mean values with SD of SSIM and CORR indices obtained comparing all filter settings for all the patients. Overall highest value of SSIM (0.66 ± 0.10) and CORR (0.62 ± 0.082) indices found between the settings 1 Hz BPF at HDF and 4 to 12 Hz BPF.

		Index, mean \pm SD			
		4 to 10 Hz	4 to 12 Hz	1 Hz BPF at HDF	Low pass
4 to 10 Hz	SSIM	1 ± 0	0.20 ± 0.11	0.22 ± 0.12	0.12 ± 0.07
	CORR	1 ± 0	0.004 ± 0.11	0.0003 ± 0.11	-0.006 ± 0.09
4 to 12 Hz	SSIM	1 ± 0	0.66 ± 0.10	0.35 ± 0.09	0.31 ± 0.11
	CORR	1 ± 0	0.62 ± 0.08	0.31 ± 0.06	0.31 ± 0.11
1 Hz BPF at HDF	SSIM	1 ± 0	1 ± 0	0.31 ± 0.06	0.30 ± 0.09
	CORR	1 ± 0	1 ± 0	0.30 ± 0.09	1 ± 0
Low pass	SSIM	1 ± 0	1 ± 0	1 ± 0	1 ± 0
	CORR	1 ± 0	1 ± 0	1 ± 0	1 ± 0

5.4 Discussion

Understanding atrial activations during AF is important. Phase mapping is interesting for this arrhythmia (Laughner *et al.* 2012) because it can demonstrate the cause-effect relationship which allows to understand the sequence of activations. The multiple wavelet hypothesis (Moe *et al.* 1964) explains that a continuous wave break collides and breaks up wavelets and creates rotors which maintain fibrillation. Whereas, the focal source hypothesis explains that stable periodic sources and centrifugal fibrillatory conduction (Jalife *et al.* 2002) are what maintains the fibrillation. Recently, Narayan *et al.* reported that detection and ablation of rotors in AF patients is effective in terminating AF and improves the clinical outcome of AF catheter ablation (Narayan *et al.* 2012). However, the detection of a rotor, which is stable and induces fibrillatory conduction (Jalife *et al.* 2002, Valderrábano 2009, Pandit and Jalife

2013, Zaman and Peters 2014) is affected by the spatiotemporal resolution of mapping, pre-processing of signals, PSs identification technique and detection parameters for tracking it in space and time. In this study, the ways how pre-processing can affect a signal are discussed and 3 techniques for detecting PSs in patients with persAF using NCM were studied and compared. It was observed that different techniques result in distinct identification of PSs and this is mainly due to the way each technique works which ultimately leads to dissimilar performances. The main factors affecting the results for each PSs identification technique are the threshold of the phase gradient and the search radius.

Automatic identification of the PSs using convolutional operations as topological charge estimation was developed by Bray *et al.* and has been used by several different studies (Gray *et al.* 1998). The main basis of the algorithm that has been used to identify PSs in this study is the TCT which is based on Bray's convolutional method (as discussed in section 2.5) and it was improvised to detect PSs in triangular mesh, which overcomes the limitation of uniformed rectangular mesh and closed geometry problems (Rantner *et al.* 2007). Studies have been performed (Tomii *et al.* 2015, Unger *et al.* 2015) in order to improve PS detection accuracy, however, they were mainly based on optical mapping and computer modelling. The TCT implemented in this study is a novel method that allows PSs investigation in global mapping on the entire atrium. This is the first time TCT was used to obtain PSs using high-density NCM during human persAF.

5.4.1 Comparing PSs identification using three different techniques

From the results, it can be observed that all three PSs detection techniques identify PSs and lead to PSs density maps but a comparison of these different maps show low SSIM and CORR index (mean \pm SD, SSIM: 0.59 ± 0.14 ; CORR: 0.30 ± 0.12). This is surprising since the methods chosen seem to affect the data and alter the content of the data (Mironov *et al.* 2006) and ultimately affect the conclusions of the studies which is identifying rotors.

As results demonstrated, we find that number of PSs detected using each method depends on choosing appropriate parameters for each algorithm, but that if any parameter can be avoided there is less complexity on detecting PSs. This leads to the other advantage of the TCT over the IPT and TMT as it is independent of the search radius. TCT also showed the best performance with phase gradient threshold of 1.8π when compared with the PS density maps with the manual annotation as well as showed lowest surface distances between the detected PSs and the manually selected PSs. Hence, demonstrating that the implemented TCT algorithm detects PSs more accurately compared to the other two techniques. On the other hand, the processing time for this technique is very low and hence resulted in 662.9 % and 372.7 % faster to run compared to IPT and TMT respectively (mean \pm SD: IPT = 596.6 ± 144.0 seconds, TMT = 335.4 ± 14.4 seconds, TCT = 0.9 ± 0.2 seconds, $P < 0.0001$). Therefore, our implemented algorithm is able to produce accurate results with reduced processing time (near-real time) to calculate targets. This is of a great advantage as fluoroscopy imaging is still considered essential to visualise catheters in real-time as long-term risks are associated with radiation both to patients and physicians during ablation. Hence, it is necessary to decrease radiation exposure (Yamagata *et al.* 2016).

5.4.2 Effect of pre-processing on PS detection

5.4.2.1 Phase singularity incidence and rotor statistics

PSs identified using the raw signal were much more spread out compared to those found using the filtered signals. Figure 25 shows two scatterplots of rotors identified using signals from one patient, unfiltered (left) and after filtering using the BWF (right).

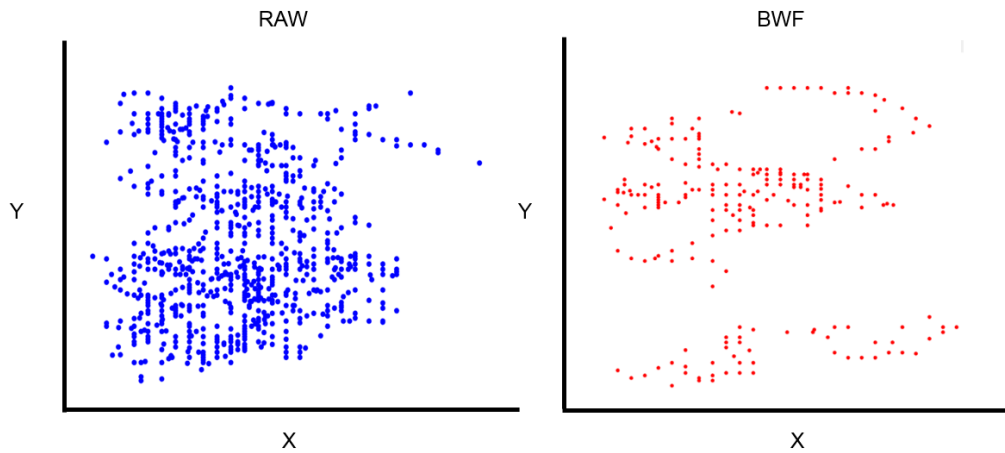


Figure 25: Scatterplots of rotors identified from one patient without any filtration (left) and with BF filter applied (right) showing on the XY plane. Unfiltered scatter plot shows a greater area of the atrium covered compared to the BWF scatterplot.

The disorganisation seen in the unfiltered scatterplot compared to the BWF scatterplot are caused by the noise and the unwanted frequencies within the signal leading to a high number of artificial PSs to be located. Total PSs incidence was consistently highest when filtering the raw signals with the EF followed by BWF and finally ICF (mean \pm SD, EF = 30580 ± 12835 , BWF = 26985 ± 13691 , ICF = 17476 ± 8903) for all the patients over interval of 20 seconds. Despite having a lower total PS incidence, a greater number of rotors were found within the BWF signal followed by the EF and ICF (mean \pm SD, BWF = 21 ± 8.9 , EF = 17.1 ± 9.0 , ICF = 8 ± 6.0).

Interestingly, despite fewer number of rotors being identified overall, the rotors identified using the ICF showed significant overlap with the rotors found using the other filtered signals. Figure 26 shows scatter plot of all rotors identified from one patient data using each of the three filters separated.

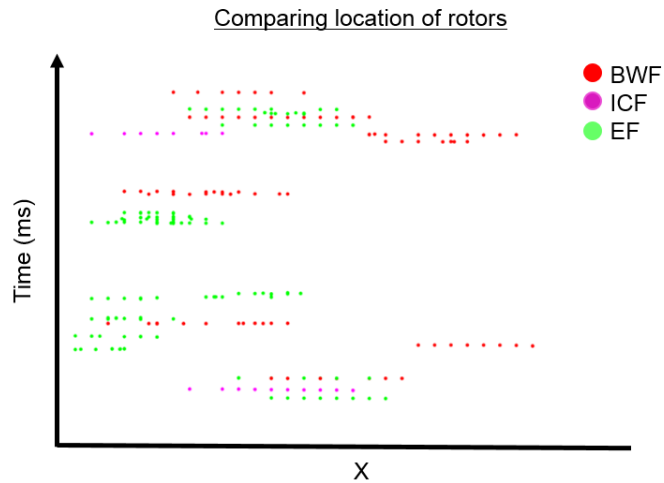


Figure 26: Scatter plot of all rotors identified from one patient signals using each of the three filters separated by colour, BF clusters in red, ICF clusters in magenta and EF clusters in green, showing variations in x-axis and time. Although rotors mostly appear in the same regions as those from other filtered signals there is little overlap at the same time window as shown by the gaps in the z-axis (time) between groups of rotors.

The overlap in the position of the rotors suggests that the differences in results between each filter type is due to the disparity in the number of points in each plot rather than a lack of similarity in position. Therefore, whilst the rotors were found to be reasonably consistent in space, there was much less overlap in time. Although this is a significant difference, this would have a negligible impact on the decision of where to target ablation, as spatial position of rotors is more important. Therefore, comparing the spatial positions for each filter type, based on results from Table 3, both mean SSIM and CORR indices for BWF and EF were found to have the highest level of similarity to each other. It is also possible that where rotors are not seen, PS were still identified but were not consistent enough to be considered for this analysis which could ultimately lead to higher SSIM and CORR indices.

Overall the comparisons of PS density maps for each filter type was above the threshold of 0.5 to be considered significantly similar. When ranking the values of CORR indices for each patient, the overall trend remained consistent in all the patients. As expected, no relationship

was found between raw density maps and all the filtered density maps, as the number and dispersion of PSs in the raw signals are so much higher than in the filtered signals. This shows that most of the PSs found in the raw signal are created by noise due to their random nature and unwanted frequency. These points are not present in the filtered signals because they are found in signal components outside of the frequency band non-attenuated by the filter. It also demonstrates that high PS identification is not a guaranteed indication of successful filter design as a high number of artificial PSs are generated by noise in under-filtered signals.

5.4.2.2 Varying filter frequency

PS incidence was highest for the low pass filter, followed by the 4 - 12 Hz bandpass, the 4 - 10 Hz bandpass and finally the 1 Hz narrow BPF around the HDF. The number of PS incidence highlights the effect of noise on the signals. It is generally accepted that to identify only signal components relating to activations responsible for AF, signals should be filtered with a BPF with a lower threshold of 4 Hz and an upper threshold in the region of 10 to 15 Hz (Sanders *et al.* 2005, Salinet *et al.* 2017). Therefore, anything outside of that bandwidth should be considered noise/artefacts or not electro-physiologically relevant. The low pass filtered signal demonstrated highest number of rotors compared to the other filter settings (Table 4). Rotors could only be found in 30% of patients when using the 1 Hz narrow BPF around the HDF. The filter also showed the lowest mean number of rotors (1.4 ± 1.96). This suggests that the 1 Hz bandwidth is too narrow to capture the range of frequencies needed to show full rotors when detected in VEGMs obtained using NCM. Also, by reducing the number of frequencies allowed through the filter, any rotors that cause activations at frequencies outside the frequency band will be completely missed, which explains the reason for detecting more PSs and rotors than in wider band of frequencies.

The only relationship seen is between the 4 - 10 Hz and 4 - 12 Hz bandpass filters. This is expected due to the large bandwidth overlap (mean \pm SD, SSIM: 0.20 ± 0.11 ; CORR: 0.004 ± 0.11). Interestingly, the SSIM and CORR indices obtained for low pass filter setting with 4

to 10 Hz BP and 4 to 12 Hz BP showed significant differences in results. The major differences between the low pass filter setting and 4 to 10/12 Hz bandpass filters must be caused by the frequency at higher range (i.e. 11 – 12 Hz) as this is the only difference between them. This therefore, further reinforces the impact that a slight modification in the frequency band can lead to a significant difference in rotor detection.

5.4.2.3 Comparison of findings to literature

In a study by Benjamin King *et al.* (King *et al.* 2017), optical mapping rabbit's myocardium under simulated fibrillation were studied to observe the effect of BPF and spatial resolution (spacing of simulated electrodes) had on the location and characterisation of PSs and rotors. The study showed a reduction in mean number of PSs when the 4 Hz BPF was applied around the DF compared to the unfiltered signals and also that these PSs were seen to have a longer duration than those found within the unfiltered maps. Leading to an increase in the number of PSs deemed rotors was higher in the BPF phase maps. The number of rotors identified using the 1 Hz narrow BPF was much lower than the number found using the unfiltered signal and this difference could be due to the greater bandwidth of the study's BPF bandwidth (4 Hz vs 1 Hz).

On the other hand, our study also used BPF wider than 4 Hz (4 - 10 Hz and 4 - 12 Hz) which still showed a lower mean number of rotors than the unfiltered signal. This emphasises the fact that the difference in results are due to the amount of noise/artefacts and unwanted frequency components found in the unfiltered signals and such that if a 'cleaner' signal is achieved, for instance by using a mapping technique that inherently has less noise, it is expected that signal components outside of the electro-physiologically relevant regions would contribute fewer perceived PSs to the phase maps. Therefore, BPF should only be applied at a maximum bandwidth to preserve the original signal in order to identify PSs which shows sufficient stability to be deemed as rotors. Hence, intracardiac signals should undergo pre-processing before being used for characterisation of atrial substrate.

5.4.3 Clinical significance

The highest procedural success rates after catheter ablation are typically seen in patients with pAF (Calkins *et al.* 2007) and deemed unsuitable in persAF (Oral *et al.* 2006). The high rates of AF recurrence support the notion that currently available procedural end points are ineffective in identifying the true atrial substrate during ablation procedure. For persAF, the absence of identified and located causes often involves damage to the atrium that could be avoided if the atrial substrate were identified and located for ablation or surgical therapy (Cox *et al.* 1991, Cox *et al.* 2000, Damiano and Bailey 2007). As mentioned earlier, FIRM seems to favour the outcomes of catheter ablation (Narayan and Krummen 2012, S.M. Narayan *et al.* 2012, Sanjiv M. Narayan *et al.* 2012, Schricker *et al.* 2014), however, other research work has shown low reproducibility of ablation outcomes using this approach (Benharash *et al.* 2015).

Studying intracardiac signals helps in understanding AF characteristics better (Papazoglou and Parthasarathy 2007). As discussed in previous chapters, intracardiac signals is a measure of hearts electrical potential versus time. It also contains unwanted components. There are various types of noises that are responsible for contamination such as baseline wander noise, electromyography interference, and 50 or 60 Hz power line interference (Chavan *et al.* 2008)(Chavan *et al.* 2008). In the case of intracardiac signals various noises such as respiratory interference, muscular noise is blended in the signal of interest. Hence it is really important to de-noise these signals. Based on our study, it could be argued that at least some of the differences in results of the above-mentioned studies could be because they characterise the atrial substrate in different way. Our results highlights that pre-processing of the signals, feature detection techniques and parameter settings of the detectors could affect PS detections, and that would result in misleading identification of the atrial substrate and hence ablation targets.

5.5 Conclusion

PSs have been believed as the source of cardiac fibrillation (Gray *et al.* 1998) and phase mapping technique can be used to track spatiotemporal changes during arrhythmia (Umapathy *et al.* 2010b). Researches showed AF re-entry sources using phase analysis techniques in invasive (S.M. Narayan *et al.* 2012) and non-invasive (Haïssaguerre *et al.* 2014) EP systems. They also showed that targeting these sources appears to improve treatment success (Pak *et al.* 2003, Narayan *et al.* 2012). In this study, the TCT method was developed to automatically calculate PSs using high-density NCM during human persAF. We have demonstrated that the implemented TCT for calculating PSs is more efficient (in terms of processing time) compared to other two techniques (IPT and TMT), while at the same time yielding higher accuracy of detection, thereby, making it more suitable for real-time purposes, such as during the EP procedures. Therefore, the algorithm proposed in this research is highly suggested to be used as it is a robust method for detecting and locating the PSs.

It has also been shown that detecting PSs from fibrillatory signals is a complex mathematical procedure, and thus it requires careful description of the parameters in order to correctly identify the PSs. We have demonstrated that different pre-processing techniques and thresholds affect the detections of PSs accordingly. Based on our results, it has also been observed that types of filters does not produce significant differences in rotor histograms as much as types of filter settings does. BPF is recommended without infringing on the frequency regions in which the relevant activations lie.

Chapter 6

Spatiotemporal Complexity of Phase Singularities as observable in the Atrial Electrograms in Human Persistent Atrial Fibrillation

6.1 Introduction

The onset and maintenance of supraventricular arrhythmias require both an initiating event and an anatomic substrate. With respect to atrial flutter (AFL), a macro re-entrant circuit triggers the electrical atrial activity, whereas, for AF, the situation is often complex. Previous researches show AF may result from an irregular atrial response to a rapidly discharging, regularly firing driver resulting from either local ectopic firing (Haïssaguerre *et al.* 1998), or a single localized re-entry circuit (Nattel 2002). Wavelets randomly re-enter tissue previously activated by the same wavelet named mother-rotor (Jalife 2003) or another wavelet (Xie *et al.* 2002). The presence of sources represents “stable” triggers that should be eliminated or isolated by curative ablation approaches in order to manage the disease (Wharton 2001). The identification and the localization of such “stable” triggers is one of the current challenges in ablation procedure. Many studies evidence that the mechanisms sustaining human AF are deterministic. However, due to the chaotic nature of AF (Ng and Goldberger 2007), finding stable electrical rotors and focal sources in either atrium is challenging. Hence, to obtain a better understanding of the rotors, it would be desirable to extract information about their spatiotemporal dynamics.

NCM technology allows generation of isopotential maps of a whole cardiac chamber from a single beat by simultaneous reconstruction of more than 3300 VEGMs (Schilling *et al.* 1998,

Gornick *et al.* 1999). It can also be used to identify mechanisms of rotor activation during AF (Yamabe *et al.* 2016).

In this study, we sought to identify rotors and analyse the complexity of the atrial activity dynamics as observable using NCM in persAF patients. We also focused on the rotor dynamics after DF guided followed by PVI ablation, whether one or more rotors are seen and study their behaviour. We used parameters that are commonly used for clinical characterization of persAF including DF, OI, and phase analysis. We also evaluated if DF-guided ablation revealed any significant anatomical differences in activation frequencies, AF organization, rotor location, and dynamics.

6.2 Methods

The methodology described below includes a complete overview of the patients' characteristics, electrophysiological set-up and electro anatomical mapping of the LA. After this, the methodology focussed on analysing the phase of the VEGMs, finding PSs and tracking the long-lived PSs.

6.2.1. Patient characteristics

This study included 10 persAF patients who underwent catheter ablation under the guidance of a 3D mapping system (Ensite Velocity, St. Jude Medical). The study was approved by the local ethics committee and all procedures were carried out after informed consent. The patient's characteristics are detailed in table 1 (see chapter 1).

6.2.2. Electrophysiological set-up and electro-anatomical mapping

Prior to the electrophysiological set-up, all drugs except amiodarone were stopped. Under fluoroscopic guidance, a quadripolar catheter and steerable decapolar catheter were inserted via femoral vein. Following trans-septal puncture, anticoagulant drugs were administered to maintain an activated clotting time between 300-350 seconds. Electro-anatomical mapping was performed in all patients to achieve detailed 3D LA geometry

(RUPV, RLPV, LUPV, LLPV, atrial roof, LAA, septum, lateral, anterior, floor, posterior and CS) with a noncontact MEA catheter. After DF-guided ablation was performed, a post procedure recording was collected for up to 5 min. The MEA was removed followed by standard PVI. In case this was insufficient to restore sinus rhythm, cardioversion was achieved by flecainide or internal defibrillation.

6.2.3 Data acquisition and signal processing

Surface ECG was recorded and band-pass filtered between 0.5 Hz and 50 Hz for all the patients. The non-contact MEA (Ensite Velocity, St. Jude Medical, USA) recorded 2048 points of AF VEGMs simultaneously from the endocardial surface of the LA. All VEGMs were resampled at 512 Hz, band-pass filtered between 1 Hz and 100 Hz and analysed offline using MATLAB (Mathworks, USA). For all 10 patients, up to 20 s of segments were analysed. Since the unipolar signals can have a significant far field ventricular component, a QRST subtraction was applied to remove the ventricular influence using a method previously described by Salinet *et al.* (Salinet *et al.* 2013a) (figure 8 of chapter 3).

6.2.4 Phase, phase singularities and rotor tracking

To obtain the phase of the VEGMs, Hilbert transform was applied to produce analytical signals from the VEGMs collected from the persAF patients. An overview of the methodology is provided in figure 10 of chapter 3. The PSs detection was implemented based on the topological charge method described by Bray *et al.* 2001. The PSs are identified as the points where there is a topological defect. Identification of spatial PSs was done by marking the sites where all phase values ($-\pi$ to $+\pi$) converged on the endocardial surface of the LA. The chirality of the PS indicates the direction in which the associated wave front circulates about the PS point (clockwise or counter-clockwise). Each LA was reshaped into 2D to study the number of PSs per surface unit along with time and the X, Y coordinates of the PSs were also recorded.

We used spatiotemporal 'thresholds' to track PSs in order to detect rotors. A maximum spatial ($\Delta d_{\max} \leq 3$ nodes) and temporal separation ($\Delta t_{\max} \leq 10$ ms) between detected PS was set. As a result of the tracking algorithm implementation, analysis of PS was more accurate and robust against losses of detection in short periods of time, for tracking long standing rotors. The overall overview of the method is shown in figure 19 of chapter 5.

PS lifespan was obtained and for those PSs lasting ≥ 100 ms (rotors), we calculated the density of rotors (defined as number of rotors arising per surface unit). The rotors are observed both in 3D and 2D and the LA was divided into ten sections. The locations of the rotors were tracked spatiotemporally to obtain the density of PSs and also PSs appearing at any instant were recorded to help visualise the complexity of the PSs clustering/appearance. This analysis was performed on both pre- and post-ablation data.

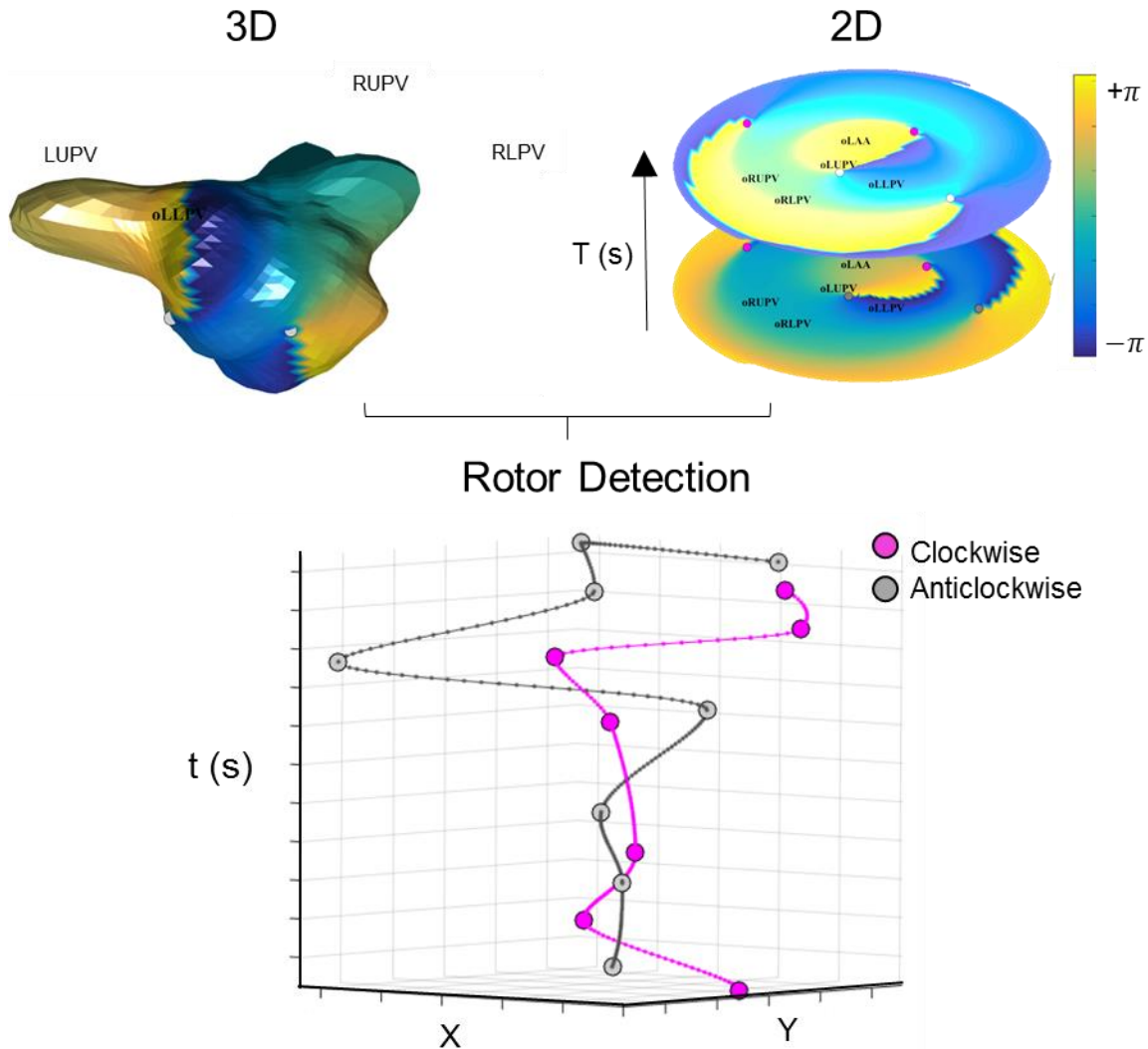


Figure 27: The location of the PSs were identified in 3D and 2D and tracked spatiotemporally to detect rotors. Its X, Y coordinates were also recorded and each LA was reshaped into 2D block for observing its behaviour. The chirality of each PS was also recorded.

6.2.5 Rotors and DF

Power spectra were estimated (Figure 28) using FFT with a Hamming window for every 1 second – long-time window with 50% overlap for all the 2048 points in the LA to find the DF, defined as the frequency component with the highest power in the frequency range between 4 and 10 Hz. Zero padding was used to increase the density of the frequency spectrum, making it smoother. HDF regions for each individual window were defined as LA geometry nodes where DF was within 0.25 Hz of the highest DF measured for that window. The OI

was also measured. The spatiotemporal correlation of HDF areas and rotors was investigated and the OI value was recorded for both in presence and absence of a rotor.

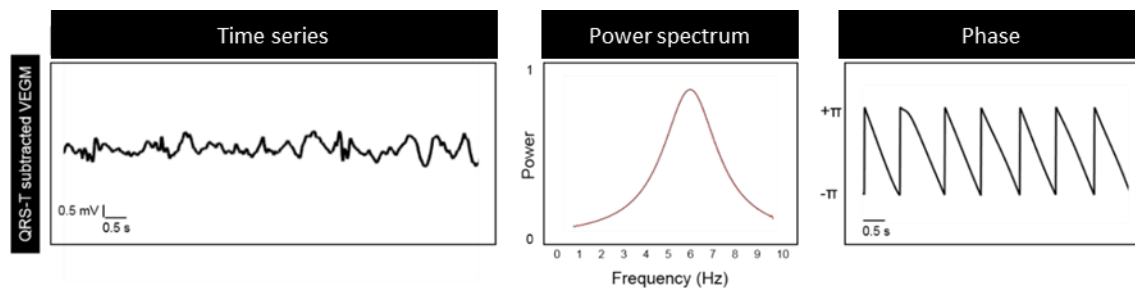


Figure 28: Shows the VEGM of a persAF patient, its frequency spectrum and the phase data extracted from it. The spectra and the phase are further analysed to study the atrial activity and dynamics of the rotor behaviour in the LA.

6.2.6 Radiofrequency ablation

Radiofrequency catheter ablation guided by DF was performed on all patients. Once the primary HDF site was identified, its CoG (Salinet *et al.* 2013c) was determined and ablation started by targeting the CoGs and their trajectory. A post procedure (after DF guided ablation) recording was collected for up to 5 minutes. The MEA was then removed and that was followed by standard PVI.

6.2.7 Statistical analysis

Nonparametric paired multiple data were analysed using the Wilcoxon matched-pairs signed rank test, while nonparametric unpaired data were analysed using the Mann–Whitney test. P-values less than 0.05 were considered statistically significant.

6.3 Results

6.3.1 Spatial distribution of PSs during AF

Figure 29 shows a representative example of one such plot where the cumulative distribution of PSs appearing at any region. Complex clustering of PSs were seen in some instances when the several PSs were detected close to each other. The red coloured bars highlights the region with PSs clustering and provides information about the spatial phase patterns during persAF. For all 10 persAF patients' cases, the number of PSs observed at any instant is shown in figure 32 (a). From our results, in 98.61 % of the time no PSs were observed prior to ablation. Also when PSs appeared, the number of PSs ranged from 1 to 21 at any instant.

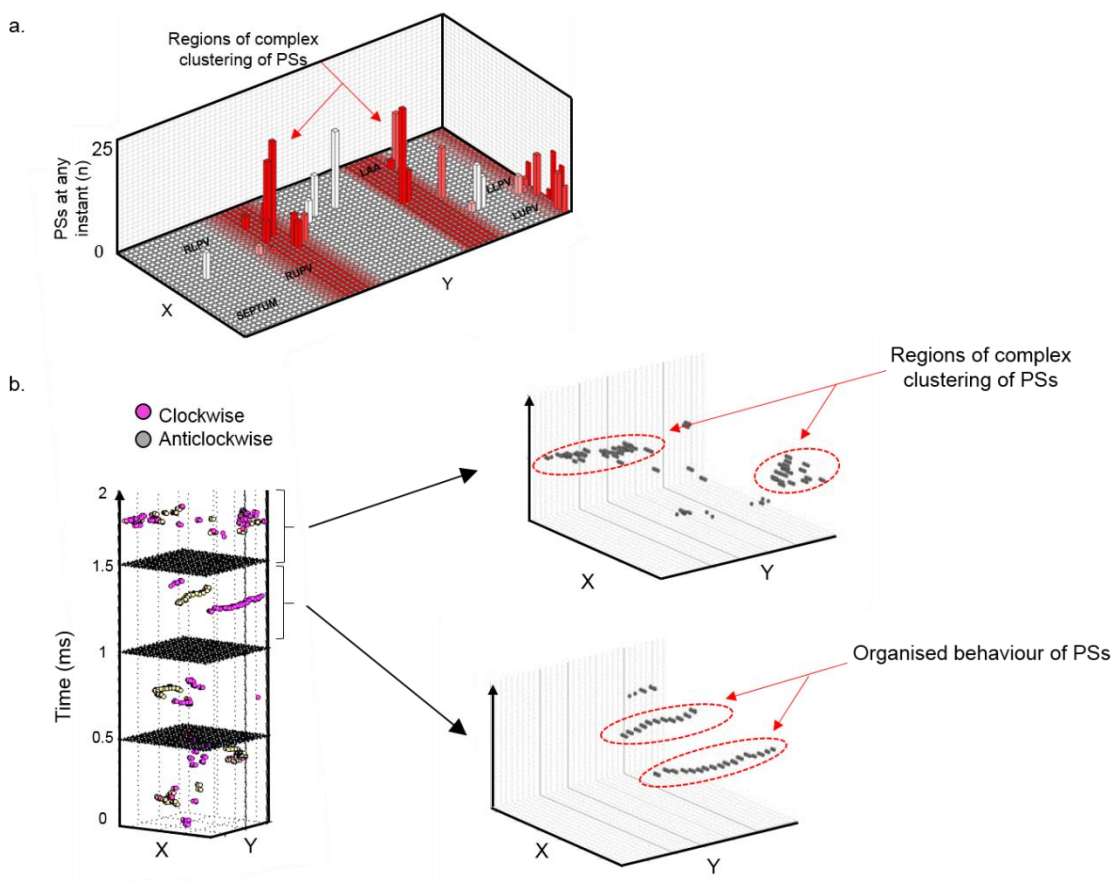


Figure 29: (a) Shows a representative example of one such plot where the cumulative distribution of PSs is shown. (b) Evolution of PSs (and their chirality) over time. In both (a)

and (b) complex clustering of PSs were seen in some instances when several PSs were detected close to each other (highlighted in red).

6.3.2 Analysis of rotor lifespan during persAF

The lifespan of tracked PSs gives an idea about the impact of rotors in the sustenance of this complex arrhythmia. For all 10 patients, figure 32 (b) shows the lifespan of tracked PSs in milliseconds. In total 2573 PSs were tracked. The lifespan distribution was skewed to the left, with 94.79% of tracked PSs lasting less than 100 ms. The mean lifespan of PSs was short, 24.13 ms (IQR: 0.74 ~ 47.52 ms), with a range that varied from 2 to 506 ms. The mean lifespan of the rotors were found 162.05 ± 79.46 ms.

6.3.3 PersAF dynamics and organization

The presence of any persistent or leading rotor(s) coincided with higher atrial activity when compared with the short lived PSs windows (Figure 30).

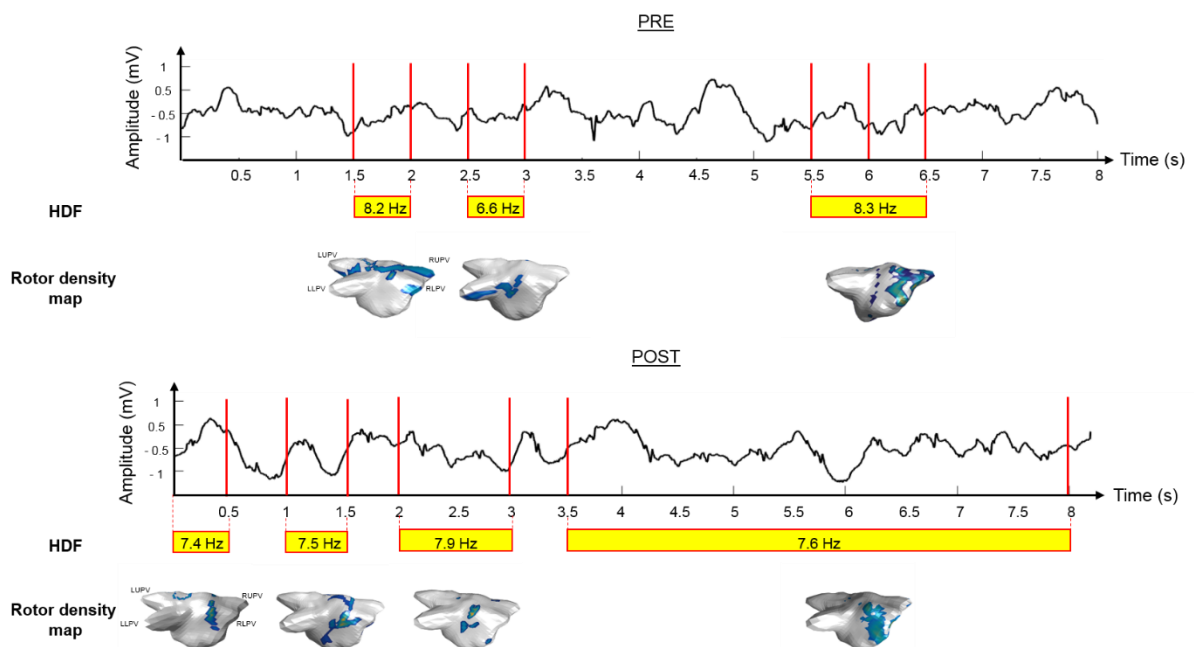


Figure 30: Shows the VEGM and the corresponding HDF value in presence of rotor(s). For the mother rotor fibrillation, the mean HDF is 8.24 ± 0.33 Hz significantly different from short

lived PSs window 7.95 ± 0.42 Hz ($p < 0.0001$) (see figure 33 (a)). The complexity of the FFT spectra as represented by the OI for mother rotor and short lived PSs window were significantly different as well (OI: 0.732 ± 0.05 vs 0.76 ± 0.05 , $p < 0.0001$) (see figure 33 (b)).

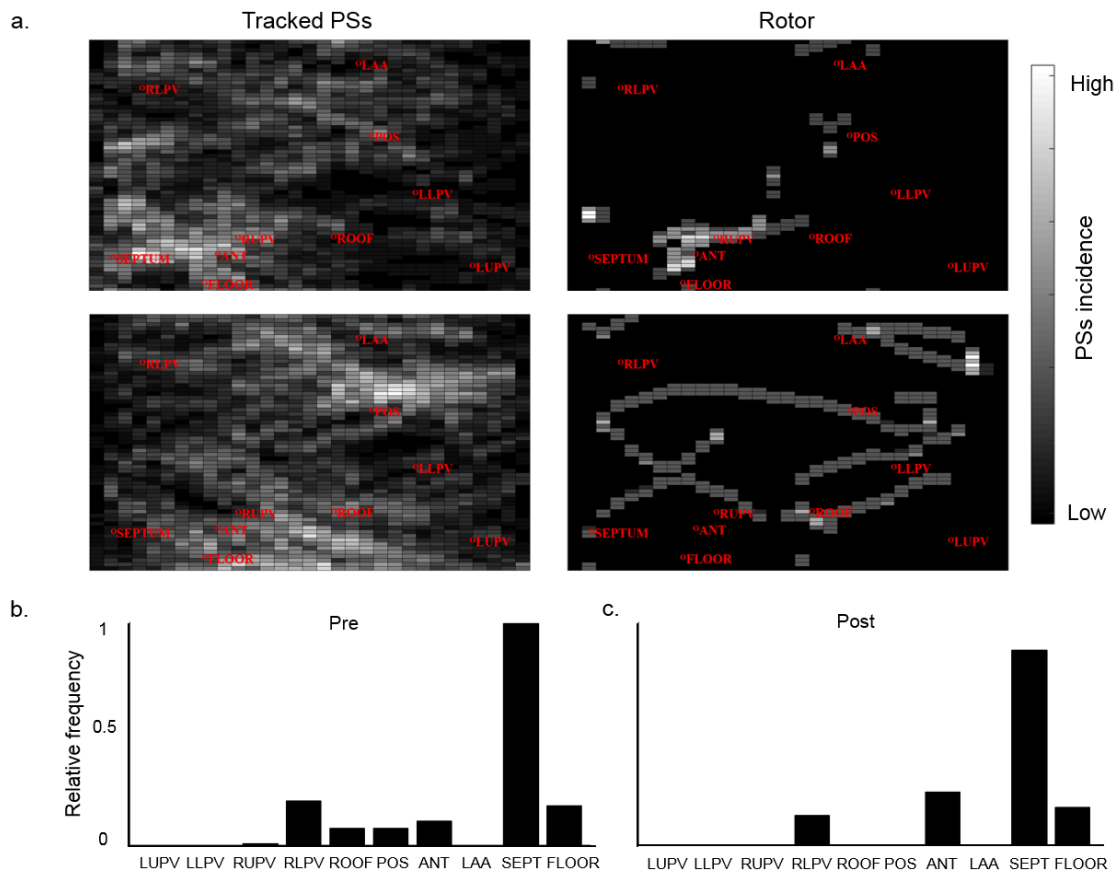


Figure 31: (a) Density maps of short lived PSs vs. rotor. For short lived PSs, a broad distribution of PSs can be seen. (b & c) Locations of rotors in the anatomical regions of the LA for both (b) pre vs. (c) post ablation data. From our results, prior to ablation, rotors were observed in several regions, with the septum having the highest incidence. (LUPV: Left upper pulmonary vein; LLPV: Left lower pulmonary vein; RUPV: right upper pulmonary vein; RLPV: right lower pulmonary vein; POS: posterior wall; ANT; anterior wall; LAA: left atrial appendage; Sept: Septum).

Our results also show the regions where the mother rotors seemed to appear. Histograms for the mother rotor and short lived PSs differed substantially (figure 31 (a)). For short lived PSs, there was a broad distribution of PSs. Although very few rotors had long life spans,

their dynamic behaviour tended to be consistent over time in the similar anatomical regions. From our results, prior to ablation, rotors were observed in several regions, with the septum having the highest incidence, followed by the RLPV, floor, anterior wall, roof and posterior wall and RUPV (figure 31 (b)).

6.3.4 Effect of DF guided ablation on the longstanding rotors

For all 10 patients, after DF guided ablation, in 90.87 % of the time no PSs were observed. Also when PSs appeared, the number of PSs ranged from 1 to 17 at any instant (see figure 32 (a)). The total number of tracked PSs for all patients did not change significantly ($n=2431$), however, the number of rotors increased (pre vs post, $n= 5.21\%$ vs 6.29%) after the ablation. These rotors were seen in more often of windows (pre vs. post, median: 17.5% vs 26.25% ; IQR: $3.75 \sim 50\%$ vs. $12.5 \sim 37.5\%$) when tracked over the same time interval. The mean lifespan of tracked PSs was short, 25.67 ± 35.30 ms, with a range that varied from 2 to 504 ms and the lifespan of the rotors was 153.48 ± 73.52 ms. Although DF guided ablation did not affect the number of rotors significantly, in particular, a significant reduction ($p < 0.0001$) in the number of rotors were more evident in the RUPV, roof and posterior wall and, interestingly, with the highest incidence in the septum.

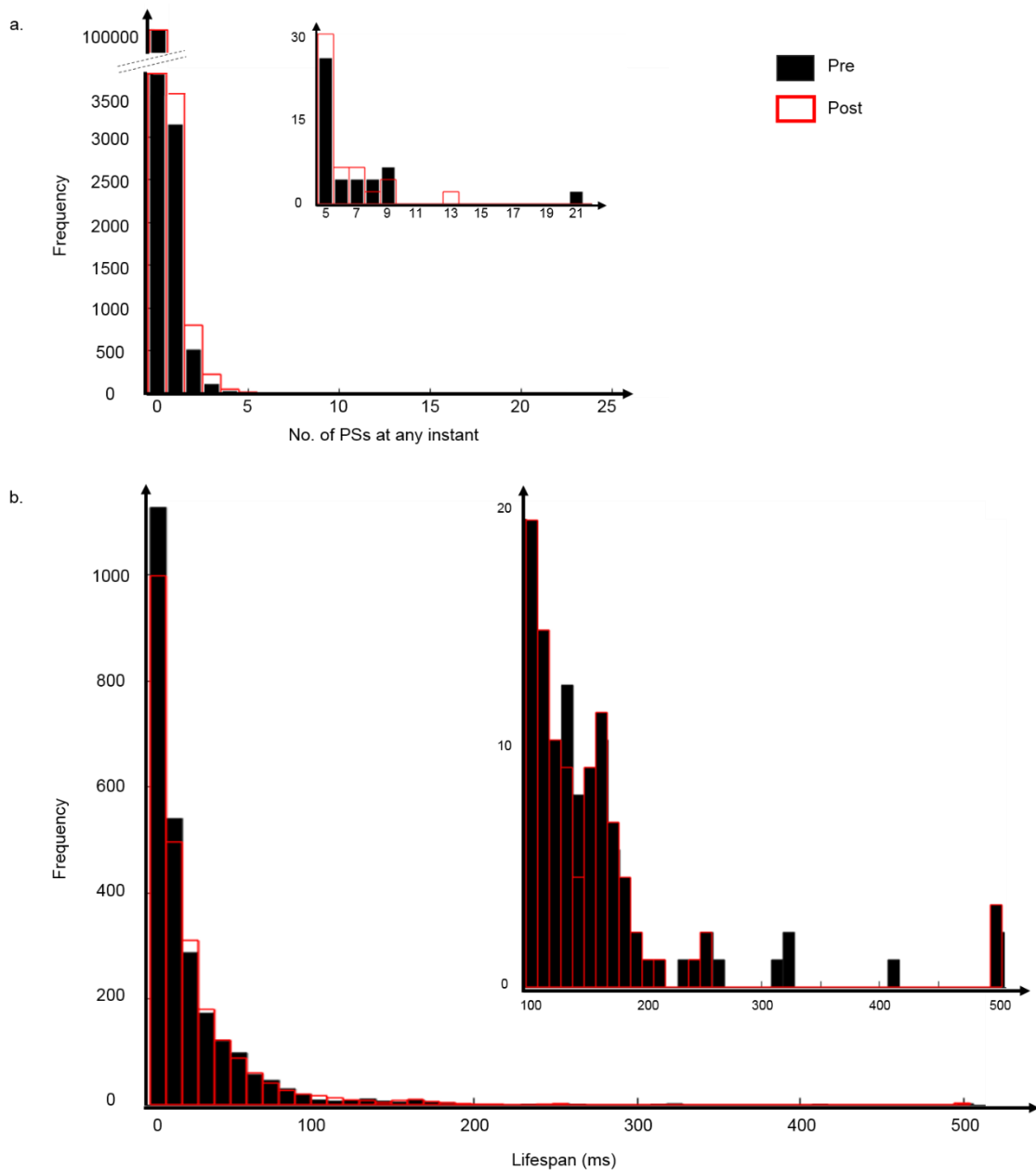


Figure 32: (a) The number of PSs observed (Pre vs Post) at any instant for all 10 persAF patients' cases. (b) The lifespan of tracked PSs (Pre vs. Post) in milliseconds.

Ablation caused significant increases in OI (pre vs.post, rotor window: 0.732 ± 0.05 vs. 0.77 ± 0.04 , $P < 0.0001$; pre vs. post, short-lived PSs window: 0.76 ± 0.05 vs. 0.79 ± 0.03 , $P < 0.0001$) and decreases in HDF (pre vs post, rotor window: 8.24 ± 0.33 Hz vs. 0.79 ± 0.50 Hz, $P < 0.0001$; pre vs. post, short-lived PSs window: 7.95 ± 0.42 Hz vs. 7.73 ± 0.50 Hz, $P < 0.0001$).

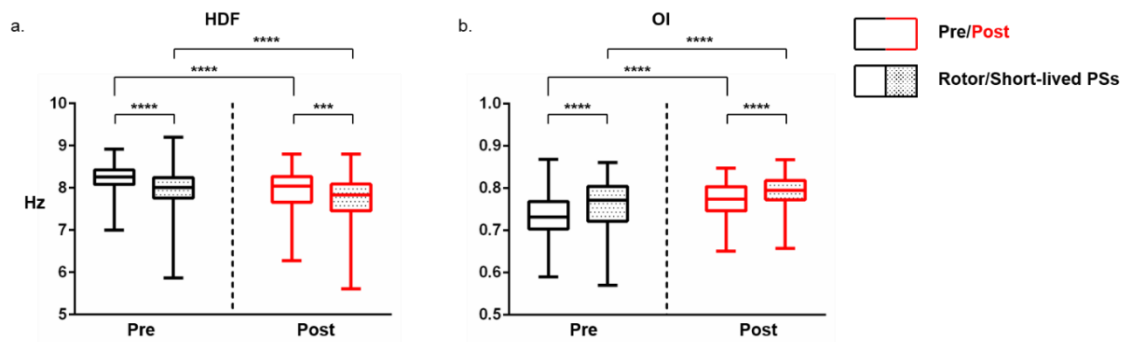


Figure 33: The mean and SD of the (a) HDF and (b) OI of rotor vs short lived PSs (for both pre vs. post ablation data).

6.4 Discussion

PS corresponds to a point that does not have a definite phase while its neighbouring sites exhibit phases that change monotonically from $-\pi$ to $+\pi$. Therefore, phase mapping illustrates the excitation recovery cycle, highlights the sequence of activation and allows the quantification of rotor dynamics. Some studies support a major role for rotors as the drivers of cardiac fibrillation, in both animal models and in humans, as the excitations are believed to rotate around a PS which acts as a pivot point (Winfree 1978). However, researches have been showing contradictory roles of rotors in persAF (Allessie and de Groot 2014, Narayan and Jalife 2014). Therefore initiation, maintenance and termination of PSs should be understood first, before an adequate strategy for treatment of persAF can be designed based on rotor ablation.

The spatial distribution of the PSs corresponds to a wave-break point (Winfree 1989, Cabo *et al.* 1996, Gray *et al.* 1998, Chen *et al.* 2000) and causes ever-changing activation patterns that characterize fibrillation (Valderrábano *et al.* 2003). According to the multiple wavelet hypothesis, fibrillation is maintained by spontaneous wave breaks that constantly generate randomly wandering daughter wavelets (Moe 1962). For all the patients, prior to ablation, up to 21 PSs were observed at any instant. Formation of pairs of PSs was also observed. Among the total time of PSs appearing at any particular instant, paired PSs seemed to

appear 54.6 % of the time. This dynamic behaviour of PSs suggests that the wave breaks were non-randomly distributed and reflects the waves propagation as a result of processes of excitation, recovery and diffusion (Gray *et al.* 1998). Each PS was subsequently present in vicinity of other PSs and therefore tracking them in space and time led to identification of rotors around which the wavelets are understood to hinge and give rise to spiralling wave fronts (Winfree 1978).

6.4.1 Characterizing long-lived PSs

In figure 27, the X and Y locations of two long-lived PSs of opposite chirality (pink and grey shaded circles) can be observed from the time of their initiation until termination. Lifespan histograms for tracked PSs indicate that the majority (pre vs. post, median: 3.21 % vs. 5.34 %; IQR: 0.85 ~ 5.32 % vs. 7.00 ~ 15.25 %) of PSs lasted less than 100 ms.

The rotor density map gives an idea about the distribution of the rotors in the LA and illustrates their wandering behaviour. Although very few rotors had long life spans, their dynamic behaviour tended to be consistent over time in the similar anatomical regions. Our results suggest that, over the 20 s interval, there was evidence of anatomical determinism in all the 9 patients who frequently re-formed at the same anatomical location with the septum being the most visited region. Kumagai and colleagues (Kumagai *et al.* 1997) concluded that unstable re-entrant circuits, principally involving the septum, appeared to be important for the maintenance of AF. Another study (Ideker and Huang 2005) on fibrillation stated that a possible common location of the mother rotor is at the region where the posterior free wall intersects with the septum. They concluded that that region is the fastest activating region and that it gives rise to activation fronts that lead to fibrillation.

Wharton (2001) (Wharton 2001) stated that if the appropriate substrate is not present, AF once initiated will not be maintained and will spontaneously terminate. Though our results show that when rotors reappeared, they re-formed at the same preferential spatial sites and had no temporal stability. In 2014, Jarman *et al.* (Jarman *et al.* 2014) reported that transient

organization of activation may occur probabilistically and that organized regions would not be expected to have temporal stability if underlying activation was truly random. This shows that rotors are not the only mechanism sustaining AF and, at times, they coexist with other mechanisms.

In the majority of instances PSs were not observed at all. And when observed, they had a propensity to drift about the surface of the LA and frequently they were not long-lived rotors. However, when tracked, rotors exhibited meandering behaviour, were rarely stationary from frame to frame and the areas of the atrium with rotors were activated at high rates and with lower organization.

6.4.2 Long lived PSs and their organisation

Fibrillatory activity may be caused directly by multiple functional re-entry circuits varying in time and space (Allessie *et al.* 1996). From our results, presence of any intermittent or spatially stable rotor contributed to the multiple components in the frequency spectra (lower OI), i.e. less organised electrograms. This suggests, the presence of multiple sources which could be the cause of multiple peaks in the frequency spectra and also supporting the idea that rotors are not the exclusive mechanism in persAF.

6.4.2.1 Effect of DF guided ablation

DF guided ablation made persAF evolve into a slower atrial arrhythmia (from ~ 8.03 Hz to ~ 7.77 Hz) and with increased organization of the VEGMS (from ~ 0.75 to ~ 0.79). High OIs indicate increased AF organization and a smaller number of wavelets (Everett *et al.* 2001). DF guided ablation also resulted in significant reduction ($P < 0.0001$) (be consistent. All your Ps should be either capital P or small-case p. I prefer capital) in the number of rotors in the RUPV, roof and posterior wall, despite the overall increase in number of rotors. Interestingly, the highest incidence of rotors observed was still in the septum and therefore, it is possible that the secondary AF drivers were eliminated and consequently, the effect of initial/dominant rotors became more marked. Studies, have also shown that, structural

remodelling of the heart has been shown to interfere with rotor behaviour (Vaquero *et al.* 2008). Regions of fibrosis may anchor fibrillatory rotors and it has been demonstrated that meandering rotors can become transiently or permanently trapped by abrupt discontinuities in the fibre architecture (Gonzales *et al.* 2014). This could explain why, despite dynamic movement of the rotors, they re-formed at the same anatomical location. Rotors had not been demonstrated directly in human AF (Vaquero *et al.* 2008) until recent advances in wide-area contact mapping and computational analysis (FIRM); however, they were indirectly supported by animal studies and some clinical analyses. Thus, the question about rotors is whether they are active drivers of fibrillation or simply represent a passive phenomenon, and the answer to that question is still unclear.

6.5 Conclusions

PersAF is being recognized increasingly as a deterministic process resulting from multiple mechanisms, such as rapidly firing foci and fibrillatory conduction, rather than a fundamentally turbulent and self-sustaining process. In the present study, we evaluated the spatiotemporal dynamics of the PSs based on the atrial VEGMs collected using noncontact mapping. PSs showed different behaviour spatially and had varying life spans. In our database, rotors were not seen very often (17.5 % of the time). They continually switched between organized and disorganized behaviours. DF guided ablation did not have a significant effect on the number of tracked PSs (pre vs. post, n= 2573 vs. 2431), however, the number of rotors increased (pre vs. post, average: 5.05 % vs. 6.34 %). Transient rotors were found in majority of mapped regions, are spatiotemporally associated with higher atrial rate as well as disorganised electrograms, and, when recurrent, demonstrate anatomical determinism.

Chapter 7

Combination of Frequency and Phase to Characterise the Spatiotemporal Behaviour of Cardiac Waves during Persistent Atrial Fibrillation in Humans

7.1 Introduction

Cardiac dysrhythmia can be due to abnormal function of the SA node or it can arise from other areas which normally do not initiate electrical impulses. AF is a very rapid, chaotic rhythm, which makes the atria and the ventricles beat irregularly. The state of AF is generally reflected using time domain analysis such as heart rate and in the shape of the ECG (absence of P waves and irregular oscillations of the baseline). VEGMs recorded from patients with persAF are the electrical recording of the LA which represent voltages on the inner surface of the LA. VEGMs contain important pointers to the nature of diseases afflicting the heart. As an alternative to time domain analysis of the atrial period during AF, frequency domain and phase analysis of atrial signals are also useful to investigate the characteristic of AF electrograms, as they provide different perspectives of how atrial activation behaves. As AF develops there are also some advancements in some factors (trigger and substrate) that help sustaining it. In case of pAF, it is the dominance of triggers that maintains it, whereas in case of persAF it is both the triggers and substrate modulation which maintain it and finally in permanent AF it is the predominance of only substrate modulation which is maintaining AF (Figure 34) (Wyse and Gersh 2004). In this chapter the combination of frequency and phase analysis of persAF signals is studied to try to help elucidate the mechanism of wave propagation and the identification of the drivers and characterisation of their dynamics, which could help to develop patient-specific ablation strategies.

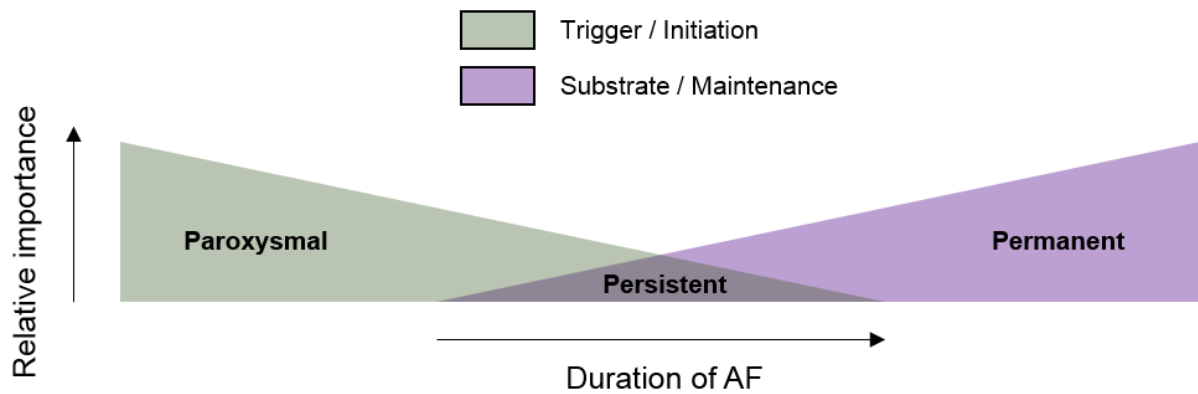


Figure 34: The figure shows the relative importance of factors that maintain the paroxysmal, persistent and permanent AF (pAF, persAF and permanent AF respectively). For pAF, it is the triggers; for persAF, it is combination of both triggers and substrate modification; for permanent AF, it is only the substrate modification which is sustaining AF.

7.2 Methods

7.2.1 Patient characteristics

This study included 10 male (36.1-76.4 years old) persAF patients with AF duration ranging from 132 to 848 days, who underwent their first procedure of catheter ablation under the guidance of 3D mapping system (Ensite Velocity, St. Jude Medical). The study was approved by the local ethics committee and all procedures were carried out after informed consent.

7.2.2 Electrophysiological set-up and electro-anatomical mapping

All antiarrhythmic drugs, except amiodarone, were discontinued for at least 5 half-lives before the start of the procedure. 3D EAM was performed in all patients. The details of the mapping procedure have been described in chapter 2.

7.2.3 Data acquisition and signal processing

The intracardiac signals were collected using MEA. VEGMs (2048 channels) were sampled at 2034.5 Hz and exported using the filter setting of 1 Hz to 150 Hz. The data were analysed offline using Matlab (Mathworks, USA). The VEGMs were resampled at 512 Hz using cubic

spline interpolation method to reduce processing time while maintaining a relatively high sampling rate for the frequency analysis. Ventricular far-field activity was removed from the recorded VEGMs using a QRST subtraction technique previously described (Ahmad *et al.* 2011, Salinet *et al.* 2013a). The VEGMs were then divided into 4 seconds long window segments with a 50 % overlap. For each segment, spectral analysis was performed using FFT. Hamming window was applied to the atrial VEGMs to reduce leakage. Zero padding was used to improve the DF identification with a resulting frequency step of 0.05 Hz. DF was defined as the peak in the power spectrum within the physiological range of 4 - 10 Hz (Salinet *et al.* 2013c).

7.2.4 Highest dominant frequency (HDF)

HDF regions for each individual window were defined as LA geometry nodes where DF was within 0.25 Hz of the highest DF measured for that window. These regions are considered to represent sites maintaining the persAF arrhythmia. Therefore, the area of a HDF forms a 'cloud' which is assumed to represent the AF activity for that region (Salinet *et al.* 2013c). In order to understand the trajectory of the HDF regions, the CoG of the HDF 'clouds' were determined by averaging the coordinates of each one node in the 'cloud' weighted by their DF values (Salinet *et al.* 2013c). These CoGs were acquired for every 4 seconds FFT window with 50 % overlap over a 75 seconds interval.

7.2.5 Phase and phase singularity points

To obtain the phase we applied Hilbert transform to produce analytical signals from the unipolar signals obtained from the VEGMs collected from the persAF patients. A phase singularity is a spatial point where all phase values converge and may be localised through calculation of the topological charge, n_t , as defined in chapter 5. The sign of the topological index derived corresponds to the chirality of the PS. This is the direction in which the associated wave front circulates about the PS point (clockwise or counter-clockwise).

7.2.6 Combining highest DF, phase maps and PS points

To study the spatiotemporal relationship between PSs and HDF, we projected the PSs and HDF on phase maps (Figure 35), and investigated the PSs and HDF distribution at regions of the LA along time. In this study, for 75 seconds of recording we analysed 37 HDF windows and 38400 phase maps corresponding to each patient. Algorithms were developed that automatically reported the PSs number of each frame in the phase map and automatically localised the PSs in the phase map. The HDF sites in each frame were also identified automatically.

To understand the co-localisation of HDF sites with PSs, the corresponding maps of cumulative PSs inside the HDF region were combined. To describe quantitatively the non-localisation or overlapping between the cumulative maps of HDF sites and PSs in corresponding frames, we calculated the spatial shifts, i.e., the median distance (as well as the IQR) between the COG of the HDF site with every PSs (37 windows per patient, total 370 windows). Median distance and IQR have been used as a better representative of distance as the number of PSs are large and many PSs have been observed to lie at a far distance from the nearest CoG.

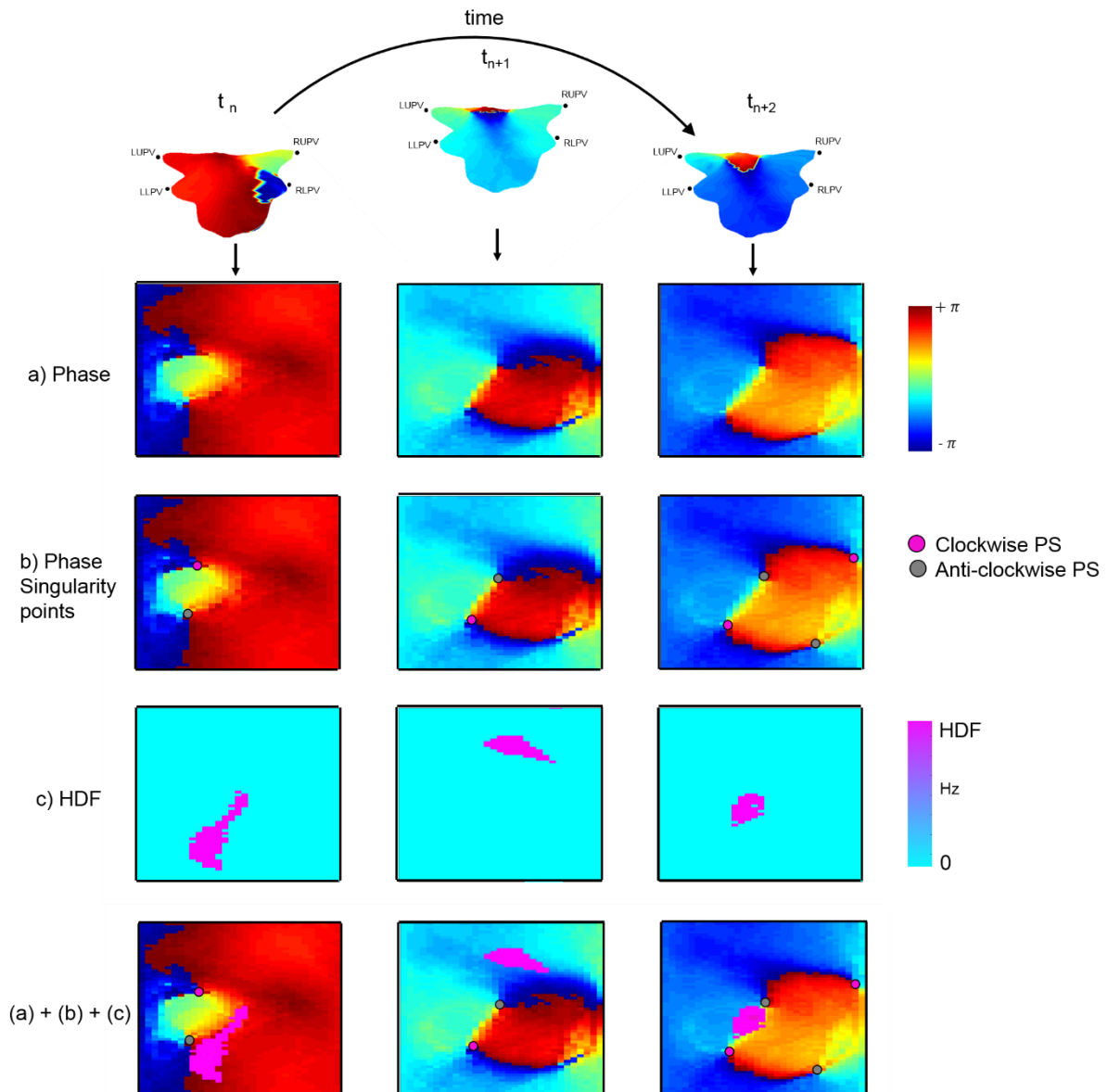


Figure 35: Illustration of the parameters characterising the atrial substrate. For one patient corresponding (a) phase, (b) PSs, (c) HDF and all the parameters combined for three different instances are shown in order to study the spatiotemporal relationship between among them.

7.2.6.1 Analysing spatiotemporal behaviour

Previously, we reported on the stability of HDF in persAF and that study offered a wider perspective about the movement of the HDF 'clouds' illustrating that they are temporarily unstable (see chapter 4) (Figure 36).

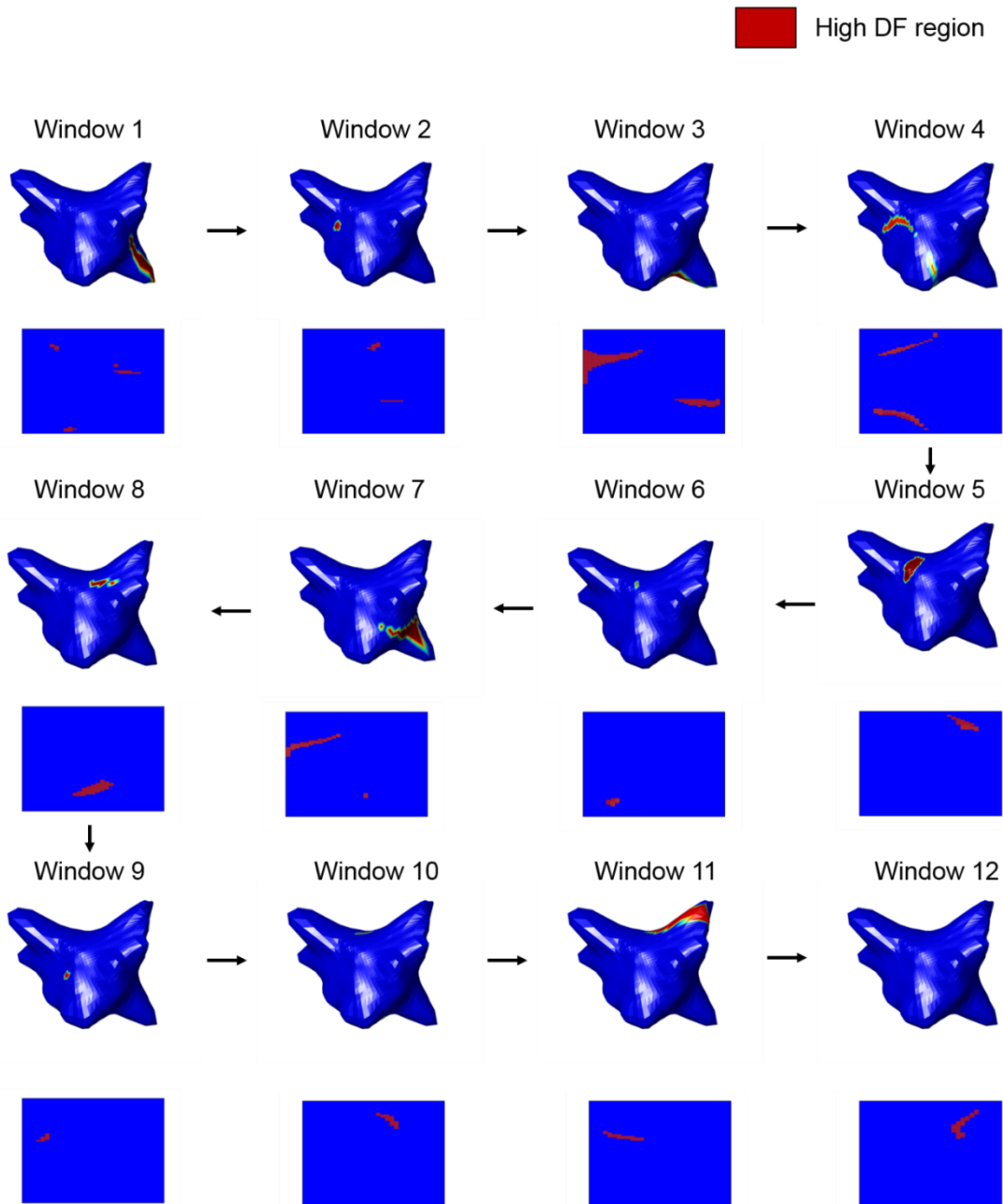


Figure 36: Illustration of corresponding 3D and 2D HDF maps for one patient for several windows. It can be seen that the HDF regions are not consistent in every window and that sometimes they reoccur in the same region after a certain while.

In this study we focused more on verifying if there is a spatiotemporal correspondence between PSs and HDF by analysing its density maps. We created an algorithm to investigate if the dense PS sites spatially correlated with the HDF

sites. It was concluded, in chapter 4, that HDF density maps produced from any random segment of VEGM recording of 75 seconds could potentially indicate consistent locations of the dense regions and may represent the individual drivers that are believed to mechanistically sustain persAF. PSs were accordingly identified for the same time period and their respective density maps were produced for comparison. In total, 70 pairs of PSs and HDF density maps were studied.

7.2.6.2 Spatiotemporal clustering of PSs

Trajectories describe the movement behaviour of PSs, and therefore clustering can be used to represent groups of PSs that appeared within a similar space and time. For instance, it is applied on PSs of similar chirality who are moving consistently together (may be in different time periods). Therefore, spatiotemporal clustering, i.e., clustering PSs based on their spatial and temporal similarity was performed (Figure 37) and the instances of PSs of opposite chirality appeared around the HDF were observed for all windows at the instant of time when the wave fronts of the two oppositely rotating wavelets propagate between the PSs.

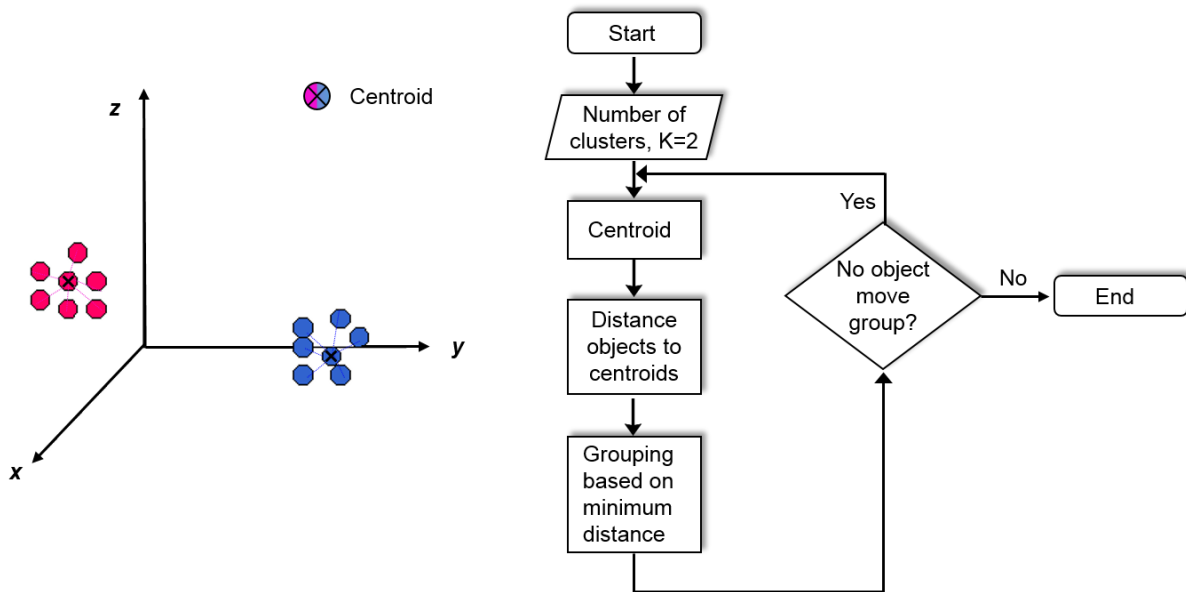


Figure 37: Illustration of how K-Means clustering algorithm. The algorithm depends on the assignment of information to a given set of partitions also known as cluster centres or the K centroids. In this study, it was defined as 2 (clockwise and anticlockwise centroids). At every step of the algorithm, each data value is assigned to the nearest centroid based on some similarity parameter that is calculated using Euclidean distance measurement. Then, the centroids are recalculated based on these hard assignments. With each successive pass, a value can change the centroid it belongs to, thus altering the values of the centroid at every pass.

7.2.6.3 Characterisation of HDF and PSs density maps

To investigate further the underlying behaviour of the density maps of the HDF and PSs, the dense regions of both the maps were characterised. The nodes in the LA were divided into groups by application of an appropriate density threshold. When a density threshold is specified, the density map shows only colours for density values above 100% minus the threshold. The threshold is specified as a percentage of the height of the colour bar (see figure 38). Thus, with a threshold of 25 %, the density maps will show the upper quarter of the colour bar. Note that a threshold of 100 % the map shows all the dense regions.

The following illustration (figure 38) shows the colour bars with thresholds set at 100 % (T_{100}), 75 % (T_{75}), 50 % (T_{50}) and 25 % (T_{25}) (from left to right). The cumulative history colour bar is the same, except the bottom colour will be the trace background colour. Accordingly, for each threshold, the OI values were obtained and compared.

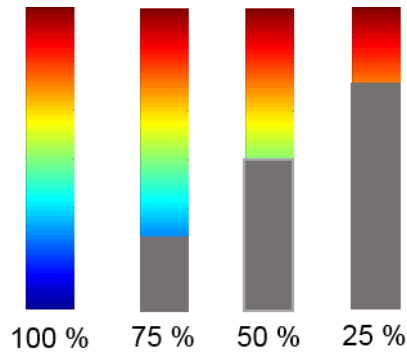


Figure 38: The illustration shows the colour bar of the density map with threshold set at 100 %, 75 %, 50 % and 25 % (from left to right). The cumulative history colour bar is the same except the bottom colour will be the trace background colour.

7.3 Results

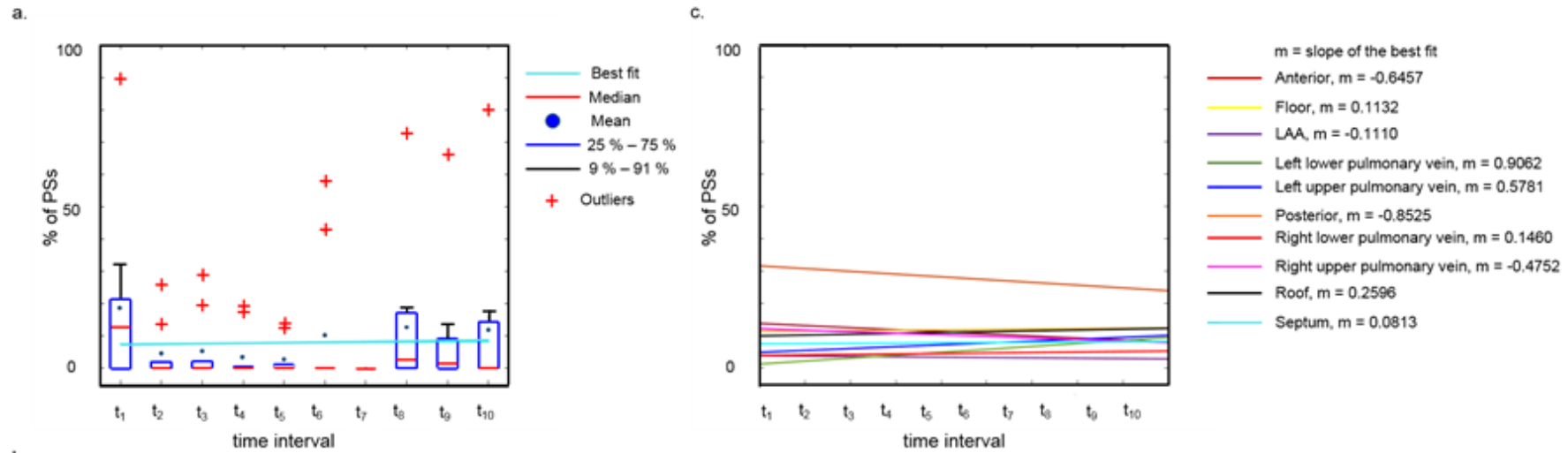
7.3.1 Observing behaviour of HDF and PSs spatiotemporally

7.3.1.1 Temporal correlation between PSs and LA regions

To study the temporal correlation between PSs and LA sites, we systematically tracked over consecutive time frames of two seconds in order to understand their behaviour and co-localisation. The first 20 seconds of persAF event were used for analysis in every patient. Figure 39 (a) shows a box plot of the cumulative number of PSs (for all 10 patients) appearing over time in one region (septum) of the LA. Except for the posterior wall and the right upper pulmonary vein region, no significant changes (P valued based on Friedman test) in the percentage of PSs were observed appearing at any other region at any interval (anterior, $P = 0.5853$; floor, $P = 0.8632$; LAA, $P = 0.2709$; left lower pulmonary vein, $P =$

0.3341; left upper pulmonary vein, $P = 0.7450$; posterior wall = 0.031^* ; right lower pulmonary vein, $P = 0.2951$; right upper pulmonary vein, $P = 0.0443^*$; roof, $P = 0.5839$; septum, $P = 0.2079$) and hence remained consistent (using linear regression) in all the patients (Figure 39 (c)), indicating a temporal correlation between regions of LA and the PSs.

The PSs seemed to have visited all the regions of the LA: posterior wall (mean \pm SD) ($24.42\% \pm 5.16\%$), floor ($16.06\% \pm 5.55\%$), right upper pulmonary vein ($10.83\% \pm 3.73\%$), anterior wall ($10.78\% \pm 3.80\%$), roof ($9.84\% \pm 3.59\%$), septum ($8.37\% \pm 3.85\%$), other PVs ($5.46\% \pm 2.87\%$), and LAA ($3.30\% \pm 1.99\%$). Therefore, in 20 seconds long segments of persAF recordings, the most preferential areas visited by the PSs were the posterior wall and the floor of the LA, with highest incidence of PS points compared with the remaining LA areas. RUPV and anterior wall of the LA presented almost half the incidences of PSs.



b.

	t_1	t_2	t_3	t_4	t_5	t_6	t_7	t_8	t_9	t_{10}
	(n, mean \pm SD, %)									
Anterior	16.19 \pm 24.38	9.49 \pm 13.28	11.57 \pm 21.06	11.74 \pm 20.29	5.62 \pm 7.48	10.81 \pm 10.46	27.83 \pm 37.73	3.57 \pm 5.60	7.01 \pm 11.63	4.77 \pm 7.87
Floor	9.87 \pm 1.65	11.98 \pm 3.23	3.93 \pm 1.45	6.87 \pm 1.45	9.38 \pm 3.15	28.13 \pm 3.25	3.77 \pm 1.69	10.44 \pm 1.35	9.95 \pm 1.30	5.68 \pm 3.88
LAA	8.36 \pm 21.33	0.51 \pm 1.17	2.99 \pm 4.29	0.92 \pm 1.49	0 \pm 0	11.13 \pm 18.76	0.8163 \pm 2.58	0.39 \pm 0.89	4.27 \pm 7.61	3.65 \pm 6.75
Left lower pulmonary vein	1.04 \pm 2.37	2.13 \pm 5.69	2.11 \pm 4.46	3.39 \pm 4.35	10.79 \pm 25.13	1.53 \pm 4.87	10.3 \pm 18.26	1.12 \pm 2.25	8.98 \pm 11.46	11.59 \pm 27.27
Left upper pulmonary vein	5.34 \pm 11.33	2.36 \pm 5.31	10.99 \pm 18.15	1.48 \pm 2.41	4.00 \pm 8.68	11.25 \pm 14.80	16.71 \pm 31.27	3.78 \pm 11.96	12.02 \pm 24.42	6.56 \pm 9.39
Posterior	22.69 \pm 32.02	30.76 \pm 19.93	25.34 \pm 21.50	34.80 \pm 24.69	45.40 \pm 30.29	25.34 \pm 26.60	18.89 \pm 28.59	38.12 \pm 21.55	19.82 \pm 13.29	16.04 \pm 9.39
Right lower pulmonary vein	1.91 \pm 5.21	7.29 \pm 13.69	8.30 \pm 18.29	2.82 \pm 5.27	1.16 \pm 2.78	2.46 \pm 7.79	0 \pm 0	8.37 \pm 12.57	10.10 \pm 19.19	3.16 \pm 8.58
Right upper pulmonary vein	9.27 \pm 11.17	9.76 \pm 11.84	12.27 \pm 18.41	19.14 \pm 17.05	6.24 \pm 7.79	9.65 \pm 17.89	5.37 \pm 11.48	18.58 \pm 12.86	4.91 \pm 8.81	5.03 \pm 6.39
Roof	7.69 \pm 16.99	14.78 \pm 22.87	13.64 \pm 11.32	9.71 \pm 13.69	10.75 \pm 18.43	8.55 \pm 13.35	9.19 \pm 15.85	5.42 \pm 10.50	9.82 \pm 25.66	21.29 \pm 29.27
Septum	18.56 \pm 27.29	4.14 \pm 8.71	5.09 \pm 10.34	3.69 \pm 7.65	2.59 \pm 5.14	10.01 \pm 21.42	0 \pm 0	12.49 \pm 22.35	9.91 \pm 20.27	11.85 \pm 24.86

Figure 39: (a) shows box plot of the cumulative number of PSs (for all 10 patients) appearing over time in the septum of the LA. (b) Summary showing the mean and SD of the number of PSs appearing at each region every two seconds. (c) Shows the best fit line for all the regions and the corresponding slope (m) value of the best fit.

7.3.1.2 Spatiotemporal behaviour of HDF and PSs

Comparing the density maps of HDF and PSs gives an overall summary of the spatiotemporal behaviour. For every patient, creating PS density maps using any random segment of 75 seconds produced very similar maps (SSIM: 0.89 ± 0.07) and demonstrated preferential areas where PSs appear more often (as highlighted in the previous section). The corresponding HDF density map when compared to the PS density map interestingly also showed similarity among them (SSIM: 0.76 ± 0.12). Some examples of the corresponding HDF and PSs density maps are presented in Figure 40 for three different patients.

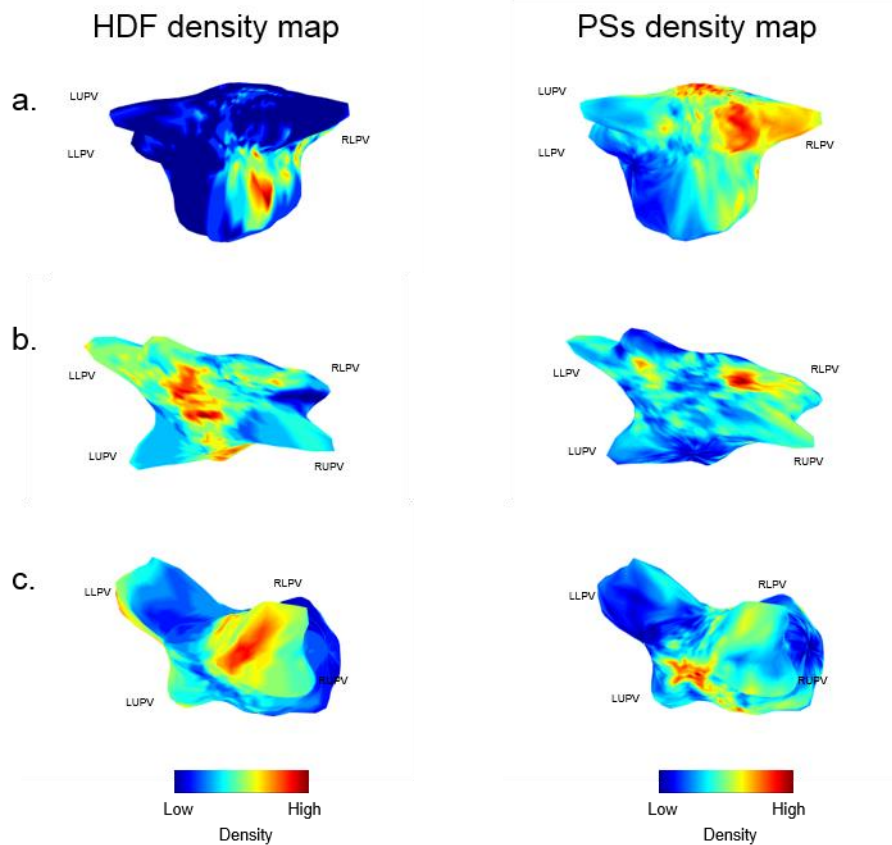


Figure 40: Comparison of the density maps of HDF and PSs to understand the overall summary of the spatiotemporal behaviour for three different patients, a, b and c.

7.3.2 Correlation between HDF sites and PSs

Spatial correspondence is referred when a HDF site overlaps with the PS map for the same time segment. To study the spatial correlation between HDF sites and PSs in depth, we superimposed the PSs and HDF for every 2 seconds frames from each patient to construct spatial maps of the HDF sites (bars) and PSs (coloured region) (Figure 41). HDF regions and highest PS occurrence did not overlap (Wilcoxon rank sum test, $P < 0.0001$). As discussed in chapter 6 that PSs drifts over the LA area, the median distance of PSs with respect to the HDF site was therefore studied. The spatial shifts, i.e., the median distance between the CoG of the HDF site with every PSs (for 37 windows per patient) were 40.32 mm (IQR: 29.59 ~ 51.02 mm). Therefore, HDF sites displaying lower degree of co-localisation with PS regions.

As mentioned earlier, in chapter 5, PSs were identified according to their chirality and also that they frequently appear in pairs, the observation of PSs not being spatially anchored at particular HDF sites let us further investigate the distribution of clockwise and anticlockwise PSs with respect to the HDF region. The spatiotemporal clustering - trajectory, provides an overview of how PSs of opposite chirality were distributed both in space and time in relation to the HDF site. It was observed that PSs have the tendency to gather separately from the PSs of opposing chirality (Figure 42 (b)). The median distance between the CoG of the HDF site with every clockwise and anticlockwise PSs (for all the patients) were 40.29 mm (IQR: 30.41 ~ 50.09 mm) and 31.99 mm (IQR: 36.47 ~ 41.79 mm) respectively (see Table 6).

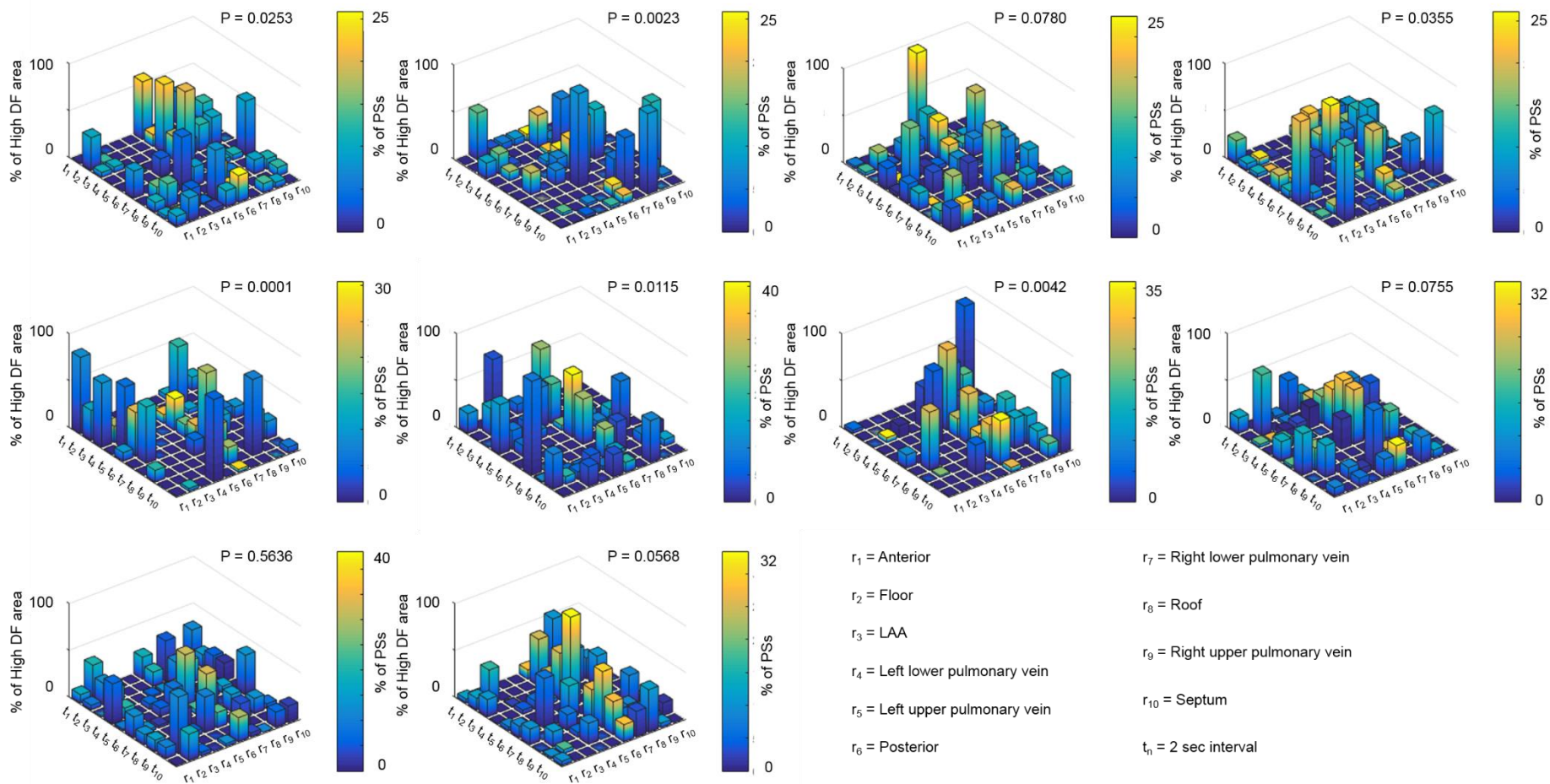


Figure 41: Shows HDF and PS detection in several regions of LA in corresponding frames.

Table 6: Summarises the spatial shifts of all the PSs from the HDF region in all corresponding frames for all the 10 patients.

PSs	Irrespective of chirality			Clockwise			Anticlockwise		
Patient	(Distance (mm), 25 th percentile, median, 75 th percentile)								
1	29.99	40.69	51.86	29.29	40.72	50.59	29.42	41.33	53.17
2	33.26	45.43	56.60	35.66	46.03	54.34	36.47	48.79	58.78
3	32.42	43.30	54.59	33.89	44.06	53.18	32.37	41.47	51.14
4	26.08	34.94	44.45	26.10	34.95	43.78	26.10	34.90	45.78
5	31.48	41.39	50.29	33.16	41.10	48.88	32.95	41.86	49.79
6	29.18	39.18	51.87	29.92	40.36	51.04	28.42	38.81	51.33
7	29.42	40.82	49.83	31.26	39.57	49.29	30.22	40.50	49.08
8	29.41	39.55	50.53	28.76	39.74	49.59	34.49	42.74	50.72
9	28.33	39.14	49.27	28.49	38.86	48.62	28.49	38.86	48.62
10	27.32	38.72	50.99	27.63	37.50	51.64	28.73	38.66	46.97

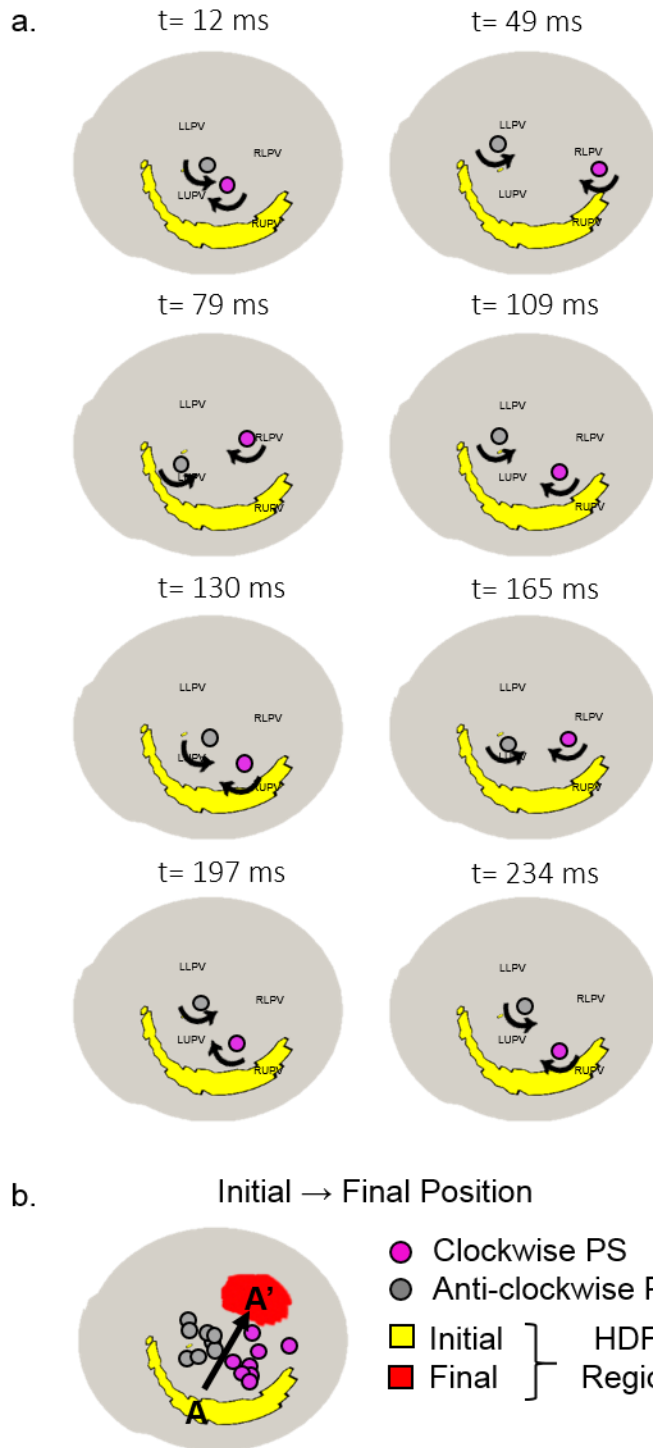


Figure 42: (a) shows an example of the PSs clustering appearing around a HDF cloud in a consecutive interval of time. The arrows indicate the propagating waves travelling across the atria giving rise to fibrillatory conduction and (b) they seem to be related to the drift direction of the HDF 'clouds' (see chapter 8).

7.3.3 Comparing OI values of the PSs and HDF density maps

The HDF and OI value of the LA (before ablation) ranged from 5.25 Hz to 8.4 Hz (mean \pm SD, 6.44 ± 0.61 Hz) and 0.11 to 0.97 (mean \pm SD, 0.52 ± 0.16 Hz) for this cohort of patients. The OI value of the dense regions of the HDF and PSs are further divided into groups according to their density (mean \pm SD: HDF density map, $T_{100} = 0.34 \pm 0.14$, $T_{75} = 0.35 \pm 0.14$, $T_{50} = 0.34 \pm 0.13$, $T_{25} = 0.36 \pm 0.014$, PSs density map, $T_{100} = 0.35 \pm 0.14$, $T_{75} = 0.35 \pm 0.15$, $T_{50} = 0.36 \pm 0.15$, $T_{25} = 0.34 \pm 0.15$).

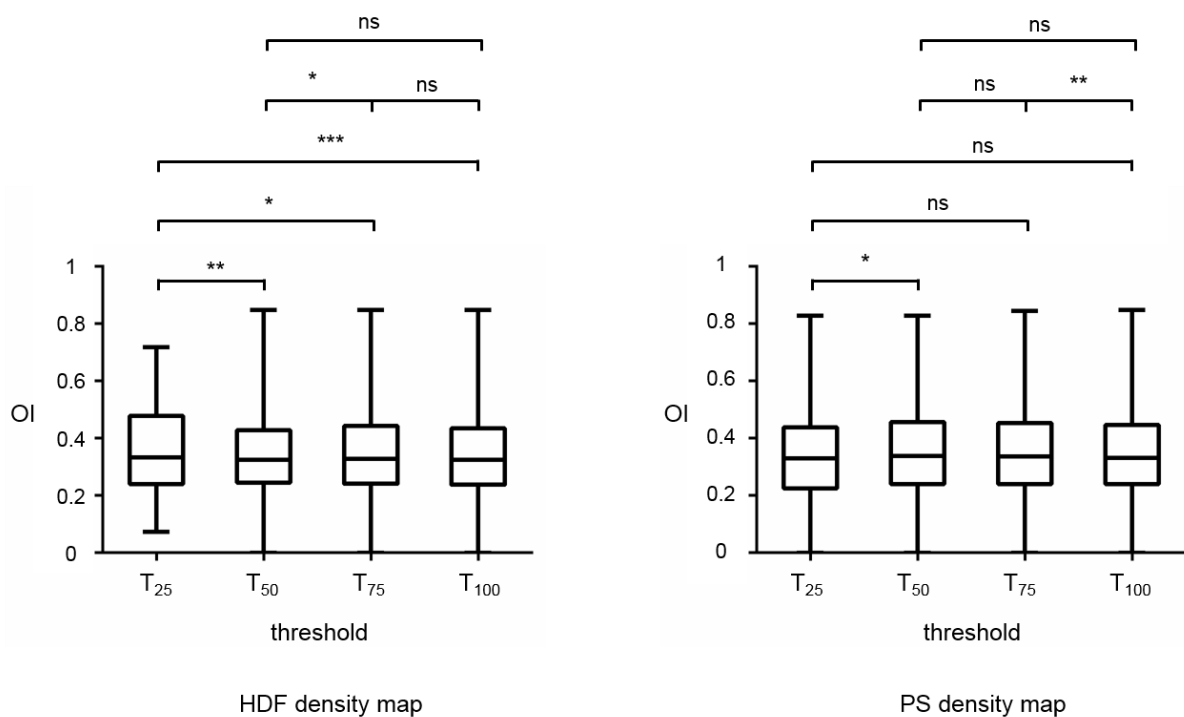


Figure 43: The mean and SD of the OI value for HDF and PS density map with change in density threshold set at 100 % (T_{100}), 75 % (T_{75}), 50 % (T_{50}) and 25 % (T_{25}).

7.4 Discussion

AF results in the absence of normal atrial contractions (Van Gelder and Hemels 2006). Although catheter ablation of AF is an effective rhythm control strategy, the recurrence rate is significant (Van Gelder *et al.* 1996). The mechanism of this disease is still poorly understood, and two major theories exist: the focal source hypothesis (Lloyd-Jones *et al.*

2004) and the multiple wavelet hypothesis (Wolf *et al.* 1991, Benjamin *et al.* 1998). Power spectral techniques provide the frequency content of the signal. However, the frequency content does not represent a complete characterisation of the dynamic AF substrate (Gutbrod *et al.* 2015). On the other hand, phase analysis allows observation of the activation patterns of the substrate and identification of PSs can lead to characterising arrhythmias (Umapathy *et al.* 2010b). However, PSs might also indicate a structural or a functional anomaly that initiates cardiac excitation waves (Pandit and Jalife 2013) which might not represent the sources maintaining the disease. In this study, the relationships among fibrillation wave dynamics parameters were examined in human persAF data by focusing on parameters such as PSs and HDF.

7.4.1 Dynamic behaviour of PSs in the LA regions

In an attempt to better understand the dynamic changes of PSs over different temporal scales, here we examine in detail the dynamic behaviour of the correlation between LA regions and the number of PSs over consecutive time frames of two seconds. Checking the number of PSs over the two second interval windows, we were able to identify several maps based solely on the frequency of the temporal fluctuations of the PSs appearing at each region. The slope of the best fit line calculated for the entire time series for each region was very low (near 'zero') implying no change in number of PSs at each region with time. We observed temporal stability in every region, except the posterior wall and right upper pulmonary vein region. From the results, PSs demonstrated preferential areas and were more likely to be located on the posterior wall, floor, right upper pulmonary vein, anterior wall and roof. These findings are in agreement with recent human studies where the spatiotemporal association between DF and re-entrant phase activation areas was studied (Salinet *et al.* 2017).

7.4.2 Correlation between HDF vs. PSs density maps

As discussed in chapter 4, HDF density maps obtained for 75 seconds recording of VEGM seemed to remain consistent and therefore could be an indicative of fixed drivers of persAF. Cumulative plotting of the HDFs along time would help identifying the potential stable sources of persAF (Dastagir *et al.* 2014). PSs are sites about which all phases of the depolarization/repolarization cycle exist simultaneously (Krummen *et al.* 2015), and its density maps are of interest because they could indicate tissues capable of supporting rotors. Accordingly PS density maps created using 75 seconds of VEGM recording showed higher SSIM index and therefore high similarity among them. However when the correlation between HDF and PSs sites were studied, the results displayed lower degree of co-localisation (see Figure 41). This was confirmed when the CoG of the HDF region with respect to the PSs were observed to be a distance apart (median: 40.32 mm, IQR: 29.59 ~ 51.02 mm). Hence, it can be concluded that the PSs tended to be located around the vicinity of the HDF areas rather than overlapping with them. The results also suggest that PSs appear in preferential locations and in similar quantity in the same interval of time, and that there is a spatial consistency with the HDF dense regions. That hints that a relationship exists between HDFs and PSs. Intriguingly, the median distance between the CoG of the HDF site with every clockwise and anticlockwise PSs (for all the patients) were 40.29 mm (IQR: 30.41 ~ 50.09 mm) and 31.99 mm (IQR: 36.47 ~ 41.79 mm) respectively and the median distance between the respective CoG of clockwise with anticlockwise PSs is 5.15 mm (IQR: 2.77 ~ 8.77 mm). Thereby demonstrating that PSs of different chirality have the tendency to gather separately from each other yet being present in the same region.

7.4.3 OI for the localisation of AF sources

Studies about the spectral organisation (T. T. Everett *et al.* 2001, Tobon *et al.* 2012, Jarman *et al.* 2014) have stated that OI provides a better approximation for the localisation of ectopic sources of high frequency and continuous activity during episodes of fibrillation. Areas of high frequency *and* high degree of organization have been proposed as critical regions for maintaining AF (Skanes *et al.* 1998, Mandapati *et al.* 2000, Mansour *et al.* 2001) and those areas have been recently proposed as ablation targets (Sanders 2005). Interestingly, as the nodes in the LA were divided into groups by application of several density thresholds, it was observed that the top most 25 % dense nodes (T_{25}) of the HDF density map had significantly higher OI ($P < 0.05$, Mann Whitney test) when compared to the T_{25} of the PS density map. With increase in threshold (see Figure 43), for all the patients, the OI value for the PS density map did not change significantly (T_{25} vs T_{50} , $P = 0.0461$; T_{25} vs T_{75} , $P = 0.0535$; T_{25} vs T_{100} , $P = 0.1378$, using Mann Whitney test) whereas for the HDF density map, for all the patients, with increase in threshold the OI value changed significantly (T_{25} vs T_{50} , $P = 0.0016$; T_{25} vs T_{75} , $P = 0.023$; T_{25} vs T_{100} , $P = 0.0009$, Mann Whitney test). Overall, the average OI was higher in the HDF sites than in the PSs. These values thereby indicate variability of frequencies in both regions (much higher in the PSs site). This suggests that the HDF sites are more representative of stable periodic sources that are inducing wave breakup (Jalife *et al.* 1998, Jalife *et al.* 2002). Also, such that, rapidly succeeding wave fronts emanate from these sources propagate through the LA and interact with anatomic and/or functional obstacles, leading to the phenomenon of "vortex shedding" and to wavelet formation (Jalife *et al.* 1998) as indicated by the PS density maps just at the vicinity of the HDF dense regions.

7.4.4 Ablation strategy suggestions based on HDF and PSs density maps

In a recent simulation study, it was demonstrated that co-localising 15 mm RFA lesions with locations of high PS density more effectively terminated fibrillation (Bayer *et al.* 2016). The study suggested targeting such regions by RFA strategies based on perforated circles and lines. This approach does not aim to targeting individual AF substrates, but to target the pathway of the electrical activity to limit its propagation in the LA. Interestingly, as discussed earlier, from our results, the halfway mean distance between PSs and HDF region for all 10 patients resulted in 20.27 ± 8.79 mm, which already highlights the region between the PS and HDF density map. Therefore, with the ablation areas covered by the perforated circle of 15 mm diameter or line of 15 mm, it could be understood that the propagation path of the excitation waves has been obstructed. As a result, it could be understood that there is a cause-effect relationship between the HDF and the PS density maps respectively which leads to the spatiotemporal organization in the activation patterns during sustained AF and such that analysing the behaviour of the two parameters can help clinicians to develop strategies for RFA.

Although the mean distance reported is close to the distance mentioned in the simulated study, the ablation might not cover exactly the mid pathway of the HDF and PSs density map in many cases because of the spread of the result. However, for clinicians to make decisions effectively, density maps of both the parameters need to be identified on a patient-by-patient basis.

7.5 Conclusion

The results shown in this chapter provide a framework for helping to understand the complex dynamics of high frequency regions – represented by the HDF – with re-entry activation – represented by the PSs – in persAF. Studies have demonstrated that re-entrant drivers as

well as atrial regions with high activation rates can be responsible for persAF maintenance (Narayan *et al.* 2012, Sanders *et al.* 2005).

Phase analysis of the VEGMs enables tracking the activation wave fronts simultaneously in the whole LA. Their spatial distribution and evolution in time provide insight into wave propagation dynamics and enable localisation and tracking of PSs. These can lead to the identification of rotors, which is one of the potential source mechanisms of persAF. Identifying the location of persistent PSs and targeting ablation at these critical regions has been shown to reduce the effects of persAF in models and patients (Narayan *et al.* 2012, Ateienza *et al.* 2014, Haïssaguerre *et al.* 2014, Miller *et al.* 2014, Hwang *et al.* 2016). Whereas, finding HDF regions allows for the global identification of areas in the LA with rapid activations. The wide range of HDFs in each patient suggests there are multiple wandering wavelets. This study therefore combined the phase, PSs and HDF to study the dynamics and spatial behaviour of the VEGMs during persAF. It was observed that the PSs and HDF density maps had a mechanistic interaction with each other such that PSs are localised mainly around or at the vicinity of the HDF regions. The analysis stated that propagating waves travel across the LA giving rise to fibrillatory conduction and they seem to have a relationship with the most visited HDF sites. Generating and analysing these spatiotemporal maps may prove helpful in understanding the spatial and temporal changes during AF and tracking the activation patterns dynamically. Therefore, analysing the relationship between HDF and PSs based on these maps could lead to understanding persAF activation, which could help clinicians establish ablation strategies. For example, when pairs of PSs of opposite chirality interact with an HDF 'cloud' that travels between them a reasonable ablation strategy could be ablating a line connecting the two centres of PSs with opposite chirality, blocking the path of propagation of HDF activation.

Chapter 8

Main findings and future investigations

In persAF patients, identification of critical areas for successful ablation remains a challenge. Therefore, improving our knowledge of the underlying AF behaviour is a key factor to contribute towards improving patient outcomes. The analysis of the atrial electrical activity plays an important role to reveal the underlying electrophysiological mechanisms responsible for its initiation, maintenance and perpetuation. DF analysis of VEGMs finds the activation rate of the dominant atrial signal in the atrium whereas phase analysis captures the wavefront dynamics through the activation-recovery cycle of the underlying tissue. Investigation and interpretation of the outcomes from these analyses are used to inform ablation strategies. In the present thesis, we investigated the spatiotemporal behaviour of the HDF sites as well as investigated the behaviour of the phase over time in the LA for understanding the activation patterns during persAF and their relationship with the underlying mechanisms for AF maintenance and perpetuation.

8.1 Main findings

The results presented in this thesis allowed for the following findings and contributions to the field:

- We developed a novel approach for studying the HDF regions over consecutive time windows in order to produce cumulative density maps and investigate spatiotemporal behaviour of HDF regions in the LA during persAF (Dastagir *et al.*, 2015). Our results show that HDF in persAF is not temporally stable and that they have a spatial 'reappearance' in certain regions of the atrium with septum being the most common location (Dastagir *et al.*, 2015). The MVR by the HDF sites also significantly appeared to have higher atrial rate along with lower degree of organisation (Dastagir *et al.*, 2015), thereby, suggesting the existence of driver regions with very rapid and

regular activity maintaining AF. We suggest that HDF density maps should be considered for HDF targeted ablation and also that it can also be used as an important tool to analyse the effect of ablation.

- We developed and tested the TCT to track PSs from human persAF data. VEGM phase was found to be as effective for PSs detection suggesting that it may be used clinically to locate rotor during fibrillation. The main basis of the algorithm is the well-established convolutional method as other research groups have been using and it was further adapted to detect PSs in triangular meshes, which overcomes the limitation of uniformed rectangular meshes and closed geometry problems (Li *et al.*, 2017). The novelty of the implemented technique in this study that it allows PSs investigation in global mapping on the entire atrium. This is the first time TCT was used to obtain PSs using high-density NCM during human persAF.
- The present work also investigated the performance of TCT compared with two other PS detection techniques for detecting PSs in patients with persAF using NCM (Li *et al.*, 2017). Comparing the three methods in the current work resulted in PS density maps with relatively low similarity suggesting that identification of the rotors is dependent on the different automated PS detection techniques (Li *et al.*, 2017).
- Moreover, the implemented algorithm, had the best performance in detecting PSs by resulting in lowest surface distances between the detected PSs and the manually identified PSs (Li *et al.*, 2017). This demonstrates that our algorithm detects PSs more precisely compared to the other two techniques. On the other hand, the processing time for it is almost 'real' time (< 1 second), being 662.9 % and 372.7 % faster compared to the other two techniques (Li *et al.*, 2017). Therefore, our implemented algorithm is able to produce accurate results with much reduced processing time (near-real time) to calculate targets. Real-time implementation of the technique represents a novelty that could have considerable impact on clinical practice, as part of the decision making process for persAF treatment. Overall, the

algorithm proposed in this research is suggested to be used as it is a robust method for identification of PSs (Li *et al.*, 2017).

- We have also shown that changing the pre-processing methods used on intracardiac signals causes significant variations in the perceived presence of PSs in atria which could ultimately affect the detection of ablation targets and consecutively the success rate of ablation. We have demonstrated the effect of varying filter type and settings on the detection of PSs (Dastagir *et al.*, 2015). By investigating the similarities and differences in PS location and stability, our results highlight that filter settings could affect PS detections, and that might result in misleading identification of the atrial substrate and hence ablation targets. Therefore, based on our results, it has also been observed that using different types of filters does not produce significant differences in PSs density maps as much as types of filter settings does. BPF between 4 to 12 Hz is recommended to be applied on VEGMs as it corresponds better to the physiological range of AF.
- In the present study, we also evaluated the spatiotemporal dynamics of the PSs based on the atrial VEGMs collected using NCM. PSs showed different behaviour spatially and had varying life spans. In our database, rotors were not seen very often and were associated with higher atrial rate as well as disorganised electrograms, and, when recurrent, demonstrate anatomical determinism with the septum having the highest incidence (Dastagir *et al.*, 2016). We also evaluated whether the ablation revealed any significant anatomical differences in activation frequencies, AF organization, rotor location, and dynamics. Our results suggest that rotors are not the sole perpetuating mechanism in persAF.
- We also studied the combination of frequency and phase analysis of persAF signals to elucidate the mechanism of wave propagation in an attempt to identify potential drivers and characterise dynamics, which could help to develop patient-specific ablation strategies. The results shown in this thesis provide a framework for helping

to understand the complex dynamics between high frequency regions and re-entry activation sites in persAF. We argue that there is an interplay between the HDF and the PS density maps such that analysing the behaviour of the two parameters can help clinicians to develop strategies for RFA (Dastagir *et al.*, 2015).

8.2 Future investigations

The results reported in this thesis helped to identify and define future investigations. Some of the suggestions below are already being conducted by the current researchers from the Bioengineering group in collaboration with the Cardiovascular Science group, and other opportunities might be considered for future PhD students.

8.2.1 Propagation of HDF region

Previously, we also reported regarding the stability of HDF in persAF and the study offered a wider perspective about the movement of the HDF 'clouds' illustrating that they are temporarily unstable (see chapter 4) (Dastagir *et al.*, 2014). In this study we also focused more on understanding their movement. We presented an algorithm to check the drift of the CoG of HDF from current time window to the next and, if so, to check whether it drifted in the resultant direction induced by the cumulative behaviour of the PSs (Figure 44 (b)). A relationship is discovered if the overall spatial and temporal appearance of PSs approximately correspond to the trajectories of the HDF.

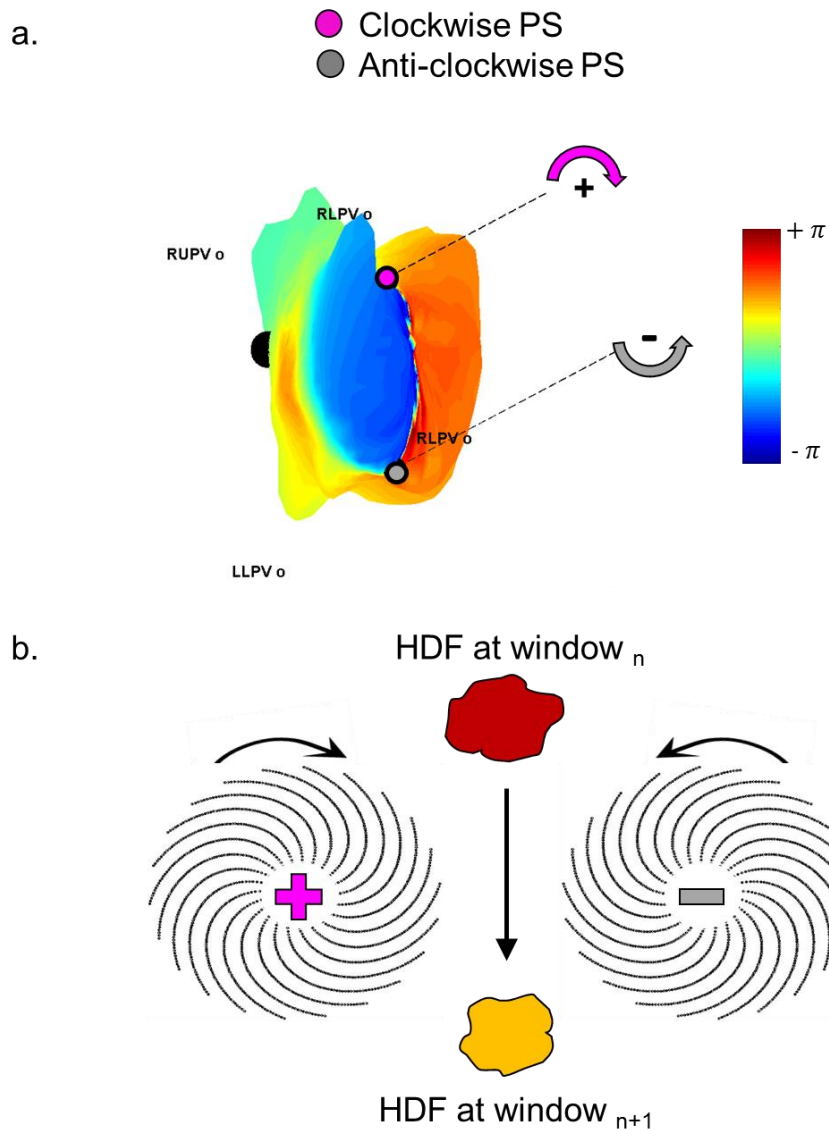


Figure 44: (a) 3D map of the left atrium showing the centre of a high DF area in black. The circles with the corresponding sign indicate clockwise and counter-clockwise PSs respectively. (b) Schematic diagram defining the direction of PSs with opposite chirality. We examine the situations when HDF channels through these PSs (arrows in the middle).

The movement of the HDF 'clouds' (as discussed in chapter 4) shows that HDF sites are temporarily unstable. PSs of opposite signs were observed for each window that might have an effect on the propagation of the HDF from current to the next window. Preliminary, using raw VEGM data, for all the 9 patients, we analysed a total of 411 windows and PSs of opposite chirality were observed in all the windows. Out of 411 windows, we observed HDF

'clouds' propagating in 293 windows (mean \pm SD: $71.3 \pm 10.7\%$) (Dastagir *et al.*, 2015). On average, 13 (± 9) times PSs of opposite signs were observed for each window that influenced the propagation of the HDF from current to the next window (Dastagir *et al.*, 2015). However, VEGM filtering affected the number of PSs significantly ($P < 0.001$) (Dastagir *et al.*, 2015). Using the same analysis the relationship of these two parameters were observed significantly less often ($P < 0.001$) when compared using the t-test. Therefore, using raw VEGMs, an interesting spatial and temporal organization of PSs with the HDF was observed. Filtering VEGMs simplifies the signal and locates selective PSs and this needs to be studied further to understand the influence of PSs on HDF as it could help developing a more successful ablation strategy.

8.2.2 Phase vector plots

We developed a visualization tool in MATLAB for visualizing phase data of the VEGMs. The tool provides the phase data, the HDF data as well as it calculates and displays the phase vectors. The technique also implements phase vector magnitude as well as vector direction. The resulting image provides, a visualization of the vector field in 2D is mapped onto the 3D surface of LA (see Figure 45) simultaneously with the phase data. The phase vectors are also shown for every sample, which therefore helps to visualise the frequent movement patterns of the phase.

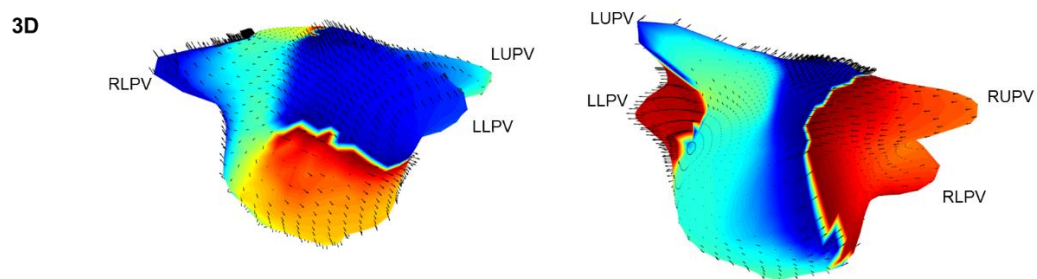
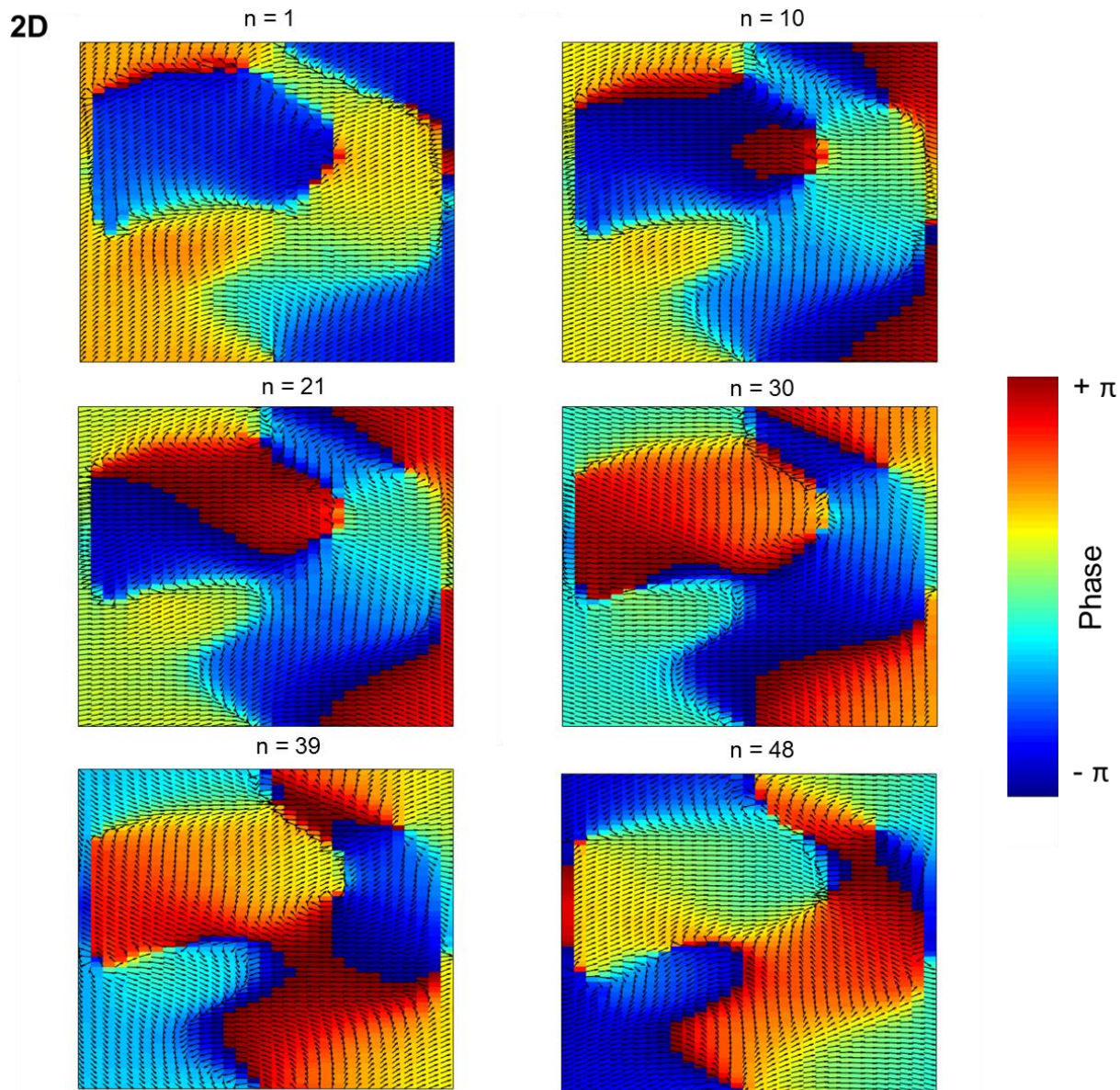


Figure 45: Representation of phase vector plots with the phase value in the background (colour) in 2D and 3D human LA. The colour represents a phase in the excitation recovery

cycle and the arrows represent the corresponding magnitude and direction of the phase propagation with time.

Developing an effective visualisation of a phase vector field is an interesting interactive tool for clinicians as it enables them to observe the formation and evolution of the atrial excitations patterns along time during AF. In areas of PSs, arrows surrounding it can be observed to appear pointing in a clockwise or counter clockwise way. It could be presented as a new technique for displaying phase data which can be applied to both 2D and 3D regular grids and surfaces. Our study so far had developed the tool to produce the plots, however, it can be further worked into for making a novel tool for visualising phase data during fibrillation.

8.2.3 DF guided persAF ablation

VEGMs with HDF are believed to represent atrial substrates with periodic activation responsible for the maintenance of persAF. This study aimed to assess the HDF spatiotemporal behaviour using high density noncontact mapping in persAF (Dastagir *et al.*, 2014, Dastagir *et al.*, 2015, Li *et al.*, 2015, Salinet *et al.*, 2013). Identifying atrial regions that are more prone to host HDF might contribute to the identification of AF drivers in persAF. Atrial areas were delimited in each frame for all VEGMs to create density maps. Such regions with highest occurrence of HDF would represent regions with highest incidence of periodic activation that could be responsible for AF perpetuation, and are potential targets for ablation. The proposed method identifies and quantifies the spatiotemporal regularity of the HDFs. The investigation of recurrent HDF regions might offer a more comprehensive dynamic overview of persAF behaviour, and the ablation targeting such regions could be considered in future works.

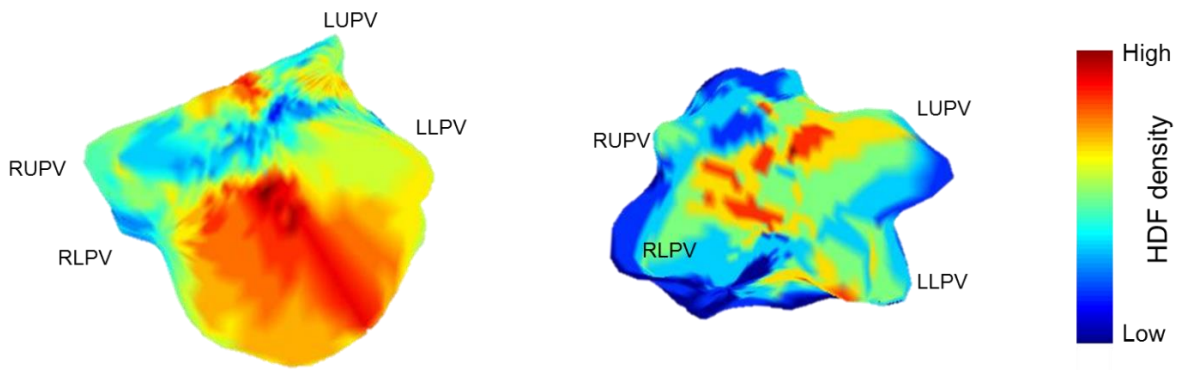


Figure 46: Representation of the cumulative HDF clouds stacked on the 3D LA (left-hand side) of 2 human persAF patients.

8.2.4 Implementing ablation strategy

Phase mapping can help to provide activation characteristics during AF. Ablation targeting PS and rotors has gained increasing interest in the past few years with early data suggesting high termination rate for persAF ablation (Haissaguerre *et al.*, 2014, Narayan *et al.*, 2012). Pak *et al.* (Pak *et al.*, 2003) reported ablation of PS points terminated fibrillation, and Narayan and collaborators (Narayan *et al.*, 2012) observed rotors in AF patients, with rotor ablation effectively terminating AF. However, details of some electrogram-based phase mapping methods have not been completely described, and rotor-based ablation has achieved mixed outcomes in terminating AF (Vijayakumar *et al.* 2016). Mandapati and collaborators (Mandapati *et al.*, 2000) found a highly significant correlation between the rotation period of rotors and the DF at the same sites. This study mapped the phase, PSs and HDF to study the dynamics and spatial behaviour of the VEGMs during persAF. It was observed that PSs are localized mainly around the HDF regions. It was also frequently observed the transit of HDF 'clouds' between rotors of opposite chirality (Dastagir *et al.*, 2015). Therefore, for mapping persAF, it would be interesting to analyse both HDF and PSs together and creating ablation lines based on the interaction between them in order to block the trajectory of the HDF 'clouds'. This study may perhaps be considered in future works.

8.3 Publications, conferences and supervisions

8.3.1 Journal publications

1. G.S. Chu, X. Li, F.J. Vanheusden, T.P. Almeida, J.L. Salinet, N. Dastagir, S.S. Varanasi, S.H. Chin, S. Siddiqui, S.H. Man, P.J. Stafford, A.J. Sandilands, F.S. Schlindwein, G.A. Ng, Targeting cyclical highest dominant frequency in the ablation of persistent atrial fibrillation, Young Investigators Competition of Heart Rhythm Congress (HRC2015), Birmingham UK, 4-7 October 2015. In: *Europace* (2015) 17 (suppl_5): v1-v2, (IF: 4.21), DOI: <https://doi.org/10.1093/europace/euv324>. Published on-line 22 February 2016.
2. Tiago P Almeida, Gavin S Chu, Michael J Bell, Xin Li, João L Salinet, Nawshin Dastagir, Jiun H Tuan, Peter J Stafford, Fernando S Schlindwein, G. André Ng, “The temporal behavior and consistency of bipolar atrial electrograms in human persistent atrial fibrillation”, submitted to *Medical & Biological Engineering & Computing*, (IF: 1.878), 6 February 2017.
3. Tiago P Almeida, Gavin S Chu; Xin Li, Nawshin Dastagir, Jiun H Tuan, Peter J Stafford, Fernando S Schlindwein, G. André Ng, “Atrial electrogram fractionation distribution before and after pulmonary vein isolation in human persistent atrial fibrillation - a retrospective multivariate statistical analysis”, submitted to *Frontiers in Physiology, Cardiac Electrophysiology*, (IF: 4.031), 10 May 2017.

8.3.2 Journal publications in preparation

1. Xin Li, Nawshin Dastagir, María S. Guillem, Tiago P. Almeida, João L. Salinet, Gavin S. Chu, Peter J. Stafford, Fernando S. Schlindwein, G. André Ng, Comparative Study on Detecting Phase Singularities for Rotor Identification using High Density Non-Contact Mapping during Atrial Fibrillation, submitted to *Heart Rhythm* (IF: 4.391), 12 April 2017.

2. Almeida TP, Chu GS, Bell MJ, Li X, Salinet JL, Dastagir N, Tuan JH, Stafford PJ, Schlindwein FS, Ng GA. The spatio-temporal consistency of atrial electrogram fractionation in persistent atrial fibrillation.
3. Dastagir N, Almeida TP, Vanheusden FJ, Li X, Salinet JL, Chu GS, Stafford PJ, Schlindwein FS, Ng GA. Using high dominant frequency density maps to understand spatiotemporal behaviour of atrial electrograms in persistent atrial fibrillation.
4. Xin Li, Gavin S. Chu, Tiago P. Almeida, Frederique J. Vanheusden, Nawshin Dastagir, João L. Salinet, Peter J Stafford, Fernando S. Schlindwein, G. André Ng. Recurrent High Dominant Frequency Spatiotemporal Patterns during Persistent Atrial Fibrillation.
5. Dastagir N, Almeida TP, Li X, Vanheusden FJ, Chu GS, Stafford PJ, Ng GA, Schlindwein FS. Spatiotemporal Complexity of Phase Singularities as observable in the Atrial Electrograms in Human Persistent Atrial Fibrillation.
6. Dastagir N, Li X, Almeida TP, Vanheusden FJ, Stafford PJ, Ng GA, Schlindwein FS. Combination of Frequency and Phase to Characterise the Spatiotemporal Behaviour of Cardiac Waves during Persistent Atrial Fibrillation in Humans.

8.3.5 Conferences

1. "Spatiotemporal Behaviour of High Dominant Frequency during Persistent Atrial Fibrillation", N Dastagir, F J Vanheusden, T P Almeida, X Li, G A Ng, F S Schlindwein, CinC2014, Computing in Cardiology, Cambridge, Mass. USA, 07 - 10 September 2014.
2. "Ablation for Persistent Atrial Fibrillation Shrinks Left Atrial High Dominant Frequency Areas", N Dastagir, Gavin S Chu, F J Vanheusden, J L Salinet, T P Almeida, X Li, P J Stafford, F S Schlindwein, G A Ng, Heart Rhythm Congress, HRC2014, Birmingham, UK, 5-8 Oct 2014.
3. "Orchestral Cacophony in the Heart: Targeting the Conductor of Atrial Fibrillation Rhythms", Dastagir, N., Ng, G.A, Schlindwein, F.S., runner up of the University's 3

Minute Thesis competition, 11th Festival of Postgraduate Research, Leicester, UK, 6 July 2015.

4. "Recurrent High Dominant Frequency Spatial Patterns in Atrial Fibrillation", X Li, GS Chu, TP Almeida, FJ Vanheusden, N Dastagir, JL Salinet, PJ Stafford, G André Ng, FS Schlindwein, CinC2015, Computing in Cardiology, Nice, France, 06 - 09 September 2015.
5. "Combination of Frequency and Phase to Characterise the Spatiotemporal Behaviour of Cardiac Waves during Persistent Atrial Fibrillation in Humans", N Dastagir, X Li, FJ Vanheusden, TP Almeida, JL Salinet, GS Chu, PJ Stafford, G André Ng, FS Schlindwein, CinC2015, Computing in Cardiology, Nice, France, 06 - 09 September 2015.
6. "Targeting cyclical highest dominant frequency in the ablation of persistent atrial fibrillation", GS Chu, X Li, FJ Vanheusden, TP Almeida, JL Salinet, N Dastagir, SS Varanasi, SH Chin, S Siddiqui, SH Man, PJ Stafford, AJ Sandilands, FS Schlindwein, GA Ng, Heart Rhythm Congress (HRC2015), Birmingham UK, 4-7 October 2015.
7. "Recurrent High Dominant Frequency Patterns in Persistent Atrial Fibrillation", X Li, GS Chu, TP Almeida, FJ Vanheusden, N Dastagir, J Salinet, PJ Stafford, FS Schlindwein, GA Ng, Heart Rhythm Congress (HRC), Birmingham UK, 4-7 October 2015.

8.3.6 Papers presented at scientific meetings

1. "Relationship of Phase Singularities and High Dominant Frequency Regions During Persistent Atrial Fibrillation in Humans", N Dastagir, JL Salinet, X Li, FJ Vanheusden, TP Almeida, GS Chu, PJ Stafford, FS Schlindwein, GA Ng, Heart Rhythm Congress (HRC), Birmingham UK, 4-7 October 2015.
2. "Frequency, phase and fractionation of atrial electrograms help guide AF ablation", Fernando S Schlindwein, Gavin S Chu, Tiago P Almeida, Xin Li, Nawshin Dastagir,

- Frederique J Vanheusden, João L Salinet, Peter J Stafford, G André Ng, Atrial Signals 2015, Karlsruhe, Germany, October 22-24, 2015.
3. "Targeting Complex Fractionated Atrial Electrograms During Persistent Atrial Fibrillation Ablation: but which ones?", Tiago P Almeida, Gavin S Chu, João L Salinet, Frederique J Vanheusden, Xin Li, Nawshin Dastagir, Jiun H Tuan, Peter J Stafford, G André Ng, Fernando S Schlindwein, Atrial Signals 2015, Karlsruhe, Germany, October 22-24, 2015.
 4. "Recurrent High Dominant Frequency Spatial Patterns in Atrial Fibrillation", Xin Li, Gavin S Chu, Tiago P Almeida, Frederique J Vanheusden, Nawshin Dastagir, João L Salinet, Peter J Stafford, G André Ng, Fernando S Schlindwein, Atrial Signals 2015, Karlsruhe, Germany, October 22-24, 2015.
 5. "Effects of Filtering Atrial electrograms on the relationship of Phase and Dominant Frequency", Nawshin Dastagir, Xin Li, Tiago P Almeida, Frederique J Vanheusden, Gavin S Chu, Peter J Stafford, G André Ng, Fernando S Schlindwein, Atrial Signals 2015, Karlsruhe, Germany, October 22-24, 2015.
 6. João L. Salinet, María S. Guillem, Tiago P. Almeida, Xin Li, Gavin S. Chu, Frederique J. Vanheusden, Nawshin Dastagir, G André Ng, Fernando S. Schlindwein. Co-localised drifting rotors and frequency activity followed by activity reduction after persistent atrial fibrillation ablation. Atrial Signals 2015, Karlsruhe, Germany; 10/2015
 7. "Cyclical Regions of Highest Dominant Frequency are Feasible Targets for Ablation in Persistent Atrial Fibrillation", Gavin S Chu, Xin Li, Frederique J Vanheusden, Tiago P Almeida, Joao L Salinet, Nawshin Dastagir, Srinivas S Varanasi, Shui Hao Chin, Shoaib Siddiqui, Sharon H Man, Peter J Stafford, Alastair J Sandilands, Fernando S Schlindwein, G André Ng, American Heart Association's Scientific Sessions 2015, Orlando, Florida, USA, 07-11 November, 2015.
 8. "Spatiotemporal Analysis of Phase and Frequency Dynamics in Human Persistent Atrial Fibrillation", Nawshin Dastagir, Frederique J Vanheusden, Gavin S Chu, João L Salinet, Xin Li, Tiago P Almeida, Peter J Stafford, Fernando S Schlindwein, G A Ng,

American Heart Association's Scientific Sessions 2015, Orlando, Florida, USA, 07-11 November, 2015. *Circulation*, November 10, 2015, Volume 132, Issue Suppl. 3, 2015; http://circ.ahajournals.org/content/132/Suppl_3/A15890.short; 132:A15890.

9. "Externally Recorded Cardiac Acoustic Signals to Assess Response to Cardiac Resynchronisation Devices", Sharon H. Man, Nawshin Dastagir, James A. Burrige, Tiago P. Almeida, Fernando S. Schlindwein, Tim Hodson, Shoaib Siddiqui, Gavin S. Chu, Subrahmanya S. Varanasi, Derek Chin, and G André Ng, *Heart Rhythm* 2016, San Francisco, CA, USA, 4-7 May, 2016.
10. "Characterization of Density of High Dominant Frequency Sites in Persistent Atrial Fibrillation Patients", Nawshin Dastagir, Tiago P. Almeida, Xin Li, Frederique J. Vanheusden, Gavin S. Chu, G André Ng, Fernando S. Schlindwein, 38th Annual International Conference of the IEEE Engineering in Medicine and Biology Society of the IEEE Engineering in Medicine and Biology Society (EMBC'16), Orlando, FL, USA, 17-20 August 2016.
11. "Dynamic Behavior of Rotors during Human Persistent Atrial Fibrillation as observed using Non-Contact Mapping", Nawshin Dastagir, Tiago P. Almeida, Xin Li, Frederique J Vanheusden, Gavin S Chu, Peter J Stafford, G André Ng and Fernando S Schlindwein, *CinC 2016, Computing in Cardiology 2016*, Vancouver, Canada, 12-14 September 2016. (paper 304)
12. "Contributing Factors Concerning Inconsistencies in Persistent Atrial Fibrillation Ablation Outcomes", Tiago P. Almeida, Gavin S. Chu, Xin Li, João L. Salinet, Nawshin Dastagir, Michael Bell, Frederique J. Vanheusden, Jiun Tuan, Peter J. Stafford, G André Ng and Fernando S. Schlindwein, *CinC 2016, Computing in Cardiology 2016*, Vancouver, Canada, 12-14 September 2016. (paper 310).
13. "The spatio-temporal behavior of atrial electrogram fractionation in persistent Atrial Fibrillation", Tiago P Almeida, Gavin S Chu, Michael J Bell, Xin Li, João L. Salinet, Nawshin Dastagir, Jiun H Tuan, Peter J Stafford, G André Ng, Fernando S

Schlindwein, XXV Congresso Brasileiro de Engenharia Biomédica – CBEB 2016, Foz do Iguaçu, Brazil, 17-20 October 2016. (manuscript 420).

14. “Analysis of cardiac acoustics obtained from the electronic stethoscope to optimize cardiac resynchronization therapy”, S H Man, O Vito, N Dastagir, J A Burr ridge, T P Almeida, S Siddiqui, G S Chu, S S Varanasi, S H Chin, W B Nicolson, R Chelliah, R K Pathmanathan, F S Schlindwein, D Chin, G A Ng, submitted to Heart Rhythm 2017, Chicago, Illinois, USA, 10-13 May, 2017.
15. “Externally recorded cardiac acoustics to optimise cardiac resynchronisation therapy”, SH. Man, O. Vito, N. Dastagir, JA. Burr ridge, TP. Almeida, S. Siddiqui, GS. Chu, SS. Varanasi, SH. Chin, FS. Schlindwein, WB. Nicolson, R. Chelliah, RK. Pathmanathan, D. Chin, GA. Ng, accepted by EHRA EUROPACE-CARDIOSTIM 2017, Vienna, Austria 18 -21 June 2017.

8.3.7 Supervisions and co-supervisions

8.3.7.1 Masters degree

1. Yi Jun. Analysis of Spatiotemporal Behavior of High Dominant Frequency clouds in the Right Atrium of Atrial fibrillation patients. 2014, M.Sc.Final Year Project. Engineering Department, University of Leicester. Supervisor: Schlindwein FS, Co-supervisor: **Dastagir N.**

8.3.7.2 BEng final year projects

1. George Fiddes. Investigating the Effects of Filtration on Phase Singularity Analysis in Human LA Atrial Fibrillation. 2017, B.Eng. Final Year Project. Engineering Department, University of Leicester. Supervisor: Schlindwein FS, Co-supervisor: **Dastagir N.**
2. Zaryawb Hussain. Estimating the concentration of phase singularity points on atrial electrograms during atrial fibrillation. 2017, B.Eng. Final Year Project. Engineering

Department, University of Leicester. Supervisor: Schlindwein FS, Co-supervisor: **Dastagir N.**

3. Abhishek Shikarwar. Tracking PSs along time to identify rotors in human persistent Atrial Fibrillation. 2016, B.Eng. Final Year Project. Engineering Department, University of Leicester. Supervisor: Schlindwein FS, Co-supervisor: **Dastagir N.**
4. Tram Ngyuen. Effect of filters on phase data on in human persistent Atrial Fibrillation. 2015, B.Eng. Final Year Project. Engineering Department, University of Leicester. Supervisor: Schlindwein FS, Co-supervisor: **Dastagir N.**

8.3.7.3 Achievements and research prizes

1. How to Beat You're a-Fib: Runner's Up Position at 3MT Thesis Competition, University of Leicester, UK, 05/05/2015.
2. Orchestral Cacophony in the Heart: Targeting the Conductor of Atrial Fibrillation Rhythms. Best Poster award for Peer-Review competition for best poster, Post Graduate Research Festival, University of Leicester, UK, 06/06/2015.
3. Representative of University of Leicester at the East Midlands University Association's (EMUA) 3MT Thesis Competition, University of Lincoln, UK, 03/09/2015.

References

- Abed, H. S., Wittert, G. A., Leong, D. P. and et al. (2013) 'Effect of weight reduction and cardiometabolic risk factor management on symptom burden and severity in patients with atrial fibrillation: A randomized clinical trial', *JAMA*, 310(19), 2050-2060.
- Ahmad, A., Salinet, J. L., Brown, P., Tuan, J. H., Stafford, P., Ng, G. A. and Schlindwein, F. S. (2011) 'QRS subtraction for atrial electrograms: flat, linear and spline interpolations', *Medical & Biological Engineering & Computing*, 49(11), 1321-1328.
- Ahmed, H. and Reddy, V. Y. (2009) 'Technical advances in the ablation of atrial fibrillation', *Heart Rhythm*, 6(8 Suppl), S39-44.
- Aizer, A., Holmes, D. S., Garlitski, A. C., Bernstein, N. E., Smyth-Melsky, J. M., Ferrick, A. M. and Chinitz, L. A. (2008) 'Standardization and validation of an automated algorithm to identify fractionation as a guide for atrial fibrillation ablation', *Heart Rhythm*, 5(8), 1134-1141.
- Alcaraz, R. and Rieta, J. J. (2013) 'Review: application of non-linear methods in the study of atrial fibrillation organization', *J Med Biol Eng*, 33.
- Aliot, E., Haissaguerre, M. and Jackman, W. (2008) *Catheter Ablation of Atrial Fibrillation*, 1 ed., Wiley-Blackwell.
- Allessie, M., Bonke, F. and Schopman, F. (1973) 'Circus Movement in Rabbit Atrial Muscle as a Mechanism of Tachycardia', *Circulation Research*, 33(1), 54-62.
- Allessie, M. and de Groot, N. (2014) 'CrossTalk opposing view: Rotors have not been demonstrated to be the drivers of atrial fibrillation', *The Journal of Physiology*, 592(15), 3167-3170.
- Allessie, M. A., Konings, K., Kirchhof, C. J. and Wijffels, M. (1996) 'Electrophysiologic mechanisms of perpetuation of atrial fibrillation', *Am J Cardiol*, 77(3), 10A-23A.
- Allessie, M. A., Lammers, W., Bonke, F. I. M. and Hollen, J. (1985) 'Experimental evaluation of Moe's multiple wavelet hypothesis of atrial fibrillation' in Zipes, D. P. and Jalife, J., eds., *Cardiac Electrophysiology and Arrhythmias* Grune {&} Stratton, 265-276.
- Andrikopoulos, G. K., Kappos, K., Tzeis, S. and Manolis, A. S. (2009) 'Contact and Non-Contact Electroanatomic Mapping in Electrophysiology', *Hospital Chronicles*, 1(1 sup), 44-48.
- Association, N. S. (1995) *The Stroke/brain Attack: Reporter's Handbook*, National Stroke Association.
- Atienza, F., Almendral, J., Jalife, J., Zlochiver, S., Ploutz-Snyder, R., Torrecilla, E. G., Arenal, A., Kalifa, J., Fernández-Avilés, F. and Berenfeld, O. (2009) 'Real-time Dominant Frequency Mapping and Ablation of Dominant-Frequency Sites in Atrial Fibrillation with Left-to-Right Frequency Gradients Predicts Long-Term Maintenance of Sinus Rhythm', *Heart rhythm : the official journal of the Heart Rhythm Society*, 6(1), 33-40.

- Atienza, F., Almendral, J., Ormaetxe, J. M., Moya, A., Martinez-Alday, J. D., Hernandez-Madrid, A., Castellanos, E., Arribas, F., Arias, M. A., Tercedor, L., Peinado, R., Arcocha, M. F., Ortiz, M., Martinez-Alzamora, N., Arenal, A., Fernandez-Aviles, F. and Jalife, J. (2014) 'Comparison of radiofrequency catheter ablation of drivers and circumferential pulmonary vein isolation in atrial fibrillation: a noninferiority randomized multicenter RADAR-AF trial', *J Am Coll Cardiol*, 64(23), 2455-67.
- Attin, M. and Clusin, W. T. (2009) 'Basic Concepts of Optical Mapping Techniques in Cardiac Electrophysiology', *Biological research for nursing*, 11(2), 195-207.
- Bayer, J. D., Roney, C. H., Pashaei, A., Jaïs, P. and Vigmond, E. J. (2016) 'Novel Radiofrequency Ablation Strategies for Terminating Atrial Fibrillation in the Left Atrium: A Simulation Study', *Frontiers in Physiology*, 7, 108.
- Bellet, S. (1963) *Clinical disorders of the heart beat*, Philadelphia: Lea & Febiger.
- Benharash, P., Buch, E., Frank, P., Share, M., Tung, R., Shivkumar, K. and Mandapati, R. (2015) 'Quantitative analysis of localized sources identified by focal impulse and rotor modulation mapping in atrial fibrillation', *Circ Arrhythm Electrophysiol*, 8(3), 554-61.
- Benjamin, E. J., Wolf, P. A., D'Agostino, R. B., Silbershatz, H., Kannel, W. B. and Levy, D. (1998) 'Impact of atrial fibrillation on the risk of death', *Circulation*, 98.
- Berenfeld, O. and Jalife, J. (2014) 'Mechanisms of Atrial Fibrillation: Rotors, Ionic Determinants and Excitation Frequency', *Cardiology clinics*, 32(4), 495-506.
- Berenfeld, O., Mandapati, R., Dixit, S., Skanes, A. C., Chen, J., Mansour, M. and Jalife, J. (2000) 'Spatially distributed dominant excitation frequencies reveal hidden organization in atrial fibrillation in the Langendorff-perfused sheep heart', *J Cardiovasc Electrophysiol*, 11(8), 869-79.
- Berenfeld, O., Zaitsev, A. V., Mironov, S. F., Pertsov, A. M. and Jalife, J. (2002) 'Frequency-Dependent Breakdown of Wave Propagation Into Fibrillatory Conduction Across the Pectinate Muscle Network in the Isolated Sheep Right Atrium', *Circulation Research*, 90(11), 1173-1180.
- Bhakta, D. and Miller, J. M. (2008) 'Principles of Electroanatomic Mapping', *Indian Pacing and Electrophysiology Journal*, 8(1), 32-50.
- 'The Boston AF Symposium 2016 Abstracts', (2016) *Journal of Cardiovascular Electrophysiology*, 27(5), 630-654.
- Bray, M. A., Lin, S. F., Aliev, R. R., Roth, B. J. and Wikswo, J. P., Jr. (2001) 'Experimental and theoretical analysis of phase singularity dynamics in cardiac tissue', *J Cardiovasc Electrophysiol*, 12(6), 716-22.
- Bray, M. A. and Wikswo, J. P. (2002) 'Use of topological charge to determine filament location and dynamics in a numerical model of scroll wave activity', *IEEE Transactions on Biomedical Engineering*, 49(10), 1086-1093.
- Burkhardt, J. D. and Natale, A. (2009) 'New Technologies in Atrial Fibrillation Ablation', *Circulation*, 120(15), 1533-1541.

- Cabo, C., Pertsov, A. M., Davidenko, J. M., Baxter, W. T., Gray, R. A. and Jalife, J. (1996) 'Vertex shedding as a precursor of turbulent electrical activity in cardiac muscle', *Biophysical Journal*, 70(3), 1105-1111.
- Cain, M. E., Ambos, H. D., Markham, J., Lindsay, B. D. and Arthur, R. M. (1991) 'Diagnostic implications of spectral and temporal analysis of the entire cardiac cycle in patients with ventricular tachycardia', *Circulation*, 83(5), 1637-48.
- Cain, M. E., Ambos, H. D., Witkowski, F. X. and Sobel, B. E. (1984) 'Fast-Fourier transform analysis of signal-averaged electrocardiograms for identification of patients prone to sustained ventricular tachycardia', *Circulation*, 69(4), 711-20.
- Calkins, H., Brugada, J., Packer, D. L., Cappato, R., Chen, S. A., Crijns, H. J., Damiano, R. J., Jr., Davies, D. W., Haines, D. E., Haissaguerre, M., Iesaka, Y., Jackman, W., Jais, P., Kottkamp, H., Kuck, K. H., Lindsay, B. D., Marchlinski, F. E., McCarthy, P. M., Mont, J. L., Morady, F., Nademanee, K., Natale, A., Pappone, C., Prystowsky, E., Raviele, A., Ruskin, J. N. and Shemin, R. J. (2007) 'HRS/EHRA/ECAS expert consensus statement on catheter and surgical ablation of atrial fibrillation: recommendations for personnel, policy, procedures and follow-up. A report of the Heart Rhythm Society (HRS) Task Force on Catheter and Surgical Ablation of Atrial Fibrillation developed in partnership with the European Heart Rhythm Association (EHRA) and the European Cardiac Arrhythmia Society (ECAS); in collaboration with the American College of Cardiology (ACC), American Heart Association (AHA), and the Society of Thoracic Surgeons (STS). Endorsed and approved by the governing bodies of the American College of Cardiology, the American Heart Association, the European Cardiac Arrhythmia Society, the European Heart Rhythm Association, the Society of Thoracic Surgeons, and the Heart Rhythm Society', *Europace*, 9(6), 335-79.
- Calkins, H., Kuck, K. H., Cappato, R., Brugada, J., Camm, A. J., Chen, S.-A., Crijns, H. J. G., Damiano, R. J., Davies, D. W., DiMarco, J., Edgerton, J., Ellenbogen, K., Ezekowitz, M. D., Haines, D. E., Haissaguerre, M., Hindricks, G., Iesaka, Y., Jackman, W., Jalife, J., Jais, P., Kalman, J., Keane, D., Kim, Y.-H., Kirchhof, P., Klein, G., Kottkamp, H., Kumagai, K., Lindsay, B. D., Mansour, M., Marchlinski, F. E., McCarthy, P. M., Mont, J. L., Morady, F., Nademanee, K., Nakagawa, H., Natale, A., Nattel, S., Packer, D. L., Pappone, C., Prystowsky, E., Raviele, A., Reddy, V., Ruskin, J. N., Shemin, R. J., Tsao, H.-M., Wilber, D., Calkins, H., Kuck, K. H., Cappato, R., Chen, S.-A., Prystowsky, E. N., Kuck, K. H., Natale, A., Haines, D. E., Marchlinski, F. E., Calkins, H., Davies, D. W., Lindsay, B. D., Damiano, R., Packer, D. L., Brugada, J., Camm, A. J., Crijns, H. J. G., DiMarco, J., Edgerton, J., Ellenbogen, K., Ezekowitz, M. D., Haissaguerre, M., Hindricks, G., Iesaka, Y., Jackman, W. M., Jais, P., Jalife, J., Kalman, J., Keane, D., Kim, Y.-H., Kirchhof, P., Klein, G., Kottkamp, H., Kumagai, K., Mansour, M., Marchlinski, F., McCarthy, P., Mont, J. L., Morady, F., Nademanee, K., Nakagawa, H., Nattel, S., Pappone, C., Raviele, A., Reddy, V., Ruskin, J. N., Shemin, R. J., Tsao, H.-M., Wilber, D., Ad, N., Cummings, J., Gillinov, A. M., Heidebuchel, H., January, C., *et al.* (2012) '2012 HRS/EHRA/ECAS Expert Consensus Statement on Catheter and Surgical Ablation of Atrial Fibrillation: Recommendations for Patient Selection, Procedural Techniques, Patient Management and Follow-up, Definitions, Endpoints, and Research Trial Design: A report of the Heart Rhythm Society (HRS) Task Force on Catheter and Surgical Ablation of Atrial Fibrillation. Developed in partnership with the European Heart Rhythm Association (EHRA), a registered branch of the European Society of Cardiology (ESC) and the European Cardiac Arrhythmia Society (ECAS); and in collaboration with the American College of Cardiology (ACC), American Heart Association (AHA), the Asia Pacific Heart Rhythm Society (APHRS), and the Society

of Thoracic Surgeons (STS). Endorsed by the governing bodies of the American College of Cardiology Foundation, the American Heart Association, the European Cardiac Arrhythmia Society, the European Heart Rhythm Association, the Society of Thoracic Surgeons, the Asia Pacific Heart Rhythm Society, and the Heart Rhythm Society', *Europace*.

- Calkins, H., Kuck, K. H., Cappato, R., Brugada, J., Camm, A. J., Chen, S., Crijns, H. J. G., Damiano, R. J., Davies, D. W. and DiMarco, J. (2012) '2012 HRS/EHRA/ECAS expert consensus statement on catheter and surgical ablation of atrial fibrillation: recommendations for patient selection, procedural techniques, patient management and follow-up, definitions, endpoints, and research trial design', *Heart Rhythm*, 9.
- Camm, A. J., Kirchhof, P., Lip, G. Y. H., Schotten, U., Savelieva, I., Ernst, S., Van Gelder, I. C., Al-Attar, N., Hindricks, G., Prendergast, B., Heidbuchel, H., Alfieri, O., Angelini, A., Atar, D., Colonna, P., De Caterina, R., De Sutter, J., Goette, A., Gorenek, B., Heldal, M., Hohloser, S. H., Kolh, P., Le Heuzey, J.-Y., Ponikowski, P., Rutten, F. H., Guidelines, E. C. f. P., Vahanian, A., Auricchio, A., Bax, J., Ceconi, C., Dean, V., Filippatos, G., Funck-Brentano, C., Hobbs, R., Kearney, P., McDonagh, T., Popescu, B. A., Reiner, Z., Sechtem, U., Sirnes, P. A., Tendera, M., Vardas, P. E., Widimsky, P., Reviewers, D., Vardas, P. E., Agladze, V., Aliot, E., Balabanski, T., Blomstrom-Lundqvist, C., Capucci, A., Crijns, H., Dahlöf, B., Folliguet, T., Glikson, M., Goethals, M., Gulba, D. C., Ho, S. Y., Klautz, R. J. M., Kose, S., McMurray, J., Perrone Filardi, P., Raatikainen, P., Salvador, M. J., Schalij, M. J., Shpektor, A., Sousa, J., Stepinska, J., Uuetoa, H., Zamorano, J. L. and Zupan, I. (2010) 'Guidelines for the management of atrial fibrillation: The Task Force for the Management of Atrial Fibrillation of the European Society of Cardiology (ESC)', *European Heart Journal*, 31(19), 2369-2429.
- Canny, J. (1986) 'A Computational Approach to Edge Detection', *IEEE Transactions on Pattern Analysis and Machine Intelligence*, PAMI-8(6), 679-698.
- Chavan, M. S., Agarwal, R. A. and Uplane, M. D. (2008) 'Suppression of Baseline Wander and power line interference in ECG using Digital IIR Filter', in *International Journal of Circuits Systems and Signal Processing*,
- Chen, J., Mandapati, R., Berenfeld, O., Skanes, A. C. and Jalife, J. (2000) 'High-Frequency Periodic Sources Underlie Ventricular Fibrillation in the Isolated Rabbit Heart', *Circulation Research*, 86(1), 86-93.
- Chinitz, L. A. and Sethi, J. S. (2006) 'How to perform noncontact mapping', *Heart Rhythm*, 3(1), 120-123.
- Chugh, S. S., Havmoeller, R., Narayanan, K., Singh, D., Rienstra, M., Benjamin, E. J., Gillum, R. F., Kim, Y. H., McAnulty, J. H., Jr., Zheng, Z. J., Forouzanfar, M. H., Naghavi, M., Mensah, G. A., Ezzati, M. and Murray, C. J. (2014) 'Worldwide epidemiology of atrial fibrillation: a Global Burden of Disease 2010 Study', *Circulation*, 129(8), 837-47.
- Clayton, R. H. and Nash, M. P. (2015) 'Analysis of cardiac fibrillation using phase mapping', *Card Electrophysiol Clin*, 7(1), 49-58.
- Cottrell, C. (2012) 'Atrial fibrillation part 1: pathophysiology', *Practice Nursing*, 23(1), 16-21.
- Cox, J. L., Boineau, J. P., Schuessler, R. B., Ferguson, T. B., Jr., Cain, M. E., Lindsay, B. D., Corr, P. B., Kater, K. M. and Lappas, D. G. (1991) 'Successful surgical treatment of atrial fibrillation. Review and clinical update', *JAMA*, 266(14), 1976-80.

- Cox, J. L., Schuessler, R. B. and Boineau, J. P. (2000) 'The Development of the Maze Procedure for the Treatment of Atrial Fibrillation', *Seminars in Thoracic and Cardiovascular Surgery*, 12(1), 2-14.
- Dagres, N., Bongiorni, M. G., Larsen, T. B., Hernandez-Madrid, A., Pison, L., Blomström-Lundqvist, C., Bongiorni, M. G., Chen, J., Dagres, N., Estner, H., Hernandez-Madrid, A., Hocini, M., Larsen, T. B., Pison, L., Potpara, T., Proclemer, A., Sciraffia, E. and Todd, D. (2015) 'Current ablation techniques for persistent atrial fibrillation: results of the European Heart Rhythm Association Survey', *Europace*, 17(10), 1596-1600.
- Damiano, R. J. and Bailey, M. (2007) 'The Cox-Maze IV procedure for lone atrial fibrillation', *Multimedia Manual of Cardio-Thoracic Surgery*, 2007(0723).
- Dastagir, N., Salinet, J., Vanheusden, F. J., Almeida, T. P., Li, X., Chu, G. S., Ng, G. A. and Schindwein, F. S. (2014) 'Spatiotemporal behaviour of high dominant frequency during persistent atrial fibrillation', in *Computing in Cardiology Conference (CinC), 2014*, 7-10 Sept. 2014, IEEE Conference Publications, 653-656.
- Davidenko, J. M., Kent, P. F., Chialvo, D. R., Michaels, D. C. and Jalife, J. (1990) 'Sustained vortex-like waves in normal isolated ventricular muscle', *Proceedings of the National Academy of Sciences of the United States of America*, 87(22), 8785-8789.
- Davidenko, J. M., Pertsov, A. V., Salomonsz, R., Baxter, W. and Jalife, J. (1992) 'Stationary and drifting spiral waves of excitation in isolated cardiac muscle', *Nature*, 355(6358), 349-351.
- Earley, M. J., Showkathali, R., Alzetani, M., Kistler, P. M., Gupta, D., Abrams, D. J., Horrocks, J. A., Harris, S. J., Sporton, S. C. and Schilling, R. J. (2006) 'Radiofrequency ablation of arrhythmias guided by non-fluoroscopic catheter location: a prospective randomized trial', *European Heart Journal*, 27(10), 1223-1229.
- Eckardt, L. and Breithardt, G. (2009) 'Construction and Interpretation of Endocardial Maps: From Basic Electrophysiology to 3D Mapping' in *Cardiac Mapping*Wiley-Blackwell, 11-26.
- Estner, H. L., Deisenhofer, I., Luik, A., Ndrepepa, G., von Bary, C., Zrenner, B. and Schmitt, C. (2006) 'Electrical isolation of pulmonary veins in patients with atrial fibrillation: reduction of fluoroscopy exposure and procedure duration by the use of a non-fluoroscopic navigation system (NavX®)', *EP Europace*, 8(8), 583-587.
- Everett Iv, T. H., Akar, J. G., Kok, L.-C., Moorman, J. R. and Haines, D. E. (2002) 'Use of global atrial fibrillation organization to optimize the success of burst pace termination', *Journal of the American College of Cardiology*, 40(10), 1831-1840.
- Everett, T. H., Moorman, J. R., Kok, L.-C., Akar, J. G. and Haines, D. E. (2001) 'Assessment of Global Atrial Fibrillation Organization to Optimize Timing of Atrial Defibrillation', *Circulation*, 103(23), 2857-2861.
- Everett, T. T., Kok, L. C., Vaughn, R. H., Moorman, J. R. and Haines, D. E. (2001) 'Frequency domain algorithm for quantifying atrial fibrillation organization to increase defibrillation efficacy', *IEEE Trans Biomed Eng*, 48.

- Fenton, F. and Karma, A. (1998) 'Vortex dynamics in three-dimensional continuous myocardium with fiber rotation: Filament instability and fibrillation', *Chaos: An Interdisciplinary Journal of Nonlinear Science*, 8(1), 20-47.
- Flaker, G., Blackshear, J., McBride, R., Kronmal, R., Halperin, J. and Hart, R. (1992) 'Antiarrhythmic drug therapy and cardiac mortality in atrial fibrillation. The Stroke Prevention in Atrial Fibrillation Investigators.', *Journal of the American College of Cardiology*, 20(3), 527-532.
- Friedman, P. (2002) 'Novel mapping techniques for cardiac electrophysiology', *Heart*, 87(6), 575-582.
- Fuster, V., Rydén, L. E., Asinger, R. W., Cannom, D. S., Crijns, H. J., Frye, R. L., Halperin, J. L., Kay, G. N., Klein, W. W., Lévy, S., McNamara, R. L., Prystowsky, E. N., Wann, L. S., Wyse, D. G., Gibbons, R. J., Antman, E. M., Alpert, J. S., Faxon, D. P., Gregoratos, G., Hiratzka, L. F., Jacobs, A. K., Russell, R. O., Smith, J. S. C., Alonso-Garcia, A., Blomström-Lundqvist, C., De Backer, G., Flather, M., Hradec, J., Oto, A., Parkhomenko, A., Silber, S. and Torbicki, A. (2001) 'ACC/AHA/ESC guidelines for the management of patients with atrial fibrillation: executive summaryA Report of the American College of Cardiology/ American Heart Association Task Force on Practice Guidelines and the European Society of Cardiology Committee for Practice Guidelines and Policy Conferences (Committee to Develop Guidelines for the Management of Patients With Atrial Fibrillation) Developed in Collaboration With the North American Society of Pacing and Electrophysiology333', *Journal of the American College of Cardiology*, 38(4), 1231-1265.
- Fuster, V., Ryden, L. E., Cannom, D. S., Crijns, H. J., Curtis, A. B., Ellenbogen, K. A., Halperin, J. L., Le Heuzey, J. Y., Kay, G. N., Lowe, J. E., Olsson, S. B., Prystowsky, E. N., Tamargo, J. L., Wann, S., Smith, S. C., Jr., Jacobs, A. K., Adams, C. D., Anderson, J. L., Antman, E. M., Halperin, J. L., Hunt, S. A., Nishimura, R., Ornato, J. P., Page, R. L., Riegel, B., Priori, S. G., Blanc, J. J., Budaj, A., Camm, A. J., Dean, V., Deckers, J. W., Despres, C., Dickstein, K., Lekakis, J., McGregor, K., Metra, M., Morais, J., Osterspey, A., Tamargo, J. L. and Zamorano, J. L. (2006) 'ACC/AHA/ESC 2006 Guidelines for the Management of Patients with Atrial Fibrillation: a report of the American College of Cardiology/American Heart Association Task Force on Practice Guidelines and the European Society of Cardiology Committee for Practice Guidelines (Writing Committee to Revise the 2001 Guidelines for the Management of Patients With Atrial Fibrillation): developed in collaboration with the European Heart Rhythm Association and the Heart Rhythm Society', *Circulation*, 114(7), e257-354.
- Garrey, W. E. (1914) 'The nature of fibrillary contraction of the heart.—Its relation to tissue mass and form', *American Journal of Physiology--Legacy Content*, 33(3), 397-414.
- Gojraty, S., Lavi, N., Valles, E., Kim, S. J., Michele, J. and Gerstenfeld, E. P. (2009) 'Dominant Frequency Mapping of Atrial Fibrillation: Comparison of Contact and Noncontact Approaches', *Journal of Cardiovascular Electrophysiology*, 20(9), 997-1004.
- Goldberger, J. J. (2000) 'Atrial Fibrillation: Identifying Sites Critical to the Maintenance of Atrial Fibrillation', *Japanese Circulation Society*, 64.
- Gonzales, M. J., Vincent, K. P., Rappel, W.-J., Narayan, S. M. and McCulloch, A. D. (2014) 'Structural contributions to fibrillatory rotors in a patient-derived computational model of the atria', *Europace*, 16(Suppl 4), iv3-iv10.

- Gornick, C. C., Adler, S. W., Pederson, B., Hauck, J., Budd, J. and Schweitzer, J. (1999) 'Validation of a New Noncontact Catheter System for Electroanatomic Mapping of Left Ventricular Endocardium', *Circulation*, 99(6), 829-835.
- Gray, R. A., Pertsov, A. M. and Jalife, J. (1998) 'Spatial and temporal organization during cardiac fibrillation', *Nature*, 392(6671), 75-8.
- Guimarães, H. N. and Santos, R. A. S. (1998) 'A comparative analysis of preprocessing techniques of cardiac event series for the study of heart rhythm variability using simulated signals', *Brazilian Journal of Medical and Biological Research*, 31, 421-430.
- Gutbrod, S. R., Walton, R., Gilbert, S., Meillet, V., Jaïs, P., Hocini, M., Haïssaguerre, M., Dubois, R., Bernus, O. and Efimov, I. R. (2015) 'Quantification of the Transmural Dynamics of Atrial Fibrillation by Simultaneous Endocardial and Epicardial Optical Mapping in an Acute Sheep Model', *Circulation: Arrhythmia and Electrophysiology*, 8(2), 456-465.
- Habel, N., Znojkwicz, P., Thompson, N., Müller, J. G., Mason, B., Calame, J., Calame, S., Sharma, S., Mirchandani, G., Janks, D., Bates, J., Noori, A., Karnbach, A., Lustgarten, D. L., Sobel, B. E. and Spector, P. (2010) 'The temporal variability of dominant frequency and complex fractionated atrial electrograms constrains the validity of sequential mapping in human atrial fibrillation', *Heart Rhythm*, 7(5), 586-593.
- Haberl, R., Jilge, G., Pulter, R. and Steinbeck, G. (1988) 'Comparison of frequency and time domain analysis of the signal-averaged electrocardiogram in patients with ventricular tachycardia and coronary artery disease: Methodologic validation and clinical relevance', *Journal of the American College of Cardiology*, 12(1), 150-158.
- Haïssaguerre, M., Hocini, M., Denis, A., Shah, A. J., Komatsu, Y., Yamashita, S., Daly, M., Amraoui, S., Zellerhoff, S., Picat, M.-Q., Quotb, A., Jesel, L., Lim, H., Ploux, S., Bordachar, P., Attuel, G., Meillet, V., Ritter, P., Derval, N., Sacher, F., Bernus, O., Cochet, H., Jaïs, P. and Dubois, R. (2014) 'Driver Domains in Persistent Atrial Fibrillation', *Circulation*.
- Haïssaguerre, M., Jaïs, P., Shah, D. C., Takahashi, A., Hocini, M., Quiniou, G., Garrigue, S., Le Mouroux, A., Le Métayer, P. and Clémenty, J. (1998) 'Spontaneous Initiation of Atrial Fibrillation by Ectopic Beats Originating in the Pulmonary Veins', *New England Journal of Medicine*, 339(10), 659-666.
- Haïssaguerre, M., Jaïs, P., Shah, D. C., Takahashi, A., Hocini, M., Quiniou, G., Garrigue, S., Le Mouroux, A., Le Métayer, P. and Clémenty, J. (1998) 'Spontaneous Initiation of Atrial Fibrillation by Ectopic Beats Originating in the Pulmonary Veins', *New England Journal of Medicine*, 339(10), 659-666.
- Hall, J. E. and Guyton, A. C. (2011) *Guyton and Hall textbook of medical physiology*.
- Harris, F. J. (1978) 'On the use of windows for harmonic analysis with the discrete Fourier transform', *Proceedings of the IEEE*, 66(1), 51-83.
- Hart, R. G. and Halperin, J. L. (2001) 'Atrial Fibrillation and Stroke: Concepts and Controversies', *Stroke*, 32(3), 803-808.

- Heist, E. K., Mansour, M. and Ruskin, J. N. (2011) 'Rate Control in Atrial Fibrillation: Targets, Methods, Resynchronization Considerations', *Circulation*, 124(24), 2746-2755.
- Hing, J., Wang, P., Al-Ahmand, A. (2009) 'Front Matter' in *Electroanatomical Mapping* Blackwell Publishing, Ltd, i-xii.
- Hornung, D., Biktashev, V. N., Otani, N. F., Shajahan, T. K., Baig, T., Berg, S., Han, S., Krinsky, V. I. and Luther, S. (2017) 'Mechanisms of vortices termination in the cardiac muscle', *Royal Society Open Science*, 4(3).
- Huang, J.-L., Tai, C.-T., Lin, Y.-J., Ting, C.-T., Chen, Y.-T., Chang, M.-S., Lin, F.-Y., Lai, W.-T. and Chen, S.-A. (2006) 'The Mechanisms of an Increased Dominant Frequency in the Left Atrial Posterior Wall During Atrial Fibrillation in Acute Atrial Dilatation', *Journal of Cardiovascular Electrophysiology*, 17(2), 178-188.
- Husser, D., Stridh, M., Sornmo, L., Olsson, S. B. and Bollmann, A. (2004) 'Frequency Analysis of Atrial Fibrillation From the Surface Electrocardiogram', *Indian Pacing and Electrophysiology Journal*, 4(3), 122-136.
- Hwang, M., Song, J.-S., Lee, Y.-S., Li, C., Shim, E. B. and Pak, H.-N. (2016) 'Electrophysiological Rotor Ablation in In-Silico Modeling of Atrial Fibrillation: Comparisons with Dominant Frequency, Shannon Entropy, and Phase Singularity', *PLOS ONE*, 11(2), e0149695.
- Ideker, R. E. and Huang, J. (2005) 'Our search for the porcine mother rotor', *Ann Noninvasive Electrocardiol*, 10(4 Suppl), 7-15.
- Ingle, V. and Proakis, J. (2012) *Digital signal processing using MATLAB*, Third ed., Stamford, Conn: Cengage Learning.
- Iyer, A. N. and Gray, R. A. (2001) 'An Experimentalist's Approach to Accurate Localization of Phase Singularities during Reentry', *Annals of Biomedical Engineering*, 29(1), 47-59.
- Jais, P., Haissaguerre, M., Shah, D. C., Chouairi, S., Gencel, L., Hocini, M. I. z. and Cle'menty, J. (1997) 'A Focal Source of Atrial Fibrillation Treated by Discrete Radiofrequency Ablation', *Circulation*, 95(3), 572-576.
- Jalife, J. (2003) 'Rotors and spiral waves in atrial fibrillation', *J Cardiovasc Electrophysiol*, 14(7), 776-80.
- Jalife, J., Berenfeld, O. and Mansour, M. (2002) 'Mother rotors and fibrillatory conduction: a mechanism of atrial fibrillation', *Cardiovascular Research*, 54(2), 204-216.
- Jalife, J., Berenfeld, O., Skanes, A. and Mandapati, R. (1998) 'Mechanisms of atrial fibrillation: mother rotors or multiple daughter wavelets, or both?', *J Cardiovasc Electrophysiol*, 9(8 Suppl), S2-12.
- Jarman, J. W. E., Wong, T., Kojodjojo, P., Spohr, H., Davies, J. E., Roughton, M., Francis, D. P., Kanagaratnam, P., Markides, V., Davies, D. W. and Peters, N. S. (2012) 'Spatiotemporal Behavior of High Dominant Frequency During Paroxysmal and Persistent Atrial Fibrillation in the Human Left Atrium', *Circulation: Arrhythmia and Electrophysiology*, 5(4), 650-658.
- Jarman, J. W. E., Wong, T. O. M., Kojodjojo, P., Spohr, H., Davies, J. E. R., Roughton, M., Francis, D. P., Kanagaratnam, P., O'Neill, M. D., Markides, V., Davies, D. W. and

- Peters, N. S. (2014) 'Organizational Index Mapping to Identify Focal Sources During Persistent Atrial Fibrillation', *Journal of Cardiovascular Electrophysiology*, 25(4), 355-363.
- Kadish, A., Hauck, J., Pederson, B., Beatty, G. and Gornick, C. (1999) 'Mapping of Atrial Activation With a Noncontact, Multielectrode Catheter in Dogs', *Circulation*, 99(14), 1906-1913.
- Kimura, K., Minematsu, K. and Yamaguchi, T. (2005) 'Atrial fibrillation as a predictive factor for severe stroke and early death in 15 831 patients with acute ischaemic stroke', *J Neurol Neurosurg Psychiatry*, 76(5), 679-683.
- King, B., Porta-Sanchez, A., Masse, S., Zamiri, N., Balasundaram, K., Kusha, M., Jackson, N., Halder, S., Umapathy, K. and Nanthakumar, K. (2017) 'Effect of spatial resolution and filtering on mapping cardiac fibrillation', *Heart Rhythm*, 14(4), 608-615.
- Kirchhof, P. and Eckardt, L. (2010) 'Ablation of atrial fibrillation: for whom and how?', *Heart*, 96(16), 1325-1330.
- Klabunde, R. (2011) *Cardiovascular Physiology Concepts*, Wolters Kluwer Health.
- Kogawa, R., Okumura, Y., Watanabe, I., Kofune, M., Nagashima, K., Mano, H., Sonoda, K., Sasaki, N., Ohkubo, K., Nakai, T. and Hirayama, A. (2015) 'Spatial and temporal variability of the complex fractionated atrial electrogram activity and dominant frequency in human atrial fibrillation', *Journal of Arrhythmia*, 31(2), 101-107.
- Krijthe, B., Kunsat, A., Benjamin, E., Lip, G., Franco, O., Hofman, A., Witteman, J., Stricker, B. and Heeringa, J. (2013) 'Projections on the number of individuals with atrial fibrillation in the European Union, from 2000 to 2060.', *European Heart Journal*, 34(35), 2746-2751.
- Krummen, D. E., Swarup, V. and Narayan, S. M. (2015) 'The role of rotors in atrial fibrillation', *Journal of Thoracic Disease*, 7(2), 142-151.
- Kumagai, K., Khrestian, C. and Waldo, A. L. (1997) 'Simultaneous Multisite Mapping Studies During Induced Atrial Fibrillation in the Sterile Pericarditis Model', *Insights Into the Mechanism of its Maintenance*, 95(2), 511-521.
- Langley, P., Bourke, J. P. and Murray, A. (2000) 'Frequency analysis of atrial fibrillation', in *Computers in Cardiology 2000*, 2000, 65-68.
- LaPage, M. J. and Saul, J. P. (2011) 'Update on rhythm mapping and catheter navigation', *Curr Opin Cardiol*, 26(2), 79-85.
- Laughner, J. I., Ng, F. S., Sulkin, M. S., Arthur, R. M. and Efimov, I. R. (2012) 'Processing and analysis of cardiac optical mapping data obtained with potentiometric dyes', *American Journal of Physiology - Heart and Circulatory Physiology*, 303(7), H753-H765.
- Lazar, S., Dixit, S., Marchlinski, F. E., Callans, D. J. and Gerstenfeld, E. P. (2004) 'Presence of Left-to-Right Atrial Frequency Gradient in Paroxysmal but Not Persistent Atrial Fibrillation in Humans', *Circulation*, 110(20), 3181-3186.
- Lewis, T. (1909) 'Auricular fibrillation: A common clinical condition', *Br Med Journal*, 2, 1528.

- Lewis, T. (1920) *The mechanism and graphic registration of the heart beat*, London: Shaw.
- Lewis, T. (1921) 'Observations upon flutter and fibrillation. Part IX. The nature of auricular fibrillation as it occurs in patients', *Heart*, 8, 293-227.
- Li, C., Lim, B., Hwang, M., Song, J.-S., Lee, Y.-S., Joung, B. and Pak, H.-N. (2016) 'The Spatiotemporal Stability of Dominant Frequency Sites in In-Silico Modeling of 3-Dimensional Left Atrial Mapping of Atrial Fibrillation', *PLOS ONE*, 11(7), e0160017.
- Lim, H. S., Derval, N., Komatsu, Y., Zellerhoff, S., Denis, A., Shah, A. J., Sacher, F., Hocini, M., Jais, P. and Haissaguerre, M. (2015) 'Is ablation to termination the best strategy for ablation of persistent atrial fibrillation? Persistent atrial fibrillation is best ablated by a strategy that terminates the arrhythmia: procedural termination is associated with improved long-term outcomes', *Circ Arrhythm Electrophysiol*, 8(4), 963-71.
- Lloyd-Jones, D. M., Wang, T. J., Leip, E. P., Larson, M. G., Levy, D., Vasan, R. S., D'Agostino, R. B., Massaro, J. M., Beiser, A., Wolf, P. A. and Benjamin, E. J. (2004) 'Lifetime Risk for Development of Atrial Fibrillation', *The Framingham Heart Study*, 110(9), 1042-1046.
- Macle, L., Jaïs, P., Scavée, C., Weerasooriya, R., Hocini, M., Shah, D. C., Raybaud, F., Choi, K.-J., Clémenty, J. and Haïssaguerre, M. (2003) 'Pulmonary Vein Disconnection Using the Localisa Three-Dimensional Nonfluoroscopic Catheter Imaging System', *Journal of Cardiovascular Electrophysiology*, 14(7), 693-697.
- MacRae, C. A. (2009) 'Symptoms in Atrial Fibrillation: Why Keep Score?', *Circulation: Arrhythmia and Electrophysiology*, 2(3), 215-217.
- Madeiro, J. P. V., Cortez, P. C., Marques, J. A. L., Seisdedos, C. R. V. and Sobrinho, C. R. M. R. (2012) 'An innovative approach of QRS segmentation based on first-derivative, Hilbert and Wavelet Transforms', *Medical Engineering & Physics*, 34(9), 1236-1246.
- Mainardi, L., Sörnmo, L. and Cerutti, S. (2008) 'Understanding Atrial Fibrillation: The Signal Processing Contribution, Part I', *Synthesis Lectures on Biomedical Engineering*, 3(1), 1-129.
- Mandapati, R., Skanes, A., Chen, J., Berenfeld, O. and Jalife, J. (2000) 'Stable Microreentrant Sources as a Mechanism of Atrial Fibrillation in the Isolated Sheep Heart', *Circulation*, 101(2), 194-199.
- Mansour, M., Mandapati, R., Berenfeld, O., Chen, J., Samie, F. H. and Jalife, J. (2001) 'Left-to-Right Gradient of Atrial Frequencies During Acute Atrial Fibrillation in the Isolated Sheep Heart', *Circulation*, 103(21), 2631-2636.
- Markides, V. and Schilling, R. J. (2003) 'Atrial fibrillation: classification, pathophysiology, mechanisms and drug treatment', *Heart*, 89(8), 939-943.
- Matsuo, S., Yamane, T., Date, T., Tokutake, K.-I., Hioki, M., Narui, R., Ito, K., Tanigawa, S.-I., Yamashita, S., Tokuda, M., Inada, K., Arase, S., Yagi, H., Sugimoto, K.-I. and Yoshimura, M. (2012) 'Substrate Modification by Pulmonary Vein Isolation and Left Atrial Linear Ablation in Patients with Persistent Atrial Fibrillation: Its Impact on Complex-Fractionated Atrial Electrograms', *Journal of Cardiovascular Electrophysiology*, 23(9), 962-970.

- McCarthy, P. M., Kruse, J., Shalli, S., Ilkhanoff, L., Goldberger, J. J., Kadish, A. H., Arora, R. and Lee, R. (2010) 'Where does atrial fibrillation surgery fail? Implications for increasing effectiveness of ablation', *The Journal of Thoracic and Cardiovascular Surgery*, 139(4), 860-867.
- McDowell, K. S., Zahid, S., Vadakkumpadan, F., Blauer, J., MacLeod, R. S. and Trayanova, N. A. (2015) 'Virtual Electrophysiological Study of Atrial Fibrillation in Fibrotic Remodeling', *PLOS ONE*, 10(2), e0117110.
- Miller, J. M., Kowal, R. C., Swarup, V., Daubert, J. P., Daoud, E. G., Day, J. D., Ellenbogen, K. A., Hummel, J. D., Baykaner, T., Krummen, D. E., Narayan, S. M., Reddy, V. Y., Shivkumar, K., Steinberg, J. S. and Wheelan, K. R. (2014) 'Initial independent outcomes from focal impulse and rotor modulation ablation for atrial fibrillation: multicenter FIRM registry', *J Cardiovasc Electrophysiol*, 25(9), 921-9.
- Miller, V. T., Rothrock, J. F., Pearce, L. A., Feinberg, W. M., Hart, R. G., Anderson, D. C. and investigators, o. b. o. t. S. P. i. A. F. (1993) 'Ischemic stroke in patients with atrial fibrillation: Effect of aspirin according to stroke mechanism', *Neurology*, 43(1 Part 1), 32.
- Mines, G. (1913) 'On dynamic equilibrium in the heart', *The Journal of Physiology*, 46(4-5), 349-383.
- Mironov, S. F., Vetter, F. J. and Pertsov, A. M. (2006) 'Fluorescence imaging of cardiac propagation: spectral properties and filtering of optical action potentials', *Am J Physiol Heart Circ Physiol*, 291(1), H327-35.
- Moe, G. (1962) 'On the multiple wavelet hypothesis of atrial fibrillation', *Arch Int Pharmacodyn Ther*, 140, 183-188.
- Moe, G. K., Rheinboldt, W. C. and Abildskov, J. A. (1964) 'A COMPUTER MODEL OF ATRIAL FIBRILLATION', *Am Heart J*, 67, 200-20.
- Nademanee, K. and Oketani, N. (2009) 'The Role of Complex Fractionated Atrial Electrograms in Atrial Fibrillation Ablation: Moving to the Beat of a Different Drum □', *Journal of the American College of Cardiology*, 53(9), 790-791.
- Narayan, D., Shivkumar, K., Clopton, P., Rappel, W. and Miller, J. (2012) 'Treatment of Atrial Fibrillation by the Ablation of Localized Sources : CONFIRM (Conventional Ablation for Atrial Fibrillation With or Without Focal Impulse and Rotor Modulation) Trial', *Journal of the American College of Cardiology*, 60(7), 628-636.
- Narayan, S. and Krummen, D. (2012) 'Targeting Stable Rotors to Treat Atrial Fibrillation', *Arrhythmia & Electrophysiology Review*, 1(1), 34-38.
- Narayan, S. M., Baykaner, T., Clopton, P., Schricker, A., Lalani, G. G., Krummen, D. E., Shivkumar, K. and Miller, J. M. (2014) 'Ablation of Rotor and Focal Sources Reduces Late Recurrence of Atrial Fibrillation Compared With Trigger Ablation Alone Extended Follow-Up of the CONFIRM Trial (Conventional Ablation for Atrial Fibrillation With or Without Focal Impulse and Rotor Modulation)', *Journal of the American College of Cardiology*, 63(17), 1761-1768.
- Narayan, S. M. and Jalife, J. (2014) 'CrossTalk proposal: Rotors have been demonstrated to drive human atrial fibrillation', *The Journal of Physiology*, 592(15), 3163-3166.

- Narayan, S. M., Krummen, D. E., Clopton, P., Shivkumar, K. and Miller, J. M. (2013a) 'Direct Or Coincidental Elimination of Stable Rotors or Focal Sources May Explain Successful Atrial Fibrillation Ablation: On-Treatment Analysis of the CONFIRM (CONventional ablation for AF with or without Focal Impulse and Rotor Modulation) Trial', *Journal of the American College of Cardiology*, 62(2), 138-147.
- Narayan, S. M., Krummen, D. E. and Rappel, W. (2012) 'Clinical Mapping Approach To Diagnose Electrical Rotors and Focal Impulse Sources for Human Atrial Fibrillation', *Journal of Cardiovascular Electrophysiology*, 23(5), 447-454.
- Narayan, S. M., Patel, J., Mulpuru, S. and Krummen, D. E. (2012) 'Focal impulse and rotor modulation ablation of sustaining rotors abruptly terminates persistent atrial fibrillation to sinus rhythm with elimination on follow-up: A video case study', *Heart rhythm : the official journal of the Heart Rhythm Society*, 9(9), 1436-1439.
- Narayan, S. M., Shivkumar, K., Krummen, D. E., Miller, J. M. and Rappel, W.-J. (2013b) 'Panoramic Electrophysiological Mapping but not Electrogram Morphology Identifies Stable Sources for Human Atrial Fibrillation: Stable Atrial Fibrillation Rotors and Focal Sources Relate Poorly to Fractionated Electrograms', *Circulation. Arrhythmia and electrophysiology*, 6(1), 58-67.
- Natale, A. and Jalife, J. (2008) *Atrial fibrillation : from bench to bedside*, Totowa, N.J.: Humana Press.
- Nattel, S. (2002) 'New ideas about atrial fibrillation 50 years on', *Nature*, 415(6868), 219-226.
- Ng, J. and Goldberger, J. J. (2007) 'Understanding and Interpreting Dominant Frequency Analysis of AF Electrograms', *Journal of Cardiovascular Electrophysiology*, 18(6), 680-685.
- Ng, J., Kadish, A. H. and Goldberger, J. J. (2006) 'Effect of electrogram characteristics on the relationship of dominant frequency to atrial activation rate in atrial fibrillation', *Heart Rhythm*, 3(11), 1295-1305.
- Ng, J., Kadish, A. H. and Goldberger, J. J. (2007) 'Technical Considerations for Dominant Frequency Analysis', *Journal of Cardiovascular Electrophysiology*, 18(7), 757-764.
- NHS (2013) *Atrial fibrillation* [online], available: <http://www.nhs.uk/conditions/Atrial-fibrillation/Pages/Introduction.aspx> [accessed 25/07].
- Nocedal, J. and Wright, S. (2006) *Numerical Optimization*, 2 ed., Springer-Verlag New York.
- Oral, H., Knight, B. P., Tada, H., Özaydin, M., Chugh, A., Hassan, S., Scharf, C., Lai, S. W. K., Greenstein, R., Pelosi, F., Strickberger, S. A. and Morady, F. (2002) 'Pulmonary Vein Isolation for Paroxysmal and Persistent Atrial Fibrillation', *Circulation*, 105(9), 1077-1081.
- Oral, H., Pappone, C., Chugh, A., Good, E., Bogun, F., Pelosi, F. J., Bates, E. R., Lehmann, M. H., Vicedomini, G., Augello, G., Agricola, E., Sala, S., Santinelli, V. and Morady, F. (2006) 'Circumferential Pulmonary-Vein Ablation for Chronic Atrial Fibrillation', *New England Journal of Medicine*, 354(9), 934-941.
- Ortigosa, N., Fernandez, C., Galbis, A. and Cano, O. (2015) 'Phase information of time-frequency transforms as a key feature for classification of atrial fibrillation episodes', *Physiol Meas*, 36(3), 409-24.

- Pachon, J., Pachon, E., Lobo, T., Pachon, M., Vargas, R., Pachon, D., Lopezm, F. and Jatene, A. (2004) 'A new treatment for atrial fibrillation based on spectral analysis to guide the catheter RF-ablation', *Europace*, 6.
- Pak, H.-N., Hwang, C., Lim, H. E., Kim, J. W., Lee, H. S. and Kim, Y.-H. (2006) 'Electroanatomic Characteristics of Atrial Premature Beats Triggering Atrial Fibrillation in Patients with Persistent Versus Paroxysmal Atrial Fibrillation', *Journal of Cardiovascular Electrophysiology*, 17(8), 818-824.
- Pak, H. N., Liu, Y. B., Hayashi, H., Okuyama, Y., Chen, P. S. and Lin, S. F. (2003) 'Synchronization of ventricular fibrillation with real-time feedback pacing: implication to low-energy defibrillation', *Am J Physiol Heart Circ Physiol*, 285(6), H2704-11.
- Pandit, S. V. and Jalife, J. (2013) 'Rotors and the Dynamics of Cardiac Fibrillation', *Circulation Research*, 112(5), 849-862.
- Papazoglou, E. S. and Parthasarathy, A. (2007) 'BioNanotechnology', *Synthesis Lectures on Biomedical Engineering*, 2(1), 1-139.
- Piorkowski, C. and Hindricks, G. (2009) 'Principles of NavX Mapping' in *Cardiac Mapping*Wiley-Blackwell, 71-79.
- Qinghua, Z., Manriquez, A. I., Medigue, C., Papelier, Y. and Sorine, M. (2006) 'An Algorithm for Robust and Efficient Location of T-Wave Ends in Electrocardiograms', *Biomedical Engineering, IEEE Transactions on*, 53(12), 2544-2552.
- Rantner, L. J., Wieser, L., Stuhlinger, M. C., Hintringer, F., Tilg, B. and Fischer, G. (2007) 'Detection of phase singularities in triangular meshes', *Methods Inf Med*, 46(6), 646-54.
- Rieta, J., Zarzoso, V., Millet-Roig, J., García-Civera, R. and Ruiz-Granell, R. (2000) 'Atrial activity extraction based on blind source separation as an alternative to QRST cancellation for atrial fibrillation analysis', in *Computers in Cardiology 2000*, IEEE, 69-72.
- Rolf, S., Hindricks, G., Sommer, P., Richter, S., Arya, A., Bollmann, A., Kosiuk, J. and Koutalas, E. (2014a) 'Electroanatomical mapping of atrial fibrillation: Review of the current techniques and advances', *Journal of Atrial Fibrillation*, 7(4), 1140.
- Rolf, S., Kircher, S., Arya, A., Eitel, C., Sommer, P., Richter, S., Gaspar, T., Bollmann, A., Altmann, D., Piedra, C., Hindricks, G. and Piorkowski, C. (2014b) 'Tailored Atrial Substrate Modification Based on Low-Voltage Areas in Catheter Ablation of Atrial Fibrillation', *Circulation: Arrhythmia and Electrophysiology*, 7(5), 825-833.
- Roney, C. H., Cantwell, C. D., Qureshi, N. A., Chowdhury, R. A., Dupont, E., Lim, P. B., Vigmond, E. J., Tweedy, J. H., Ng, F. S. and Peters, N. S. (2016) 'Rotor Tracking Using Phase of Electrograms Recorded During Atrial Fibrillation', *Annals of Biomedical Engineering*, 1-14.
- Roney, C. H., Cantwell, C. D., Siggers, J. H., Ng, F. S. and Peters, N. S. (2014) 'A novel method for rotor tracking using bipolar electrogram phase', in *Computing in Cardiology 2014*, 7-10 Sept. 2014, 233-236.

- Rosenbaum, D. S. and Cohen, R. J. (1990) 'Frequency Based Measures Of Atrial Fibrillation In Man', in *Engineering in Medicine and Biology Society, 1990., Proceedings of the Twelfth Annual International Conference of the IEEE*, 1-4 Nov 1990, 582-583.
- Sahadevan, J., Ryu, K., Peltz, L., Khrestian, C. M., Stewart, R. W., Markowitz, A. H. and Waldo, A. L. (2004) 'Epicardial Mapping of Chronic Atrial Fibrillation in Patients: Preliminary Observations', *Circulation*, 110(21), 3293-3299.
- Salinet, J., Schlindwein, F. S., Stafford, P., Almeida, T. P., Li, X., Vanheusden, F. J., Guillem, M. S. and Ng, G. A. (2017) 'Propagation of Meandering Rotors Surrounded by High Dominant Frequency Areas in Persistent Atrial Fibrillation', *Heart Rhythm*.
- Salinet, J. L., Madeiro, J. P. V., Cortez, P. C., Stafford, P. J., André Ng, G. and Schlindwein, F. S. (2013a) 'Analysis of QRS-T subtraction in unipolar atrial fibrillation electrograms', *Medical & Biological Engineering & Computing*, 51(12), 1381-1391.
- Salinet, J. L., Oliveira, G. N., Vanheusden, F. J., Comba, J. L. D., Ng, G. A. and Schlindwein, F. S. (2013b) 'Visualizing intracardiac atrial fibrillation electrograms using spectral analysis', *Comput Sci Eng*, 15.
- Salinet, J. L., Tuan, J. H., Sandilands, A. J., Stafford, P. J., Schlindwein, F. S. and André Ng, G. (2013c) 'Distinctive patterns of dominant frequency trajectory behavior in drug-refractory persistent atrial fibrillation: preliminary characterization of spatiotemporal instability', *J Cardiovasc Electrophysiol*, 25(4), 371-9.
- Samie, F. H., Berenfeld, O., Anumonwo, J., Mironov, S. F., Udassi, S., Beaumont, J., Taffet, S., Pertsov, A. M. and Jalife, J. (2001) 'Rectification of the Background Potassium Current. A Determinant of Rotor Dynamics in Ventricular Fibrillation', *Circulation Research*.
- Sanders, P. (2005) 'Spectral analysis identifies sites of high-frequency activity maintaining atrial fibrillation in humans', *Circulation*, 112.
- Sanders, P., Berenfeld, O., Hocini, M., Jaïs, P., Vaidyanathan, R., Hsu, L.-F., Garrigue, S., Takahashi, Y., Rotter, M., Sacher, F., Scavée, C., Ploutz-Snyder, R., Jalife, J. and Haïssaguerre, M. (2005) 'Spectral Analysis Identifies Sites of High-Frequency Activity Maintaining Atrial Fibrillation in Humans', *Circulation*, 112(6), 789-797.
- Saxon, L. A., Kalman, J. M., Olgin, J. E., Scheinman, M. M., Lee, R. J. and Lesh, M. D. (1996) 'Results of radiofrequency catheter ablation for atrial flutter', *The American Journal of Cardiology*, 77(11), 1014-1016.
- Schwartz, Y. and Ben-Haim, S. A. (2009) 'Principles of Nonfluoroscopic Electroanatomical and Electromechanical Cardiac Mapping' in *Cardiac Mapping*Wiley-Blackwell, 49-70.
- Scherf, D. (1947) 'Studies on Auricular Tachycardia Caused by Aconitine Administration', *Proceedings of the Society for Experimental Biology and Medicine*, 64(2), 233-239.
- Scherr, D., Dalal, D., Cheema, A., Cheng, A., Henrikson, C. A., Spragg, D., Marine, J. E., Berger, R. D., Calkins, H. and Dong, J. (2007) 'Automated detection and characterization of complex fractionated atrial electrograms in human left atrium during atrial fibrillation', *Heart Rhythm*, 4(8), 1013-20.

- Schilling, R. J., Peters, N. S. and Davies, D. W. (1998) 'Simultaneous Endocardial Mapping in the Human Left Ventricle Using a Noncontact Catheter', *Comparison of Contact and Reconstructed Electrograms During Sinus Rhythm*, 98(9), 887-898.
- Schilling, R. J., Peters, N. S. and Davies, D. W. (1999) 'Feasibility of a Noncontact Catheter for Endocardial Mapping of Human Ventricular Tachycardia', *Circulation*, 99(19), 2543-2552.
- Schneek, D. (1999) 'An Outline of Cardiovascular Structure and Function' in *The Biomedical Engineering Handbook, Second Edition. 2 Volume Set* CRC Press.
- Schricker, A. A., Lalani, G. G., Krummen, D. E. and Narayan, S. M. (2014) 'Rotors as drivers of atrial fibrillation and targets for ablation', *Curr Cardiol Rep*, 16(8), 509.
- Schuessler, R. B., Grayson, T. M., Bromberg, B. I., Cox, J. L. and Boineau, J. P. (1992) 'Cholinergically mediated tachyarrhythmias induced by a single extrastimulus in the isolated canine right atrium', *Circulation Research*, 71(5), 1254-67.
- Schuessler, R. B., Kay, M. W., Melby, S. J., Branham, B. H., Boineau, J. P. and Damiano Jr, R. J. (2006) 'Spatial and temporal stability of the dominant frequency of activation in human atrial fibrillation', *Journal of Electrocardiology*, 39(4, Supplement), S7-S12.
- Semmlow, J. L. (2004) 'Spectral Analysis' in *Biosignal and Biomedical Image Processing* CRC Press.
- Shea, J. B. and Sears, S. F. (2008) 'A Patient's Guide to Living With Atrial Fibrillation', *Circulation*, 117(20), e340-e343.
- Sherwood, L. (2011) *Fundamentals of Human Physiology*, Cengage Learning.
- Skanes, A. C., Mandapati, R., Berenfeld, O., Davidenko, J. M. and Jalife, J. (1998) 'Spatiotemporal Periodicity During Atrial Fibrillation in the Isolated Sheep Heart', *Circulation*, 98(12), 1236-1248.
- Smith, S. W. (1997) *The Scientist and Engineer's Guide to Digital Signal Processing*, California Technical Pub.
- Sörnmo, L. and Laguna, P. (2006) *Bioelectrical signal processing in cardiac and neurological applications*, Amsterdam; Heidelberg [u.a.]: Elsevier Academic Press.
- Sosnowski, M., Macfarlane, P. W. and Tendra, M. (2011) 'Determinants of a Reduced Heart Rate Variability in Chronic Atrial Fibrillation', *Annals of Noninvasive Electrocardiology*, 16(4), 321-326.
- Sra, J. and Akhtar, M. (2007) 'Mapping techniques for atrial fibrillation ablation', *Curr Probl Cardiol*, 32(12), 669-767.
- Stewart, S., Murphy, N., Walker, A., McGuire, A. and McMurray, J. J. V. (2004) 'Cost of an emerging epidemic: an economic analysis of atrial fibrillation in the UK', *Heart*, 90(3), 286-292.
- Stridh, M. and Sörnmo, L. (2001) 'Spatiotemporal QRST cancellation techniques for analysis of atrial fibrillation', *Biomedical Engineering, IEEE Transactions on*, 48(1), 105-111.

- Sy, R. W., Thiagalingam, A. and Stiles, M. K. (2012) 'Modern Electrophysiology Mapping Techniques', *Heart, Lung and Circulation*, 21(6), 364-375.
- Takahashi, Y., Sanders, P., Jaïs, P., Hocini, M., Dubois, R., Rotter, M., Rostock, T., Nalliah, C. J., Sacher, F., Clémenty, J. and Haïssaguerre, M. (2006) 'Organization of Frequency Spectra of Atrial Fibrillation: Relevance to Radiofrequency Catheter Ablation', *Journal of Cardiovascular Electrophysiology*, 17(4), 382-388.
- Tan, E. S., Mulder, B. A., Rienstra, M., Wiesfeld, A. C. P., Ahmed, S., Zijlstra, F. and Van Gelder, I. C. (2009) 'Pulmonary vein isolation of symptomatic refractory paroxysmal and persistent atrial fibrillation: A single centre and single operator experience in the Netherlands', *Netherlands Heart Journal*, 17(10), 366-372.
- Tobon, C., Rodriguez, J. F., Ferrero, J. M., Jr., Hornero, F. and Saiz, J. (2012) 'Dominant frequency and organization index maps in a realistic three-dimensional computational model of atrial fibrillation', *Europace*, 14 Suppl 5, v25-v32.
- Tomii, N., Yamazaki, M., Arafune, T., Honjo, H., Shibata, N. and Sakuma, I. (2015) 'Detection Algorithm of Phase Singularity Using Phase Variance Analysis for Epicardial Optical Mapping Data', *IEEE Trans Biomed Eng*, PP(99), 1-1.
- Tortora, G. J. and Derrickson, B. (2011) *Principles of anatomy & physiology*, International student version, 13th ed ed., Hoboken, N.J.: Wiley.
- Traykov, V., Pap, R. and Saghy, L. (2012) 'Frequency Domain Mapping of Atrial Fibrillation - Methodology, Experimental Data and Clinical Implications', *Current Cardiology Reviews*, 8(3), 231-238.
- Tsuchiya, T. (2012) 'Three-dimensional mapping of cardiac arrhythmias - string of pearls', *Circ J*, 76(3), 572-81.
- Uetake, S., Miyauchi, Y., Osaka, M., Hayashi, M., Iwasaki, Y.-k., Yodogawa, K., Horie, T., Tsuboi, I., Hayashi, H., Takahashi, K. and Shimizu, W. (2013) 'Frequency analysis of surface electrocardiograms (ECGs) in patients with persistent atrial fibrillation: Correlation with the intracardiac ECGs and implications for radiofrequency catheter ablation', *Journal of Arrhythmia*, (0).
- Umaphathy, K., Nair, K., Masse, S., Krishnan, S., Rogers, J., Nash, M. P. and Nanthakumar, K. (2010a) 'Phase mapping of cardiac fibrillation', *Circ Arrhythm Electrophysiol*, 3(1), 105-14.
- Umaphathy, K., Nair, K., Masse, S., Krishnan, S., Rogers, J., Nash, M. P. and Nanthakumar, K. (2010b) 'Phase Mapping of Cardiac Fibrillation', *Circulation: Arrhythmia and Electrophysiology*, 3(1), 105-114.
- Unger, L. A., Rottmann, M., Seemann, G. and Dössel, O. (2015) 'Detecting phase singularities and rotor center trajectories based on the Hilbert transform of intraatrial electrograms in an atrial voxel model', *Current Directions in Biomedical Engineering*, 1(1), 38-41.
- Unger Laura, A., Rottmann, M., Seemann, G. and Dössel, O. (2015) 'Detecting phase singularities and rotor center trajectories based on the Hilbert transform of intraatrial electrograms in an atrial voxel model', *Current Directions in Biomedical Engineering*, 1(1), 38.

- Valderrábano, M. (2009) 'Atrial fibrillation: The mother rotor and its rebellious offspring take turns sustaining the family', *Heart Rhythm*, 6(7), 1018-1019.
- Valderrábano, M., Chen, P.-S. and Lin, S.-F. (2003) 'Spatial Distribution of Phase Singularities in Ventricular Fibrillation', *Circulation*, 108(3), 354-359.
- Van Gelder, I. C., Crijns, H. M., Tieleman, R. G. and et al. (1996) 'Chronic atrial fibrillation: Success of serial cardioversion therapy and safety of oral anticoagulation', *Archives of Internal Medicine*, 156(22), 2585-2592.
- Van Gelder, I. C. and Hemels, M. E. W. (2006) 'The progressive nature of atrial fibrillation: a rationale for early restoration and maintenance of sinus rhythm', *Europace*, 8(11), 943-949.
- Van Wynsberghe, D., Noback, C. R. and Carola, R. (1995) *Human anatomy and physiology*, McGraw-Hill.
- Vaquero, M., Calvo, D. and Jalife, J. (2008) 'Cardiac Fibrillation: From Ion Channels to Rotors in the Human Heart', *Heart rhythm : the official journal of the Heart Rhythm Society*, 5(6), 872-879.
- Waktare, J. E. P. (2002) 'Atrial Fibrillation', *Circulation*, 106(1), 14-16.
- Waldo, A. L. (2002) 'Mechanisms of atrial flutter and atrial fibrillation: distinct entities or two sides of a coin?', *Cardiovascular Research*, 54(2), 217-229.
- Walters, T. E., Lee, G., Morris, G., Spence, S., Larobina, M., Atkinson, V., Antippa, P., Goldblatt, J., Royse, A., O'Keefe, M., Sanders, P., Morton, J. B., Kistler, P. M. and Kalman, J. M. (2015) 'Temporal Stability of Rotors and Atrial Activation Patterns in Persistent Human Atrial FibrillationA High-Density Epicardial Mapping Study of Prolonged Recordings', *JACC: Clinical Electrophysiology*, 1(1), 14-24.
- Wharton, J. M. (2001) 'Ablation of atrial fibrillation: a procedure come of age?', *Current Controlled Trials in Cardiovascular Medicine*, 2(2), 67-70.
- Wiggers, C. J. (1940) 'Ventricular fibrillation due to single, localized induction and condenser shocks applied during the vulnerable phase of ventricular systole', *American Heart Journal*, 19(3), 372.
- Winfree, A. T. (1978) 'Stably Rotating Patterns of Reaction and Diffusion A2 - EYRING, HENRY' in Henderson, D., ed., *Theoretical Chemistry* Academic Press, 1-51.
- Winfree, A. T. (1989) 'Electrical instability in cardiac muscle: phase singularities and rotors', *J Theor Biol*, 138(3), 353-405.
- Winfree, A. T. (1997) *Rotors, fibrillation and dimensionality* Chichester John Wiley & Sons Ltd
- Winner, C. (2007) *Circulating Life: Blood Transfusion from Ancient Superstition to Modern Medicine*, Twenty-First Century Books.
- Winter, J. B. and Crijns, H. J. G. M. (2000) 'Atrial Flutter and Atrial Fibrillation', *Journal of Cardiovascular Electrophysiology*, 11(8), 859-860.

- Wolf, P. A., Abbott, R. D. and Kannel, W. B. (1991) 'Atrial fibrillation as an independent risk factor for stroke: the Framingham Study', *Stroke*, 22(8), 983-8.
- Wyse, D. G. and Gersh, B. J. (2004) 'Atrial Fibrillation: A Perspective: Thinking Inside and Outside the Box', *Circulation*, 109(25), 3089-3095.
- Xie, F., Qu, Z., Garfinkel, A. and Weiss, J. N. (2002) 'Electrical refractory period restitution and spiral wave reentry in simulated cardiac tissue', *American Journal of Physiology - Heart and Circulatory Physiology*, 283(1), H448-H460.
- Xie, Z. X., Yin, Y. H., Chen, L. C., Xu, X. H., Liu, Z. Z., Zhi, D., Neng, Z., Xia, D. M. and Lu, H. D. (1998) 'Analysis for atrial fibrillation waves', in *Proceedings of the 20th Annual International Conference of the IEEE Engineering in Medicine and Biology Society. Vol.20 Biomedical Engineering Towards the Year 2000 and Beyond (Cat. No.98CH36286)*, 29 Oct-1 Nov 1998, 115-118 vol.1.
- Yamabe, H., Kanazawa, H., Ito, M., Kaneko, S. and Ogawa, H. (2016) 'Prevalence and mechanism of rotor activation identified during atrial fibrillation by noncontact mapping: Lack of evidence for a role in the maintenance of atrial fibrillation', *Heart Rhythm*, 13(12), 2323-2330.
- Yamagata, K., Aldhoon, B. and Kautzner, J. (2016) 'Reduction of Fluoroscopy Time and Radiation Dosage During Catheter Ablation for Atrial Fibrillation', *Arrhythm Electrophysiol Rev*, 5(2), 144-9.
- Yoshida, K., Chugh, A., Ulfarsson, M., Good, E., Kuhne, M., Crawford, T., Sarrazin, J. F., Chalfoun, N., Wells, D., Boonyapisit, W., Veerareddy, S., Billakanty, S., Wong, W. S., Jongnarangsin, K., Pelosi, F., Jr., Bogun, F., Morady, F. and Oral, H. (2009) 'Relationship between the spectral characteristics of atrial fibrillation and atrial tachycardias that occur after catheter ablation of atrial fibrillation', *Heart Rhythm*, 6(1), 11-17.
- Zaman, J. A. B. and Peters, N. S. (2014) 'The Rotor Revolution', *Conduction at the Eye of the Storm in Atrial Fibrillation*, 7(6), 1230-1236.
- Zlochiver, S., Yamazaki, M., Kalifa, J. and Berenfeld, O. (2008) 'Rotor Meandering Contributes to Irregularity in Electrograms during Atrial Fibrillation', *Heart rhythm : the official journal of the Heart Rhythm Society*, 5(6), 846-854.